Roles of the HOPS complex and Sec1/Munc18 proteins in membrane fusion

Braden T. Lobingier

A dissertation
submitted in partial fulfillment of the
requirements for the degree of

Doctor of Philosophy

University of Washington

2013

Reading Committee:
Alexey Merz, Chair
David Kimelman
David R. Morris

Program Authorized to Offer Degree:

Biochemistry

University of Washington

Abstract

Roles of the HOPS complex and Sec1/Munc18 proteins in membrane fusion

Braden T. Lobingier

Chair of the Supervisory Committee:
Professor Alexey Merz
Department of Biochemistry

A fundamental feature of the eukaryotic cell is its diversity of membrane bound compartments. Despite a constant flux of proteins and lipids through these compartments, organelle identity and function is maintained by regulating membrane fusion. Membrane fusion is driven by the coordinated action of a several families of proteins: Rabs, tethers, SMs, and SNAREs. Each compartment has its own paralogs of these proteins, and compartment identity is maintained by the specificity of this membrane fusion machinery. Individual SNARE proteins form a complex to catalyze membrane fusion, while Rabs, tethers, and SM proteins regulate SNARE activity. The universal factors Sec18 and Sec17, an ATPase and its adaptor, prime the SNARE proteins after each round of membrane fusion by disassembling the SNARE complex. The mechanisms by which these processes occur, however, are not fully understood. I have studied the conserved membrane fusion machinery of the lysosomal-vacuole using the *S. cerevisiae* model system, and then expanded my observations to the fusion machinery involved in ER to Golgi transport. Using biochemical and cell biological assays, I have examined the architecture of the vacuole-lysosomal tethering complex, and identified interactions sites within it for the other components of the fusion machinery. I have specifically focused on the role of

SM proteins in membrane fusion. Using biochemical assays with purified components, I have characterized the SNARE binding properties of two SM proteins and identified a mechanistic function for SM proteins in kinetically shielding SNARE complexes from disassembly by ATPase Sec18.

TABLE OF CONTENTS

LIST OF FIGURES

LIST OF TABLES

Acknowledgements

I would like to start by thanking Alex Merz for his mentorship. He allowed me to pursue "the big problems," and believed early on that I was onto something interesting. Without his willingness to let me try, and try again, to solve seemingly intractable problems, many of the most exciting results in this thesis would not have been obtained.

I am deeply appreciative of my all of my co-workers past and present, especially those who were instrumental in my early training. Chris Brett is a consummate scientist, and he taught me three critical lessons: 1) Always remember the big picture; 2) An experiment without controls is not an experiment; 3) A failed experiment—a good one—is simply a marker to point you in the right direction. Cortney Angers was essential in teaching me the technical side of science. Her willingness to trouble-shoot my mistakes was essential to my scientific growth. I also am very thankful to my collaborators, especially Margaret Lo and Dan Nickerson, who came in to help when time got short.

I am thankful to all my friends during graduate school. A special thanks goes to William Hyman, who gave me a home during the last six months of my thesis. You went above and beyond the call of friendship, and I am deeply in your debt.

I would like to thank the Schultz Travel Fellowship and the Cell and Molecular Biology training grant for support and training opportunities. Both were instrumental in expanding my scientific viewpoint.

Finally, I would like to thank my family: my parents, my sister, and my wife. Your support, and your love, has helped me through six years and these final six months.

Dedication

To Jill.

My wife and my love.

For the six years and the six months.

Chapter One — Introduction

1.1 –Overview of Membrane Trafficking and Membrane Fusion

A fundamental feature of the eukaryotic cell is that its contents are divided between the cytoplasm and numerous functionally specialized compartments. Membrane-enclosed organelles allow for disparate and even opposing chemistries—such as protein synthesis and protein degradation—to occur in proximity. Intracellular trafficking carries specific proteins and lipids between these different compartments with selectivity. Trafficking has three general phases: vesicle budding, vesicle transport, and membrane fusion (Bonifacino and Glick, 2004).

During vesicle budding, a subset of luminal and membrane-bound contents of an organelle are packaged into a vesicle. This process is achieved by coordinated action of coat proteins (Brodsky, 2012; Popoff et al., 2011; Zanetti et al., 2012). Adaptor proteins (also called inner coat proteins) enrich an area of the bilayer for particular cargos, and this patch of membrane is deformed. Once the vesicle separates from the donor membrane through a membrane fission event, it traffics through the cytoplasm until nearby the surface of an acceptor compartment. This can occur by passive diffusion or via cytoskeletal motors. It should be noted that in addition to vesicular traffic, some pathways—such as endosomal recycling of receptors to the plasma membrane— use tubular networks to move material (Puthenveedu et al., 2010; Temkin et al., 2011).

Once a vesicle reaches an acceptor compartment, a conserved protein machinery initiates merging of bilayers and mixing of the lumenal contents (Rizo and Sudhof, 2012; Wickner and

Schekman, 2008; Wickner, 2010). Membrane fusion starts with activation of signaling molecules called Rabs. Activated Rabs recruit tethering factors to make initial contacts between the compartments. Rabs and tethers also coordinate recruitment of additional proteins, including SM proteins, and these factors work together to coordinate the protein catalysts of membrane fusion. The proteins that physically drive membrane fusion are called SNAREs. To fuse two compartments, SNAREs anchored within each bilayer form a co-complex spanning the two membranes. The free energy release from SNARE complex formation is coupled to deformation of the membrane and dehydration of intermembrane space, leading to bilayer fusion. After fusion, a universally conserved ATPase (Sec18/NSF) and its essential adaptor (Sec17/α-SNAP) disassemble the SNARE complex so that additional rounds of membrane fusion can occur. SNARE assembly/disassembly operates similarly throughout the cell, but each compartment employs its own paralogs of the basic membrane fusion factors: Rabs, tethers, SMs, and SNAREs. There is a notable exception to this rule. Both the mitochondria and smooth ER use the large GTPase of the dynamin superfamily for membrane fusion (Hu et al., 2011; Meeusen and Nunnari, 2005).

1.2 –Proteins of Membrane Fusion

Rab small G proteins

Rab proteins are small G proteins of the Ras superfamily that are physically linked to a membrane through a post-translational lipid modification (*bis*-geranylgeranylation) (Mizuno-Yamasaki et al., 2012). Rabs are key markers of organelle identity (Behnia and Munro, 2005). Rab proteins regulate membrane fusion by acting as signaling molecules. When bound to GTP, the Rab protein adopts an activated conformation that is recognized by specific effector proteins,

which in turn mediate downstream effects of Rab activation. Rab signaling is turned off by GAPs (GTPase accelerating proteins), which dramatically increase the basal rate of Rab GTP hydrolysis (Barr and Lambright, 2010). GAPs coordinate the nucleotide-binding pocket of the Rab, as well as a nucleophilic water molecule, so that hydrolysis of the γ-phosphate of GTP occurs much more efficiently. This is in contrast to GTPases like dynein or dynamin, which coordinate the GTP nucleotide and water molecule without additional proteins, and consequently have a much higher rate of basal GTPase activity. Hydrolysis of the γ-phosphate of GTP leaves the Rab bound to GDP and inorganic phosphate, and the latter diffuses away from the GDP-Rab. GDP-Rabs can be removed from and re-inserted into membranes by a specialized chaperone, GDI (GDP dissociation inhibitor).

GEFs (guanine nucleotide exchange factors) catalyze nucleotide exchange in order to activate the GDP-Rab (Barr and Lambright, 2010). GEFs typically function *in vivo* toward a small subset of the Rabs, and a single Rab may have multiple cognate GEFs. While there is no universal GEF mechanism, there are similarities in the methods by which GEFs act. First, GEF proteins bind to the Rab and destabilize the nucleotide binding pocket, which causes release of nucleotide. Second, as GEF proteins bind to GDP-Rab, release of GDP causes loss of the GEF binding surface and dissociation of the GEF. Consequently, GEFs are not thought to promote selective binding of GTP *vs.* GTP to the nucleotide-free Rab. However, since the cytoplasm has a 10-fold greater concentration of GTP than GDP, GEFs functionally promote GDP for GTP exchange. TRAPP (transport protein particle), the only GEF known to function as an obligate multi-subunit complex, is a notable exception to this rule. Unlike other GEFs, the TRAPP complex directly promotes nucleotide re-binding to the Rab (Cai et al., 2008; Chin et al., 2009).

Tethers

Tethers are the most diverse family of proteins associated with membrane docking and fusion. Other conserved membrane fusion proteins—Rabs, SM proteins, SNAREs—all have compartment-specific paralogs that carry out similar functions. Tethers are compartment-specific as well, and each organelle has at least one unique tether that tends to be highly conserved from yeast to humans (Koumandou et al., 2007). Comparisons of the resident tethers at different organelles, however, demonstrate that tethers can be quite different in structure and function. Thus, tethers are defined by the property of making initial contacts between two membranes. Tether proteins are separated into at least two major families: long coiled-coil proteins (p115/Uso1, GMAP-210, GCC185, GM130, and giantin) and multisubunit tethering complexes (exocyst, HOPS, CORVET, TRAPPI/II, GARP, COG, Dsl1). To catalog the vast number of studies of these different tethers, and summarize the known functions, would be a review in itself (for excellent examples of such a review, see (Angers and Merz, 2011; Yu and Hughson, 2010)). The goal here is to underscore some important features that are generally conserved among tethers, and highlight some of the functional diversity.

Most tethering proteins have been shown to interact with Rabs or other small G proteins, and many have been shown to interact with SNAREs. The prototypical member of the long coiled-coil family of tethers is p115 (Uso1 in yeast). p115/Uso1 functions in intra-Golgi transport, and the resident Golgi Rab (Rab1/Ypt1) recruits p115/Uso1 to the membrane (Allan et al., 2000; Cao et al., 1998). p115 makes contacts with Golgi SNAREs, and can accelerate SNARE complex assembly *in vitro* (Bentley et al., 2006; Shorter et al., 2002). In the multisubunit tethering complex family (MTC), several complexes have been shown to contact Rabs and SNAREs. The four-subunit GARP complex (retrograde traffic from the endosome to

Golgi), the eight-subunit COG complex (retrograde traffic within the Golgi), the eight subunit exocyst complex (traffic to the plasma membrane), and the six subunit HOPS and CORVET complexes (trafficking from the late endosome to lysosome) all contact both Rabs and SNAREs (Guo et al., 1999; Perez-Victoria and Bonifacino, 2009; Sato et al., 2000; Seals et al., 2000; Sivaram et al., 2005; Suvorova et al., 2002).

A few tethers are thought to contact either Rabs or SNAREs, but not both. For example, the long coiled-coil tether GCC185, which functions in Golgi trafficking, has at least five Rab binding sites but does not interact with SNAREs (Hayes et al., 2009). The MTC tether Dsl1, which functions in retrograde traffic to the ER, has no Rab binding sites but can interact with SNAREs (Kraynack et al., 2005; Tripathi et al., 2009). Like the long coiled-coil tether p115, the Dsl1 complex has been shown to accelerate SNARE complex formation *in vitro* (Ren et al., 2009). This underscores that while not all properties are shared among tethers, subsets of structurally and functionally distinct tethers do perform common functions. For tethers that contact both Rabs and SNAREs, a proposed mechanism of tethering is to link a Rab on one compartment to SNAREs on the other. It is less clear how tethers that can only bind Rabs or SNAREs might tether, although the long coiled-coil tether GCC185 has been shown to interact with other SNARE-binding tethers, suggesting that tethers can act cooperatively. In the case of the Dsl1 complex, it is thought that tethering is achieved through its second affinity for the vesicle coat proteins of the COPI family (Zink et al., 2009).

A subset of tethers are peripheral membrane proteins that directly contact lipids. The long coiled-coil tether GMAP210 functions in Golgi traffic. GMAP210 forms a parallel dimer that is predicted to be greater than 200 nm in length. Each monomer has a binding site for a small G protein at its N-terminus, and at its C-terminus GMAP210 has an ALPS motif

(amphiphatic lipid-packing sensor) that binds to the highly curved membrane of a vesicle (Drin et al., 2008). The MTC HOPS, which consists of six subunits, functions in traffic to the lysosome. Like GMAP210, one of the HOPS subunits, Vps41, can both bind a small G protein **(see Chapter 2)** and has an APS motif that will bind to highly curved membranes (Cabrera et al., 2010). Also, the entire HOPS complex has been shown to have affinity for phosphoinositides, and preferentially binds singly phosphorylated phosphoinositides (Stroupe et al., 2006).

The common picture of tether function is that tethering proteins make initial contacts between membranes, but the methods by which tethers make these contacts is variable. To make these contacts, tethers are thought to reside on the acceptor compartment prior to the arrival of vesicle or incoming compartment (Yu and Hughson, 2010). It should be noted, however, that tethers are not found as static residents of their cognate compartment; rather, they are temporally recruited by an activation of signaling factors such as Rab small G proteins. Some tethers contact Rabs and SNAREs, or Rabs and lipids, or multiple Rabs. It should be pointed out that tethers are not limited to just two different affinities. The HOPS complex has been shown to bind to Rabs, SNAREs, highly curved membranes, and phosphoinosities. The binding affinities of the HOPS complex are explored in more detail in **Chapters 2, 3, and 4.**

SNAREs

A great deal of evidence suggests that SNARE (SNAP receptor) proteins are primary catalysts of membrane fusion (**Figure 1.1**). All SNARE proteins have a 60-70 amino acid SNARE domain that is defined by amphiphilic heptad repeats. Most SNARE proteins are tail-anchored in the membrane, with a C-terminal transmembrane domain adjacent to the cytoplasmic SNARE domain. SNARE proteins drive membrane fusion by forming a complex of different SNARE proteins from each bilayer: three SNARE from one membrane and one

SNARE from the opposing membrane form a four-helical coiled-coil bundle through their SNARE domains. The asymmetric distribution of SNAREs gave rise to the early SNARE nomenclature: t-SNAREs enriched on the target membrane pair with v-SNAREs on the vesicle. Sequence alignments showed there was not one family of t-SNAREs, but three subfamilies. SNARE nomenclature was updated based on sequence and structural studies; also, the change in nomenclature better accommodated description of homotypic fusion events (in which each compartment carries the t- and v-SNAREs) (Fasshauer et al., 1998). The new nomenclature for SNAREs was based on the structural observation that the packing residues of the coiled-coil SNARE bundle are hydrophobic repeats (thus, every third and fourth amino acid is hydrophobic, with the rest of the amino acids facing the cytoplasm), with the exception on a single layer of packing residues in the center of the four-helical bundle: almost every t-SNARE has a conserved glutamine (Q) in the center of its SNARE domain and v-SNAREs have a conserved arginine (R). These Q and R residues form the central packing layer of the SNARE complex bundle. Consequently, t-SNAREs were renamed Q-SNAREs (and the three subfamilies differentiated by homology into Qa, Qb, and Qc), and the v-SNARE was renamed the R-SNARE.

When Qa, Qb, and Qc SNAREs from one bilayer are in close proximity with a R-SNARE from an apposed bilayer, SNARE domains can zipper together into a tetrahelical coiled-coil bundle. Zippering appears to initiate at the N-terminal, (membrane-distal) end of the SNARE domains, proceeding toward the membrane and drawing the two bilayers together (Fasshauer and Margittai, 2004; Pobbati et al., 2006; Schwartz and Merz, 2009; Sorensen et al., 2006). While zippering, the Q- and R-SNAREs are still in separate bilayers, and this partially zippered SNARE complex is called a *trans*-SNARE complex. When the SNARE complex fully forms, free energy release is coupled to distortion of the bilayer through the SNARE transmembrane

domains. In fact, the distance between the SNARE domain and transmembrane domain is critical for membrane fusion. If more than a few residues separate the SNARE and transmembrane domains, membrane fusion fails (McNew et al., 1999). Free energy release upon complex formation has been measured at 65 k_BT, which exceeds the estimated 40 k_BT needed to deform the bilayer and drive membrane fusion (Gao et al., 2012). After membrane fusion, the Q- and R-SNAREs are in a single bilayer, and this structure is called a *cis*-SNARE complex.

Not only do SNAREs drive membrane fusion, but they also are involved in regulating the specificity of membrane fusion. Each trafficking pathway in the cell uses its own complement of SNARE proteins; consequently, SNARE complex formation between non-cognate SNARE could drive off-pathway fusion. *In vitro* assays with liposomes have showed, however, that membrane fusion is driven preferentially by cognate SNAREs (McNew et al., 2000). A notable exception to this rule is that some R-SNAREs have been shown to drive membrane fusion *in vitro* with non-cognate Q-SNAREs (Izawa et al., 2012). Thus, SNARE molecules themselves contribute to part of the membrane fusion specificity determinants.

In addition to their SNARE domains, many SNARE proteins have N-terminal regulatory domains. In general, SNARE NTDs function in SNARE regulation or as recruitment motifs for other proteins. Perhaps the most well studied SNARE NTD is the trihelical H_{abc} domain of the Qa family of SNAREs. For example, the Qa SNARE that functions in the exocytosis of synaptic vesicles, syntaxin-1a, has a H_{abc} domain that can fold back into a closed conformation that holds the SNARE domain in an auto-inhibited conformation (Yang et al., 2000). It is hypothesized that this closed conformation may prevent syntaxin-1a from forming non-cognate complexes as it traffics from the endoplasmic reticulum, where it is inserted into the membrane, through the Golgi, and to its destination at the plasma membrane (Zhou et al., 2013). Autoinhibitory

functions of SNARE NTDs have been seen for other SNAREs. For example, the R-SNARE VAMP-7, which functions in endocytic trafficking, has a N-terminal "longin" domain. Recent work has shown that this R-SNARE longin domain can be stabilized in a closed, autoinhibited form by the effector protein Varp (Schafer et al., 2012). It should be pointed out that some SNAREs with NTDs, including some Qa SNAREs, do not seem to adopt a closed conformation. For example, the H_{abc} domain of the Qa SNARE that functions at the yeast vacuole, Vam3, does not have an autoinhibitory mode (Dulubova et al., 2001). Instead, the Vam3 H_{abc} domain is involved in recruiting the tethering complex HOPS (Laage and Ungermann, 2001; Lobingier and Merz, 2012). See **Chapter 3** for more details.

NSF/Sec18 and αSNAP/Sec17

Membrane fusion is driven by the trans-SNARE complex, consisting of SNAREs in two membranes, fully zippering into a *cis*-SNARE complex in one membrane. The *cis*-SNARE complex is enormously stable. Melting temperatures have been measured for several SNARE complexes. For the early endosomal SNARE complex, the unfolding transition for the SNARE bundle was measured at 87˚ C (Zwilling et al., 2007). The SNARE complex that functions in exocytosis in yeast has a melting temperature of 64˚ C. The most stable SNARE complex that has been measured functions in syntaptic vesicle exocytosis. It has a melting temperature of 95˚ C, and is resistant to denaturation by the detergent SDS up to 60˚ C (Ernst and Brunger, 2003; Strop et al., 2008). It is unsurprising, then, that *cis*-SNARE complexes do not fall apart spontaneously, and must be actively disassembled for the individual SNARE proteins to participate in subsequent round of membrane fusion.

ATP hydrolysis is coupled to SNARE complex disassembly by the universal factors NSF (N-ethylmaleimide-sensitive factor) and its obligate cofactor α-SNAP (soluble NSF attachment

protein). The *S. cerevisiae* homologs of NSF and α-SNAP are Sec 18 and Sec17 (**Figure 1.1**). Here, the will be referred to using yeast nomenclature. Sec17 and Sec18 are essential proteins. Loss of either results in accumulation of *cis*-SNARE complexes, stalled intracellular trafficking, and cell death (Griff et al., 1992; Kaiser and Schekman, 1990). While it is not fully understood how Sec18 and Sec17 disassemble SNARE complexes, a general model has been established. Sec18 cannot bind or disassemble SNARE complexes by itself, and requires Sec17 to act as an adaptor. Three copies of Sec17 bind around the four-helical SNARE complex bundle. Recent work has shown that residues in the N-terminus of Sec17 and α-SNAP dip into the membrane, and this membrane dipping aids—but is not necessary for—engagement of the SNARE complex (Winter et al., 2009). As Sec17 must interact with every SNARE complex in the cell, and because these SNARE complexes do not have conserved surfaces, it has been proposed that Sec17 recognizes the general shape and negative charge of the SNARE complex surface (Marz et al., 2003; Rice and Brunger, 1999).

Sec18 is an obligate homo-hexamer that forms a ring surrounding a central pore. Each Sec18 molecule has three domains: an "N" domain necessary for Sec17 interaction and two ATP-binding "D" domains form the stacked rings of the hexamer. The D1 domain functions primarily in SNARE complex disassembly while the D2 domain is primarily responsible for hexamerization. Both D1 and D2 functions require ATP. Upon binding of ATP, Sec18 hexamer changes into a conformation that is competent to engage the Sec17-bound SNARE complex. Sec18 has a low basal rate of ATP hydrolysis in solution and can only hydrolyze ATP efficiently when bound to Sec17 and a SNARE complex (Matveeva and Whiteheart, 1998). Once bound, Sec18 hydrolyzes ATP, the SNARE complex is disassembled, and Sec17 and Sec18 dissociate. It is not known how Sec18 disassembles SNARE complexes. There are (at least) two models (Zhao

et al., 2012). First, ATP hydrolysis allows Sec18 to pull a single SNARE out of the SNARE complex and into its central pore. In the second model, ATP hydrolysis causes subunits of the Sec18 hexamer to twist relative SNARE complex, which applies torque through Sec17 to untwist the coiled-coil SNARE complex bundle.

1.3 –Sec1/Munc18 (SM) Proteins

A longstanding mystery in the intracellular trafficking field, and a central issue addressed by this thesis, is the function of SM (Sec1/Munc18) proteins in membrane fusion (Rizo and Sudhof, 2012). SM proteins are highly conserved, interact with SNAREs, and are essential for the process of membrane fusion. For example, deletion of the SM that functions in neurons, Munc18-1, causes a complete loss of neurotransmission (Verhage et al., 2000). There are four subfamilies of SM proteins and each is required for fusion at the trafficking steps in which they function: Sly1 (ER to Golgi), Sec1/Munc18 family (exocytosis), Vps45 (endosomal traffic), and Vps33 (late-endolysosomal traffic) **(Figure 1.2)**. Crystal structures have been solved for several SM proteins, and the 60-70 kDa soluble proteins share a clasp-like structure (Bracher et al., 2000). Despite their essential functions in important processes and over a decade of intense study, the mechanistic role(s) of SM proteins is still unresolved and controversial.

At the heart of the confusion about SM proteins are two seemingly contradictory observations. First, SM proteins interact with SNAREs. Second, the mode of SNARE interaction varies between the SM protein subfamilies (Carr and Rizo, 2010). It has been very difficult to reconcile genetic and structural lines of evidence, which suggest that SM protein subfamilies have a common general role, with biochemistry that has shown very divergent modes of SNARE

association. There are three major SNARE binding modes that have been identified for SM proteins (**Figure 1.2**).

Munc18 binds with nanomolar affinity to the closed form of its cognate Q_a-SNARE, syntaxin-1a (Burkhardt et al., 2008). In this configuration, Munc18 makes contacts with the H_{abc} domain, the SNARE domain, and a short "N-peptide" motif at the syntaxin-1a N-terminus. Munc18 binding to the closed Q_a SNARE prevents SNARE complex formation. This observation, and overexpression experiments, initially suggested that Munc18 might have a preventative role in membrane fusion (Yang et al., 2000). Paradoxically, genetic studies demonstrated that ablation of Munc18 completely prevents neurotransmission, suggesting that the protein in fact promotes fusion process (Verhage et al., 2000). More recent studies have shown that only the N-peptide and SNARE domain of syntaxin are required for Munc18 to promote fusion; the H_{abc} domain and the closed form of syntaxin are not necessary (Rathore et al., 2010; Shen et al., 2010). Rather, it seems that Munc18 binding to the closed form of syntaxin suppresses spontaneous and aberrant fusion events, but that this is a secondary role of the protein (Zhou et al., 2013). Like Munc18, the Vps45 subfamily also binds its cognate Q_a SNARE in its closed conformation, making contacts with the N-peptide, H_{abc}, and SNARE domain (Carpp et al., 2006; Furgason et al., 2009).

The Sly1 subfamily of SM proteins uses the second binding mode of SM proteins. It binds to the N-peptide of its cognate Qa SNARE, and this interaction is low nanomolar in affinity (Grabowski and Gallwitz, 1997; Peng and Gallwitz, 2002; Yamaguchi et al., 2002). Sly1 does not appear to bind the closed form of its Qa SNARE Sed5 (it is not known if Sed5 can enter an autoinhibited conformation). The biochemistry of the Sly1 subfamily can be viewed as a variation on Munc18 and Vps45, as all three interact with the Qa SNARE N-peptide motif, but

only Sly1 exclusively uses this mode. It has been proposed that N-peptide binding functions primarily to recruit SM proteins to their cognate Q_a SNAREs (Rathore et al., 2010; Shen et al., 2010).

The third mode of association between SNAREs and SM proteins was first described in studies of the Sec1 subfamily. Sec1, which functions in exocytosis in yeast, lacks strong affinity for any individual SNARE. Sec1 has primary affinity for the quaternary SNARE complex (Carr et al., 1999; Morgera et al., 2011; Togneri et al., 2006). In this thesis, I show that the Vps33 subfamily of SM proteins has a similar primary affinity for its cognate SNARE complex (see **Chapters 3 and 4**). Interestingly, the cognate Qa SNAREs of Vps33 and Sec1 do *not* include the consensus N-peptide motif (Hu et al., 2007). It is intriguing that Sec1 and Munc18--which seemingly use the most disparate modes of SNARE association—are by sequence alignment part of the same subfamily of SM proteins that function in exocytosis, and are closer in sequence to each other than either is to Vps45, Vps33, or Sly1 subfamilies. More recently, it has been shown that Munc18 can bind to the quaternary SNARE complex as well, although with a much lesser affinity (mid-micromolar) compared to the closed Qa SNARE (low nanomolar) (Xu et al., 2010b). This data suggests that despite differences in primary SNARE binding mode, the SNARE complex might be the universal target of SM proteins (see **Chapters 3 and 4**).

The primary *in vitro* evidence for a common, evolutionarily conserved SM function comes from studies of membrane fusion. SNARE proteins reconstituted into proteoliposomes can drive fusion. Addition of either Sec1 or Munc18 has been shown to moderately increase the rate of SNARE-mediated liposome fusion *in vitro* (Scott et al., 2004; Shen et al., 2007). However, more recent studies with SNARE mediated liposome fusion have shown that SM protein alone is not capable of driving fusion, and that additional proteins—such as Rabs,

effectors, tethers, and Sec17/Sec18—are all required (Ma et al., 2013; Ohya et al., 2009; Stroupe et al., 2009). It is not clear how SM proteins increase the rate of membrane fusion *in vitro*, or whether this is their primary function *in vivo.*

Several hypotheses have been suggested for SM protein function (Carr and Rizo, 2010). The first is that SM proteins accelerate the rate of SNARE complex formation (as this seems to be a rate limiting step in membrane fusion). However, many *in vitro* studies have shown that SMs proteins do not alter the rate of SNARE complex assembly. A second idea is that SM proteins bind the assembling *trans*-SNARE complex, and this contributes to membrane fusion by aiding the SNARE complex in applying torque on the membrane. No direct evidence exists in support of this theory. A third hypothesis suggests that SM proteins bind to the *trans*-SNARE complex and keep it from diffusing away from the fusion vertex (especially into the space between the apposed bilayers). Again, no direct evidence exists to support this theory.

1.4 – HOPS and CORVET complexes

The tethering complexes that function in traffic from the late endosome to the vacuolar-lysosome are the CORVET (class C core vacuole/endosome tethering) and HOPS (homotypic fusion and protein sorting) complexes. The hexameric 659kDa CORVET and hexameric 633kDA HOPS complexes share a four subunit core—Vps11, Vps16, Vps18, and the SM protein Vps33—and each have two complex-specific subunits: Vps3 and Vps8 for CORVET and Vps39 and Vps41 for HOPS. These complexes are essential for the process of membrane fusion in the late-endo-lysosomal pathway. Loss of any core subunit leads to severe fragmentation of the vacuolar-lysosomal compartment, consistent with a failure of early endosomes to mature in the endo-lysosomal pathway. These mutants also exhibit total failures of protein targeting to the

vacuole through biosynthetic, endocytic, and autophagic pathways, severe sterol storage defects (probably due to mistargeting of the NPC1 and NPC2 sterol transport proteins), and, in mammalian cells, immunity to Ebola virus, which uses NPC2 as a portal for cellular entry (Raymond et al., 1992) (Carette et al., 2011). Loss of the HOPS-specific subunits, Vps39 or Vps41, leads to failure of late endosome to fuse, and partial fragmentation of the vacuole and a subset of the above trafficking defects. The vacuole swells dramatically with the loss of the CORVET subunits Vps3 or Vps8, consistent with an imbalance of traffic into and out of the vacuole.

With the exception of the SM protein Vps33, computational folding algorithms predict that HOPS and CORVET subunits have a similar architecture, consisting of an N-terminal beta-propeller followed by a C-terminal alpha-solenoid (Plemel et al., 2011). This architecture is shared with coat proteins like clathrin, COPI and COPII, and subunits of the nuclear pore complex. The possibility of a shared origin has led to the beta-propeller/alpha-solenoid fold being called an ancestral coat element (ACE) (Brohawn et al., 2008). As the HOPS complex has been studied in much more depth than the CORVET complex, this review will focus on the former. It is likely that many of the general functions described for HOPS will also hold true for CORVET.

HOPS complex, as discussed in the introduction on tethers, has affinities for Rabs, SNAREs, curved membranes, and phosphoinositides (some of these observations are from this thesis; see **Chapter 2, 3, and 4**) (Epp et al., 2011; Nickerson et al., 2009; Solinger and Spang, 2013). In addition to its binding affinities, much insight into the function of the HOPS complex—and in fact all the membrane fusion machinery—has been gained using an *in vitro* assay of vacuole fusion. Using this system, the HOPS complex has been demonstrated to

function not only in tethering, but also in a subsequent step, docking, during which the SNAREs are prepared for action. The HOPS complex has been shown to accumulate at the membrane fusion sites of vacuole:vacuole contact called fusion vertices, along with SNAREs, the Rab Ypt7, and a subset of lipids (Wang et al., 2002; Wang et al., 2003). HOPS has been shown to have several functional roles with the SNARE complex. The HOPS complex appears to suppress the fusion of vacuoles when one of the SNAREs has a mutation in its central layer, suggesting an assembly-coupled proofreading function (Starai et al., 2008). HOPS also protects *trans*-SNARE complexes from Sec18-mediated disassembly (Xu et al., 2010a). Further insight into the HOPS complex has been gained from *in vitro* fusion assays using liposomes. Early work in this system demonstrated that HOPS could accelerate the rate of SNARE-mediated liposome fusion (Mima et al., 2008). Later work, which included optimization of the lipid composition of the liposomes, confirmed results from intact vacuole experiments, showing that HOPS is necessary for membrane fusion along with the Rab Ypt7 and the SNARE disassembly machinery Sec17 and Sec18 (Stroupe et al., 2009; Stroupe, 2012).

The goal of my thesis was to understand how HOPS and CORVET interact with Rabs and SNAREs to drive membrane fusion. While these proteins had been studied in the context of the heteroligomeric complexes, a deeper understanding of HOPS and CORVET functions required characterization of isolated subunits and subcomplexes. To better understand HOPS function, I expressed and purified HOPS and CORVET subunits using the baculovirus and insect cell system. In **Chapter 2**, the architecture of the HOPS and CORVET complexes and interactions with compartment-specific Rabs are examined. In **Chapter 3,** HOPS-SNARE interactions are studied. In **Chapter 4,** I identify a novel co-complex of the HOPS SM-family subunit Vps33, Sec17, and the vacuolar SNARE complex. I extend this result to the Golgi SM, Sly1, and I

demonstrate that these SM proteins protect their cognate SNARE complexes from Sec18-mediated disassembly

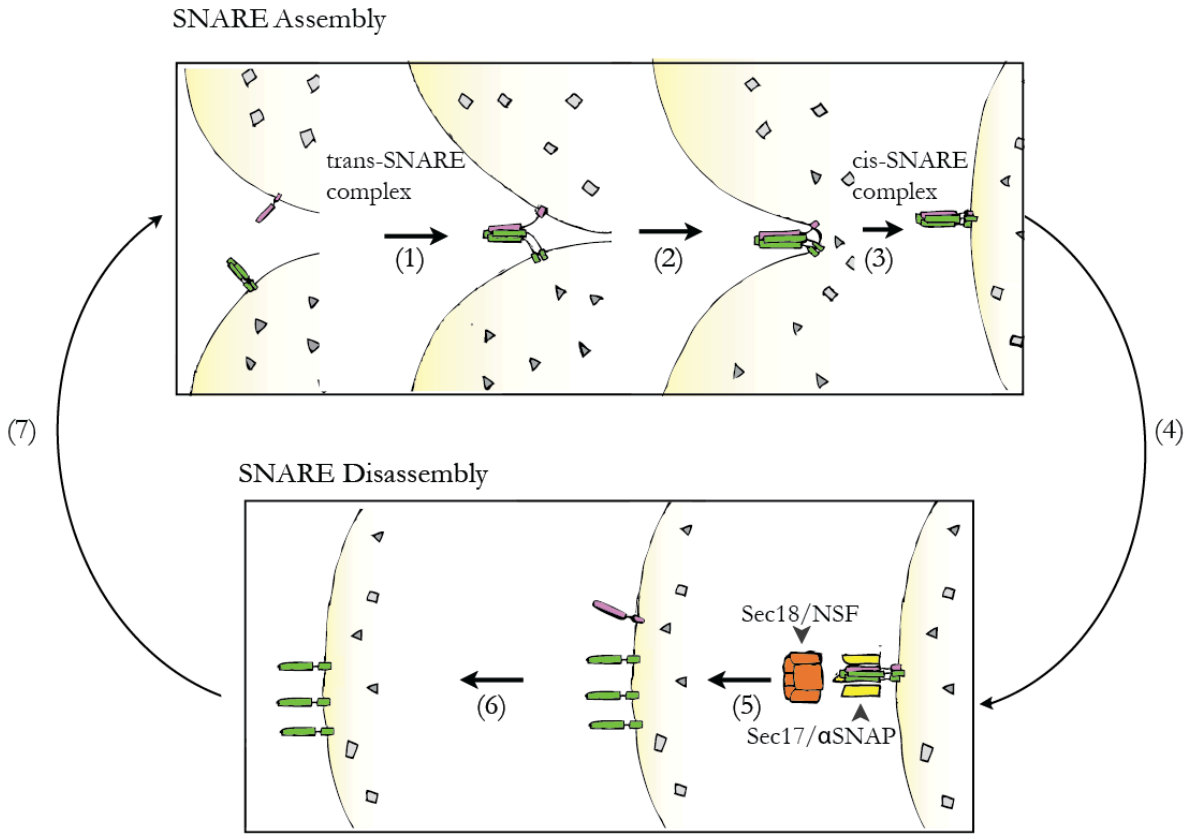

Figure 1.1. The SNARE Cycle
SNARE-mediated membrane fusion begins with an asymmetric distribution of Q- (green) and R-SNAREs (pink) in separate bilayers. (1) trans-SNARE complex forms when the Q- and R-SNAREs are brought into close proximity (in the cell, this involves the associated proteins of membrane fusion including Rabs and tethers which are not diagramed here). (2) Full zippering of the trans-SNARE complex leads to deformation of the membrane, fusion of the bilayers, and mixing of lumenal contents. (3) At the end of membrane fusion, the cis-SNARE complex of Q- and R-SNAREs is in the membrane of the newly fused compartment. (4) For the SNAREs to participate in additional rounds of membrane fusion, the cis-SNARE complex must be separated. This process begins with three copies of the cofactor Sec17/αSNAP binding around the SNARE complex bundle. (5) Once Sec17/αSNAP is bound to the SNARE complex, it recruits the hexameric ATPase Sec18/NSF. Sec18 couples the hydrolysis of ATP to disassembly of the SNARE complex. (6) In the cases of non-homotypic fusion, the R-SNARE is recycled away from the compartment. (7) The Q-SNAREs form an acceptor complex for another round of membrane fusion.

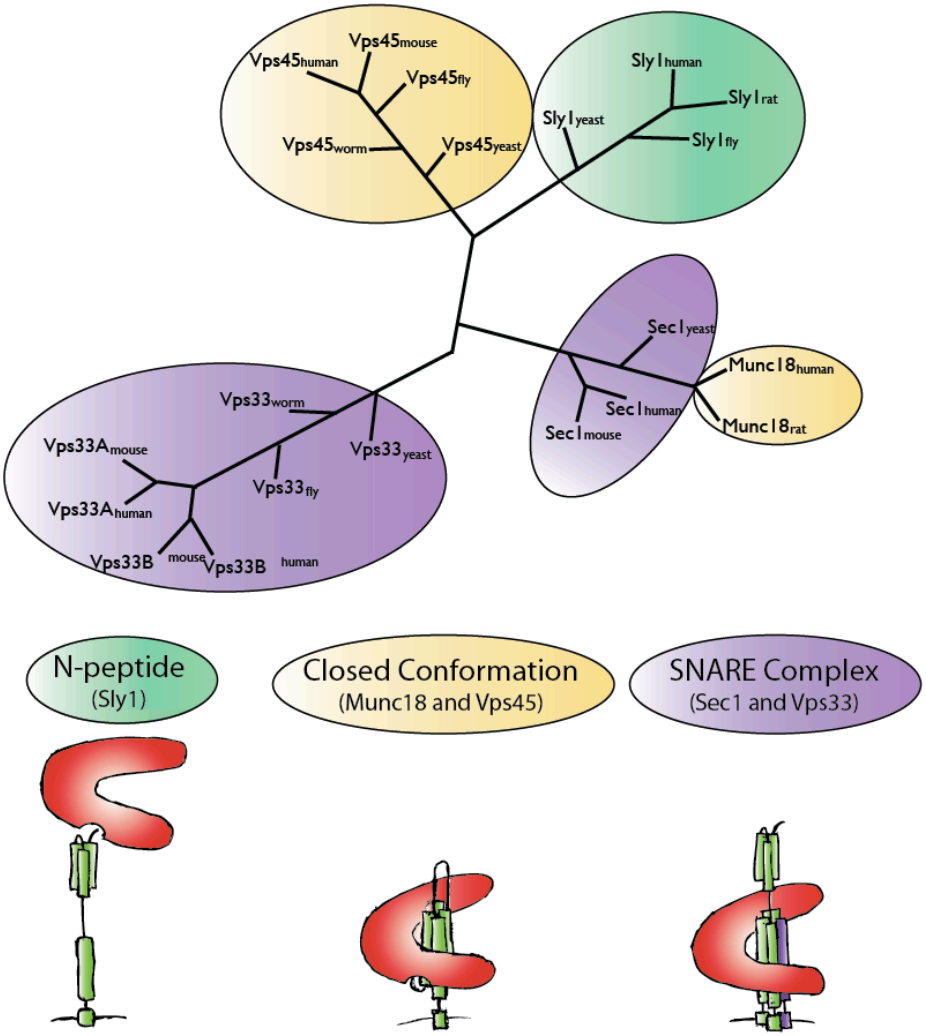

Figure 1.2. SM protein subfamilies and divergent primary SNARE binding modes
A phylogenetic tree shows the genetic relationship between the different SM protein subfamilies. The three different SM primary SNARE binding modes have been color-coded. It should be noted that many of the SM proteins have a secondary binding mode, and the diagram above is based on the strongest affinity binding mode. For example, Munc18 can weakly associate with the N-peptide alone, and also has a weak affinity for the SNARE complex bundle. Vps45 can also use the N-peptide binding mode, and associate with the SNARE complex bundle.

Chapter Two — Subunit organization and Rab interactions of Vps-C protein complexes that control endolysosomal membrane traffic[1]

2.1 –Introduction

Membrane traffic entails cycles of vesicle budding, transport, tethering, docking, and fusion with target membranes. These processes are regulated by the Rab-Arf family of small G proteins, which act as switches that confer specificity and directionality, and as timers that control rates of membrane ingress and egress at each compartment. In current models, a patch of membrane moving (or maturing) through a sequence of compartments is signified by the presence of a specific associated Rab. As the patch matures, a handoff occurs in which one Rab is replaced by the next, an arrangement called a Rab cascade or relay (Grosshans et al., 2006). Traffic through the endocytic-lysosomal pathway is controlled by members of the Rab5 and Rab7 families, which operate at earlier and later compartments, respectively. The Rab5-to-Rab7 handoff is controlled by signaling state of each Rab and by the Vps-C regulatory complexes CORVET and HOPS (Peplowska et al., 2007; Rink et al., 2005). The Rab5-to-Rab7 handoff is also controlled by a second evolutionarily unrelated complex, Mon1(SAND1)-Ccz1 (Kinchen and Ravichandran, 2010; Kucharczyk et al., 2001; Kucharczyk et al., 2009; Nordmann et al., 2010; Poteryaev et al., 2010), which has also been called "HOPSII" (Wang et al., 2003).

The Vps-C protein complexes were discovered in *Saccharomyces cerevisiae* (Nickerson et al., 2009; Rieder and Emr, 1997; Srivastava et al., 2000). They contain a four subunit core

[1] **Chapter 2** was adapted with permission from *Plemel RL, *Lobingier BT, Brett CL, Angers CG, Nickerson DP, Paulsel A, Sprague D, Merz AJ, 2011. MBOC Apr: 22(8): 1353-63. *equal contributors. http://www.molbiolcell.org/content/22/8/1353.long. B.T.L and A.J.M wrote the paper. B.T.L performed Figures 2.2; 2.3B, C, D, F; 2.5D.

(Pep5/Vps11, Vps16, Pep3/Vps18, and Vps33) and two additional, compartment-specific subunits. CORVET, which contains the Vps-C core plus Vps3 and Vps8 (Horazdovsky et al., 1996; Peplowska et al., 2007; Peterson and Emr, 2001; Raymond et al., 1990), operates at late endosomes, and interacts with the Rab5 ortholog Vps21 (Horazdovsky et al., 1996; Peplowska et al., 2007). HOPS, which contains the Vps-C core plus Vps39 (also called Vam6) and Vps41 (Seals et al., 2000), operates at the lysosomal vacuole and interacts with the Rab7 ortholog Ypt7 (Brett et al., 2008; Seals et al., 2000; Wurmser et al., 2000).

CORVET controls traffic into late endosomes, while HOPS controls all traffic – including late endosomes, autophagosomes, and Golgi-derived AP-3 vesicles – into the vacuole. Accordingly, loss of any Vps-C core subunit results in the absence or malformation of all late endosomal compartments and severe conditional growth defects. Conversely, loss of CORVET- or HOPS-specific subunits causes selective defects at late endosomes or vacuoles (Nickerson et al., 2009). HOPS promotes Ypt7-dependent membrane tethering (Stroupe et al., 2006) and SNARE-mediated membrane fusion (Mima et al., 2008; Sato et al., 2000). The HOPS subunit Vps39 was reported to be an activating GEF (guanosine nucleotide exchange factor) of Ypt7 (Binda et al., 2009; Wurmser et al., 2000), but highly purified preparations of Vps39 and HOPS do not exhibit intrinsic nucleotide exchange activity toward Ypt7 (Nordmann et al., 2010; Ostrowicz et al., 2010; and B.T.L., C.L.B., and A.J.M., unpublished data). Moreover, strong genetic (Kucharczyk et al., 2000; Kucharczyk et al., 2001; Wang et al., 2002) and biochemical (Nordmann et al., 2010) evidence indicates that another complex, Mon1-Ccz1, is a *bona fide* Ypt7 GEF. The Vps41 subunit of HOPS directly interacts with Ypt7, and it is essential for stable HOPS binding to Ypt7-GTP (Brett et al., 2008). Functions analogous to HOPS have been proposed for CORVET (Peplowska et al., 2007), though CORVET is not known to tether

membranes directly or to promote SNARE assembly. Hybrid complexes containing both CORVET- and HOPS-specific subunits (Peplowska et al., 2007) raise the possibility that Vps-C complexes are remodeled on-the-fly concomitantly with the endolysosomal Rab cascade. However, dynamic subunit exchange has neither been demonstrated nor linked to specific trafficking pathways.

Here, we present domain-level dissections of Vps-C subunit interactions with one another and with Rab small G-proteins. We employ yeast two-hybrid (Y2H) miniarrays to systematically search for Vps-C subunit–subunit and subunit–Rab contacts, and purify three dimeric subassemblies. Two subassemblies are composed of HOPS- or CORVET-specific subunits; we show that they function as integrated Rab-interaction modules. Through genetic analyses, we show that the core subunit Vps11 is a key scaffold for Vps-C complex assembly and demonstrate that its C-terminal domain (CTD) is of special importance, physically and functionally linking the HOPS and CORVET Rab-interaction modules to the Vps-C core.

2.2 –Materials and Methods

Strains and plasmids

For information on yeast strains and plasmids for Y2H screening, see (Plemel et al., 2012). Plasmids were constructed either by conventional cloning or by gap repair methods.

Y2H Assays

Two-hybrid vectors were constructed using gap-repair and homologous recombination (Uetz et al., 2000). Prey domains were cloned into the plasmid pOAD and transformed into the yeast strain PJ69-4a. Bait domains were cloned into pOBD-2 and transformed into PJ69-4**α**. Clonal

isolates were obtained and verified by PCR, and in many cases by DNA sequencing. Interaction tests were performed by mating haploid strains containing the bait and prey vectors. Liquid cultures of the bait and prey strains were grown in selective media, then mixed in 96-well plates and pinned to YPD plates supplemented with adenine using a 48-spoke inoculating manifold. The mating plates were grown at 30° C overnight, then diploid cells were selected by replica plating onto medium lacking tryptophan and leucine, and supplemented with adenine. Diploid colonies were grown at 30°C for two days, then tested for Y2H interactions by replica plating to medium lacking tryptophan, leucine, and histidine, supplemented with adenine and various concentrations of 3-amino-1,2,4-triazole (3-AT), ranging from 1.5 to 25 mM. The use of low-copy vectors (pOAD and pOBD-2), and the assay of histidine auxotrophy in the presence 3-AT at >1 mM, together almost totally suppresses false positive signals in Y2H experiments (Braun et al., 2009; Chen et al., 2010). After 5 days at 30° C, plates were scored for growth. Bait-prey interactions were scored: very strong (3), strong (2), weak (1), none (0). Mean scores are presented; in a large majority of cases these represent results from two or three independent interaction tests. In many cases, positive hits from the Y2H surveys were also subjected to further rounds of screening, which are not reflected in the survey scores; for more detail, see (Plemel et al., 2012).

Protein Purification

His_6- and GST-fused Vps-C subunits were expressed in BTI-Tn-5B1-4 (High-5) insect cells as described (Brett et al., 2008). Baculovirus vectors were constructed and propagated using the Bac-to-Bac system as recommended by the vendor (Invitrogen). Suspension-adapted or monolayer insect cells were infected with passage-3 or passage-4 virus, grown for 3 days at 27˚ C, and harvested. All subsequent steps were done at 4° C or on ice. Cells were resuspended in

lysis buffer (50 mM HEPES, 400 mM NaCl, 5 mM BME, 10% Glycerol, 0.5% Triton X-100, supplemented with pH 7.8, 400uM PMSF, 1 μg/ml leupeptin, 1 μg/ml pepstatin, 100 μM Pefabloc SC (Roche), and 20 mM imidazole). The cells were lysed with detergent and brief sonication, and the lysate was clarified by centrifugation (18,000 × g, 25 min.). Clarified lysates were incubated with glutathione sepharose 4B (GE Heathcare) for 2 h, and resin was subsequently washed three times with the lysis buffer, and eluted with lysis buffer supplemented with 10 mM reduced glutathione. GST eluates were then incubated with pre-equilibrated Ni^{2+}-NTA resin (GE Healthcare) for 1 hr, washed three times with lysis buffer supplemented with 35 mM imidazole, eluted with lysis buffer supplemented with 500 mM imidazole, and analyzed by SDS-PAGE.

Rab Pulldowns

GST-Rab fusion proteins were cloned, expressed, and purified as described (Brett et al., 2008). Nucleotide loading of Rab proteins was performed either (Procedure 1) as described (Brett et al., 2008) or (Procedure 2) by washing the resin once with nucleotide loading buffer (50 mM Tris, 200 mM NaCl, 7. 5 mM EDTA, 5 mM 2-mercaptoethanol, pH 8.0), then incubating the resin with the nucleotide loading buffer and 20-fold molar exess of nucleotide for 2 hrs at room temperature. The reaction was terminated with an excess of quenching buffer (50 mM Tris, 200 mM NaCl, 15 mM $MgCl_2$, 5 mM, pH 8.0). The resin was washed three times with reaction buffer (50 mM Tris, 200 mM NaCl, 5 mM $MgCl_2$, 5 mM 2-mercaptoethanol, pH 8.0). Cell lysates or purified Vps-C subunits were incubated with the resin in reaction buffer for 1hr at 4˚C, and the resin was then washed with reaction buffer three times. Bound protein was eluted from the beads in reaction buffer supplemented with 10 mM reduced glutathione, pH 8.0 (final), and the eluates were analyzed by SDS-PAGE.

Immunoprecipitation

Cell lysates were prepared, and immunoprecipitations were performed as described (Angers and Merz, 2009).

Protein sorting and vacuole morphology

Mutant yeast strains were propagated at room temperature to minimize selection for suppressor mutations. Liquid cultures were grown to log phase (OD_{600} = 0.6-1.0) in complex or synthetic media at 26°C. Cell pellets were chilled on ice and washed in 10 mM NaN_3. Washed pellets were resuspended in 40 µl SDS-PAGE sample buffer per 1 ml × OD_{600}. After addition of sterile glass beads, samples were boiled 15 min. and vortexed 3 min. Western blots were probed using monoclonal mouse antibodies against CPY, ALP and PGK (all from Invitrogen) and analyzed with a LICOR (Lincoln, NE) Odyssey fluorescence scanner. Colorimetric assays to detect secretion of CPY-invertase were performed as described previously (Darsow et al., 2000). Vacuole morphology was evaluated by pulse-chase labeling with the endocytic tracer FM4-64 (Invitrogen) as described (Brett et al., 2008). Subcellular fractionation by differential centrifugation was performed as described (Angers and Merz, 2009). Fluorescence microscopic analysis of GFP-CPS localization in FM4-64 labeled cells employed the plasmid pGO47 (Odorizzi et al., 1998).

2.3 –Results

Domain architecture of Vps-C subunits

We analyzed yeast and human Vps-C subunits using the *ROBETTA* suite of structure prediction algorithms (Chivian et al., 2005; Kim et al., 2004). Previously, ~200 residues of sequence

homology to clathrin proximal leg were detected in C-terminal regions of Vps8, 11, 18, 39, and 41 (Conibear and Stevens, 1998; Ybe et al., 1999). Vps39 was reported to contain a short motif similar to a COPI outer-shell coat subunit (Conibear and Stevens, 1998). Vps41 was shown to contain WD40 repeats that typically form β-propellers (Rehling et al., 1999). Our analyses (**Figure 2.1**; Nickerson et al., 2009) revealed pervasive similarity to vesicle coat and nuclear pore proteins: seven of eight subunits contain a predicted N-terminal β-propeller followed by a C-terminal α-solenoid. In addition, Vps8, Vps11, and Vps18 have C-terminal RING motifs, and Vps39 has a partial RING motif, although this region lacks residues that would coordinate a second Zn^{2+} ion. Similar predictions were obtained for human and yeast orthologs. These findings provided the basis for our domain-level dissection of Vps-C subunits.

Domain-level interaction topology of Vps-C complexes

HOPS and CORVET are sufficiently stable to withstand affinity isolation, chromatographic purification, and sedimentation (Angers and Merz, 2009; Peplowska et al., 2007; Rieder and Emr, 1997; Seals et al., 2000; Stroupe et al., 2006), but only a few direct intersubunit contacts have been identified, using disparate approaches and organisms. To obtain a broader inventory of intersubunit contacts we performed exhaustive yeast two hybrid (Y2H) analyses.

Y2H can be very sensitive, potentially reporting bridging interactions mediated by proteins not encoded by the query constructs, so we employed a de-tuned Y2H system originally designed to minimize false-positive signals in high-throughput screens (Uetz et al., 2000). This system employs single-copy bait and prey vectors, rather than the more commonly-employed multi-copy vectors. Recent quantitative assessments demonstrate that of single-copy Y2H vectors, used in combination with the *HIS3* reporter gene and 3-aminotriazole (3-AT) in colony growth assays, nearly eliminates false-positive signals in Y2H interaction experiments (Chen et

al., 2010; Venkatesan et al., 2009). Identical highly stringent assay conditions were used throughout the present study.

The Y2H-derived Vps-C interaction topology is summarized in **Figure 2.1.** Our survey replicated (and in most cases mapped to higher resolution) almost all published interactions within Vps-C complexes across all organisms studied to date (Nakamura et al., 1997; Nakamura et al., 1997; Peplowska et al., 2007; Peterson and Emr, 2001; Pulipparacharuvil et al., 2005; Sevrioukov et al., 1999; Srivastava et al., 2000; Wurmser et al., 2000). This suggests that not only the subunit folds, but the interaction topologies and functional dynamics of Vps-C complexes are broadly conserved. Our survey also revealed candidate interactions that to our knowledge have not previously been reported. The minimal regions sufficient for each interaction are largely non-overlapping, strongly suggesting that most interactions detected in this survey are direct rather than bridged through other subunits.

Vps11, particularly in its C-terminal region, is a densely-connected hub (**Figure 2.1E**), interacting with Vps18, Vps8, Vps3, and Vps39. Vps39 and Vps3 share substantial sequence homology, with the region of highest similarity within a stretch of ~100 residues at near their C-termini. The Vps3 and Vps39 CTDs interacted strongly with residues 736-926 in the Vps11 CTD, suggesting that they may bind to a single site within Vps11 (**Figure 2.1C and D**). The HOPS subunit Vps39 also interacts with the HOPS subunit Vps41. The Vps39-Vps41 interaction was relatively weak, but was detected in both bait-prey and prey-bait configurations; this was the strongest interaction detected between Vps41 and any other HOPS subunit.

Isolation of three Vps-C sub-complexes

To examine the ability of subunits to heterodimerize in in the absence of the HOPS and CORVET holocomplexes, pairs of subunits were co-expressed in insect cells. In each case, one

subunit was expressed as a GST fusion, the other as a His_6 fusion, and complexes were purified using the two affinity tags in sequence. From several tested pairs, three sub-complexes were identified (**Figure 2.2**). Vps16 is required for Vps33 association with Vps11 and 18 (Rieder and Emr, 1997), and a region corresponding to yeast Vps16 residues 451-595 mediates binding between *Drosophila* Vps16A and B and Vps33A and B (Pulipparacharuvil et al., 2005). Our Y2H survey mapped an overlapping site within Vps16 (residues 479-798; **Figure 2.1**) and indeed Vps16 and Vps33 form a subcomplex when co-expressed (**Figure 2.2A**). The CORVET subunits Vps3 and Vps8 also form a sub-complex (**Figure 2.2B**). This binding interaction has not to our knowledge been reported previously, and was not detected in our Y2H survey. Like Vps3 and Vps8, the HOPS subunits Vps39 and Vps41 formed a binary complex (**Figure 2.2 C and D**); the interacting domains were mapped by Y2H to the N-termini of both proteins (**Figure 2.2C**). The Vps39 CTD was sufficient to interact with Vps11 and was necessary for stable Vps39 association with HOPS (**Figure 2.1**; Wurmser et al., 2000). However, the Vps39 CTD was not needed for Vps39 binding to Vps41 (**Figure 2.2D**). Both subcomplexes exhibited signs of lability, suggesting that their interactions are stabilized when they reside within the HOPS and CORVET holocomplexes.

Y2H identification of Vps-C Rab interaction sites

CORVET interacts with the Rab5 ortholog Vps21, and HOPS interacts with the Rab7 ortholog Ypt7. Vps39 binds GDP- or GTP-Ypt7, and was previously reported to harbor Ypt7 GEF activity (Binda et al., 2009; Wurmser et al., 2000). Vps41 binds directly to Ypt7 and is essential for stable binding of HOPS to Ypt7-GTP (Brett et al., 2008). Until recently, no Rab binding sites were definitively identified within CORVET, though there was genetic evidence that Vps3 and Vps8 contribute to the CORVET Vps21 binding activity (Horazdovsky et al., 1996; Markgraf et

al., 2009; Pawelec et al., 2010; Peplowska et al., 2007). To identify Rab-binding sites, Y2H miniarrays comprising the eleven yeast Rabs were prepared. In addition to wild type Rabs, Rab point mutants were included in the arrays, including mutants favoring specific nucleotide states or lacking C-terminal sites of covalent prenylation (LF, lipid-free). Rab miniarrays were used to probe Vps-C miniarrays in both bait and prey configurations (for more information see (Plemel et al., 2012)). At least six candidate interactions were identified by Y2H. Vps21 interacted with CORVET subunits Vps3 and Vps8, and with the NTD of Vps-C core subunit Vps11 (for more information see (Plemel et al., 2012)). Ypt7 interacted with HOPS subunits Vps39 and Vps41 (**Figure 2.3A**; Brett et al., 2008; Wurmser et al., 2000), and weakly with the core subunit Vps33.

The HOPS Ypt7 interaction module

In pulldowns, native HOPS interacts preferentially with Ypt7-GTPγS versus Ypt7-GDP (Brett et al., 2008; Peplowska et al., 2007; Price et al., 2000; Seals et al., 2000). However, under conditions that yielded highly selective binding of native HOPS to Ypt7-GTP, there was no GTP *vs* GDP selectivity when purified Vps41 was tested. Further studies indicated that nucleotide stripping under our previous conditions was inefficient. With a more stringent strip-exchange procedure, purified Vps41 selectively bound Ypt7-GTPγS (**Figure 2.3B and F**), establishing Vps41 as a direct effector of Ypt7-GTP and explaining why it is required (Brett et al., 2008) for the stable association of HOPS with Ypt7-GTP.

In previous studies, Vps39 was reported to either bind Ypt7-GDP (Wurmser et al., 2000), or to show no nucleotide selectivity (Brett et al., 2008). Under our improved nucleotide-loading conditions, purified Vps39-860Δ bound Ypt7 without any detectable GNP selectivity (**Figure 2.3C and D**). Taken together, our Y2H and biochemical data show that the N-terminal predicted β-propellers of Vps39 and Vps41 interact with one another and with the vacuolar Rab Ypt7, with

Vps41 showing strong selectivity for Ypt7-GTP and Vps39 showing little or no nucleotide selectivity. Because Vps39 was the only HOPS subunit that interacted with Vps41 in our Y2H experiments, we asked whether Vps41 could remain associated with the remaining HOPS subunits in the absence of Vps39. Co-immunoprecipitation experiments using anti-Vps11 antibodies (**Figure 2.3E**) demonstrated that the five remaining HOPS subunits remain stably associated in the absence of Vps39. This result indicates that in addition to Vps39, Vps41 has additional binding interactions with the core that were not detected in our Y2H survey. In contrast to Vps39, the core subunit Vps18 has a crucial role in assembly of HOPS and the Vps-C core, as deletion of Vps18 prevented co-immunoprecipitation of Vps11 and Vps16, Vps18, Vps33, or Vps41 (**Figure 2.3E**).

As the region of Vps39 required for its interaction with Vps11 maps to the Vps39 C-terminus (residues 860-979; Wurmser et al., 2000), we analyzed the *in vivo* phenotypes of two C-terminal Vps39 deletion mutants. *In vivo* homotypic fusion was evaluated by examining vacuole morphology with the endocytic tracer dye FM4-64 (**Figure 2.4A**). Traffic to the vacuole was evaluated by subcellular fractionation followed by immunoblotting for two cargo proteins, CPY and ALP (**Figure 2.4B**). In this procedure, Golgi membranes and small vesicles fractionate to the 100,000 × g pellet (P100). Endosomes are found in the 13,000 × g pellet (P13) and P100 fractions. Vacuoles are found in the P13 fraction almost exclusively. Immunoblotting of fractions with fiduciary markers for vacuolar, endosomal, and soluble markers was performed for each experiment, and confirmed proper fractionation for each mutant (not shown). CPY is transported from the late Golgi to endosomes, and then to the vacuole. ALP is delivered from the Golgi to the vacuole through the AP-3 pathway, which bypasses endosomes. Both ALP and CPY are synthesized as inactive proenzymes (p) that are proteolytically processed into active mature (m)

enzymes upon arrival at the vacuole. Transport defects result in the accumulation of slow-migrating ALP or CPY proenzymes in the P100 and P13 fractions (**Figure 2.4B**).

The *vps39-860*Δ mutation completely phenocopies the defects in CPY and ALP localization and maturation, and vacuole morphology, conferred by *vps39*Δ or *vps41*Δ mutations (**Figure 2.4**; Brett et al., 2008). In contrast, *vps39-979*Δ mutant cells produce Vps39 with an intact Vps11-binding site and exhibit only mild trafficking defects (**Figure 2.4**). Expression of Vps39-860 from an ectopic promoter results in higher levels of Vps39-860Δ than Vps39 wt (not shown), indicating that the loss of function in the *vps39-860*Δ mutant is not due to poor expression or accelerated turnover of Vps39-860Δ protein. Since Vps39 residues 860-979 are necessary and sufficient for Vps39 binding to Vps11 and Vps39 association with HOPS, but not required for Vps39 interactions with Ypt7 or Vps41, our results suggest that Vps39 function depends on its interactions with HOPS through both Vps11 and Vps41. We conclude that the Vps39-Vps41 subcomplex is a physically and functionally integrated effector module containing two Ypt7-binding sites with distinct nucleotide specificity. These sites reside within N-terminal predicted β-propellers that physically interact with one another.

The CORVET Vps21 interaction module

In Y2H assays the two CORVET subunits, Vps3 and Vps8, interacted with wild type Vps21 and Vps21-Q66L (GTP hydrolysis-deficient), but not with Vps21-S21L (a GDP-biased mutant) or any other *Saccharomyces* Rab (**Figure 2.5A and B**). Additional controls validated the Y2H Rab constructs: the Vps21 effector Vac1 (Peterson et al., 1999) had Rab interaction patterns identical to Vps3 and Vps8, while the Vps21 GEF Vps9 interacted strongly with Vps21-S21L but not with wild type Vps21 or Vps21-Q66L (Hama et al., 1999; R.P. and A.J.M, submitted). Vps3, like Vps41 and Vps39, interacted with its cognate Rab thorough a predicted N-terminal β-propeller.

In contrast, Vps8 interacted with Vps21 through the Vps8 C-terminal predicted α-solenoid (**Figure 2.5A**; see also Pawelec et al., 2010). The Vps3-Vps21 interaction was validated biochemically. Vps3 in cell lysates, presumably as a subunit of CORVET, bound to Vps21-GTPγS with high specificity (**Figure 2.5C**; Peplowska et al., 2007). Moreover, purified Vps3 bound to Vps21 with strong selectivity for Vps21-GTPγS vs. -GDP (**Figure 2.5D**). These experiments suggest that both Vps3 and Vps8 contain Vps21 binding sites and establish that Vps3 is a direct, GTP-selective effector of Vps21.

The Vps3 CTD is highly homologous to the Vps39 CTD. As with Vps39, the Vps3 CTD is required for its interaction with the Vps11 CTD, and as with the Vps39 CTD it is functionally indispensable: deletion of the Vps3 CTD (*vps3-901*Δ) phenocopied the vacuole morphology and trafficking defects of a *vps3*Δ null mutant (**Figure 2.5E**). Thus, homologous CTDs within Vps3 and Vps39 are essential for the functions of both proteins and bind a ~100 residue region within the Vps11 CTD.

Genetic suppression experiments show that the Vps8-Vps21 interaction detected by Y2H (**Figure 2.5A and B**) is functionally important, and suggest that the Vps8-Vps21 interaction is, like the Vps3-Vps21 interaction, direct. Truncation of Vps11 to residue 445 causes conditional growth defects, complete defects in biosynthetic traffic to late endosomes and vacuoles (**Figure 2.6A**; Woolford et al., 1998), and class C vacuole morphology (**Figure 2.6B**). The *VPS8-200* allele suppresses several of these *vps11-445*Δ phenotypes: it rescues growth defects, restores endosomal (but not vacuolar) trafficking, and results in a class B vacuole morphology similar to *vps39*Δ, *vps41*Δ, or *ypt7*Δ mutant cells (**Figure 2.6A and B**; Woolford et al., 1998). In Y2H screens we found that Vps21 interacted more strongly with Vps8-200 than with wild type Vps8 (**Figure 2.6C**). This difference in interaction strength was not attributable to differences in

expression of the Vps8 and Vps8-200 prey constructs (**Figure 2.6D**). Moreover, neither GTP preference nor selectivity for Vps21 vs. other Rabs was modified by the Vps8-200 mutation, and the difference between Vps8 and Vps8-200 was seen with either full-length constructs or with truncated constructs containing the Vps21-binding region (**Figure 2.6C**). We sequenced *VPS8-200* and identified a single missense substitution at an evolutionarily conserved residue (L830 to R), which is near the middle of the Vps21 interaction region (**Figure 2.5A**). Taken together, our results indicate that Vps21 interacts with both Vps3 and Vps8, and suggest a biochemical basis — enhanced Vps21 binding to Vps8 — for the genetic suppression of *vps11-445*Δ trafficking phenotypes by *VPS8-200*.

The Vps11 CTD organizes Vps-C assembly and signaling

Among the Vps-C subunits Vps11 had the densest web of interactions with other subunits, particularly within its CTD (**Figure 2.7A**). Notably, both the CORVET-specific subunit Vps3 and its HOPS-specific paralog Vps39 interact *via* their conserved CTDs with the Vps11 CTD; these regions in Vps3 and Vps39 are functionally indispensable (**Figures 2.4 and 2.5E**). To dissect the functional architecture of the Vps11 CTD, we prepared a set of Vps11 truncation alleles (**Figure 2.7A**) and evaluated their *in vivo* phenotypes.

Each *vps11* allele was prepared as a chromosomal replacement driven by the *VPS11* promoter. *vps11*Δ null mutants exhibited defects in endosomal delivery indicated by pro-CPY accumulation and CPY secretion into the extracellular medium (**Figure 2.7B**), defects in vacuolar delivery, indicated by accumulation of pro-ALP and pro-CPY, and defects in late endosome and vacuole fusion, indicated by class C vacuole morphology (**Figure 2.7C**). Four C-terminal Vps11 truncations (350Δ, 445Δ, 505Δ, and 735Δ) completely phenocopied the *vps11*Δ null allele (**Figure 2.7B and C**). The total loss of function in the *VPS11-735*Δ mutant is

particularly important, as this mutant lacks binding sites for Vps3 and Vps39 (**Figure 2.7A**).

In contrast to the more severe truncation mutants, a mutant lacking the Vps11 RING motif (*vps11-926*Δ) exhibited more selective defects: slightly impaired CPY processing and limited CPY secretion from the cell, but a severe defect in ALP processing (**Figure 2.7B**). These phenotypes are diagnostic of defective docking or fusion at the vacuole, but not at the endosome. Consistent with this interpretation, *vps11-926*Δ cells had Class B fragmented vacuoles similar to *vps39*Δ or *vps41*Δ cells (**Figure 2.7C**). Because the Vps11 RING motif interacted weakly with other Vps-C subunits including Vps16, co-immunoprecipitation experiments were performed to ascertain whether HOPS is intact in *vps11-926*Δ mutant cells (**Figure 2.5D**). The results show that Vps11, Vps16, Vps18, and Vps41 all co-precipitate at least as efficiently with Vps11-926Δ as with wild type Vps11. Together, these results indicate that the Vps11 RING is not needed for HOPS complex assembly, but instead functions predominantly to regulate fusion at the vacuole, presumably through binding interactions with other HOPS subunits or interactions with other fusion factors.

In addition to Vps11, three other Vps-C subunits contain RING/Zn^{2+} finger motifs at their extreme C-termini (**Figure 2.1**). We compared the functions of these motifs by deleting each one; all are functionally important. The severity of the trafficking defects observed in each ΔRING/Zn^{2+} finger mutant, from most severe to least, was: *vps18-826*Δ > *vps11-926*Δ >> *vps39-979*Δ > *vps8-1188*Δ (**Figures 2.4B and 2.7B**). The Vps8 and Vps18 RING domains appear to heterodimerize (**Figure 2.1**). However, the more severe vacuolar and endosomal defects observed upon deletion of the Vps18 RING *vs.* the Vps8 RING indicate that Vps8 cannot be the sole functional target of the Vps18 RING. Vps39 might be capable of a self-interaction mediated through its RING-like domain (**Figure 2.1C**). Weak Y2H interactions were sometimes detected

between the Vps11 RING and other subunits including Vps16. Taken together, these data show that the four Vps-C RING/Zn^{2+} finger motifs have distinct functions in endolysosomal trafficking.

The Vps11 CTD (residues 736-926) interacts with ~100 residue CTDs of high similarity in Vps3 and Vps39, so we asked whether the *vps11-735*Δ truncation might be complemented *in trans* by the missing Vps11-(736-1029) fragment. Remarkably, co-expression of this fragment rescued the vacuole morphology (**Figure 2.8A**) of both *vps11-736*Δ and *vps11-936*Δ cells, but it failed to rescue in *vps11-350*Δ, -*445*Δ, or -*505*Δ cells. Identical rescue results were obtained with expression of GFP-tagged or untagged Vps11-(736-1029). The CPY and ALP maturation defects of *vps11-735*Δ cells were also rescued by Vps11-(736-1029) (**Figure 2.8B**). We also evaluated the formation of multivesicular endosomes (MVEs) in *vps11-735*Δ cells expressing Vps11-(736-1029). GFP-CPS is sorted through the multivesicular endosome (MVE) pathway into the vacuole lumen. Defects in formation of MVEs result in missorting of GFP-CPS to the vacuole limiting membrane. The two-fragment complemented strain correctly sorted GFP-CPS to the vacuole lumen, indicating that MVE function is intact in these cells. Together, the results indicate that endolysosomal traffic is essentially normal in cells expressing both Vps11-(735Δ) and Vps11-(736-1029).

In every *vps11* mutant strain tested, the GFP-Vps11-(736-1029) fragment exhibited a discrete subcellular localization (**Figure 2.8A**). In *vps11-735*Δ or *vps11-926*Δ cells, it localized predominantly to the vacuole limiting membrane and to perivacuolar foci, which are probably late endosomes. In *vps11-350*Δ, -*445*Δ, and -*505*Δ cells, GFP-Vps11-(736-1029) usually localized to a single bright punctate spot. In wild type cells, however, GFP-Vps11-(736-1029) was exclusively cytoplasmic, indicating that the C-terminus of native Vps11 saturates the site(s)

required for localization of Vps11-(736-1029). This was confirmed in co-immunoprecipitation experiments (**Figure 2.8C**). GFP-Vps11-(736-1029) co-precipitated Vps16, 18, 33, and 41 in the truncation mutants (**Figure 2.8C, lanes 2-6**). In cells containing full-length Vps11, co-isolation of other subunits with GFP-Vps11-(736-1029) was almost eliminated (**Figure 2.8C, lane 1**), consistent with its diffuse localization in *VPS11* cells (**Figure 2.8A**). Together, these data show that Vps11 can be split in two and retain nearly its full function. However, in the absence of a central domain (*e.g.,* when 1-505 and 736-1029 are co-expressed), the phenotype is equivalent to a *vps11*Δ null, even though a HOPS complex of apparently normal composition is assembled (**Figure 2.8C, lanes 4 and 5**). Thus, the central domain of Vps11 (residues 351-735 is also crucial for its function. The split N- and C- terminal fragments of Vps11 probably assemble on Vps18 (**Figure 2.7A**). This conclusion is supported by our finding that the integrity of the entire wild type complex is lost when Vps18 is deleted (**Figure 2.3E, lanes 4**). Taken together, these experiments underscore the complex and critical functions of the Vps11 CTD in both HOPS and CORVET function.

2.4 –Discussion

Our main conclusions are that the CORVET subunits Vps3 and Vps8, and the HOPS subunits Vps39 and Vps41 form discrete complex-specific subassemblies that function in Rab recognition. The activities of these subassemblies are coordinated with the core through contacts between the CTDs of Vps3 or Vps39, and the CTD of Vps11. The core subunits Vps16 and Vps33 also form a stable subassembly. Vps33 belongs to the SM family of cofactors (Sudhof and Rothman, 2009), which are universally required for SNARE-mediated membrane fusion, so Vps16 and Vps33 likely link the Rab signaling activities of HOPS and CORVET to SNARE-

mediated fusion.

In early studies, HOPS was identified as an effector of Ypt7-GTP (Price et al., 2000; Seals et al., 2000) and the Vps39 subunit was reported to be a Ypt7 GEF (Binda et al., 2009; Wurmser et al., 2000). Vps41 binds Ypt7-GTP directly (**Figure 2.3B**), explaining why Vps41 is essential for stable binding of the HOPS holocomplex to Ypt7-GTP (Brett et al., 2008). However, while Vps39 shows a lack of nucleotide specificity in Ypt7 binding, as might be expected for a GEF, highly purified preparations of Vps39 or Vps39-860Δ failed to exhibit any nucleotide exchange activity in fluorescence and radioisotopic assays that readily detected the activities of *bona fide* GEFs (Nordmann et al., 2010; Ostrowicz et al., 2010; B.T.L., C.L.B., and A.J.M., unpublished results). Instead, the major Ypt7 GEF activity appears to reside within the Ccz1/Mon1 complex (Kucharczyk et al., 2000; Kucharczyk et al., 2001; Nordmann et al., 2010). The Vps39 CTD is dispensable for Vps39 binding to Ypt7 and Vps41 (**Figure 2.1 and 2.2D**), and for binding of HOPS to Ypt7-GTPγS (C.L.B. and A.J.M., unpublished results). The Vps39 CTD is, however, essential for Vps39 function *in vivo*, as its deletion phenocopies a *vps39*Δ null mutant (**Figure 2.4**; Wurmser et al., 2000).

Like Vps39 and Vps41, the CORVET subunits Vps3 and Vps8 function as a Rab-recognition module that signals through Vps11. As with Vps39, the Vps3 CTD binds the Vps11 CTD, and this domain is needed for Vps3 function. In Y2H analyses we identified Vps21-interacting domains in both Vps3 and Vps8. While this manuscript was in preparation, Y2H hits between Vps8 and Vps21 were reported by two other groups (Markgraf et al., 2009; Pawelec et al., 2010). Moreover, we obtained genetic data, using the *VPS8-200* suppressor of *vps11-445*Δ, that Vps8 and Vps21 functionally interact. In our Y2H analyses, both Vps8 and Vps8-200 exhibited a preference for Vps21-GTP. In our experiments, Vps3 always exhibited preferential binding to

activated Vps21. Native Vps3, as a CORVET substituent, is selectively retained on Vps21-GTP (**Figure 2.4C**). Using purified proteins we demonstrated that Vps3 binds Vps21-GTPγS directly (**Figure 2.4D**). In contrast, recent work suggested that Vps3 contributes to GDP-selective Vps21 binding by the CORVET holocomplex, and it was proposed in this work that Vps3 might function as a Vps21 GEF (Peplowska et al., 2007). However, as with Vps39, we have been unable to detect any nucleotide exchange activity mediated by purified Vps3 using assays that readily detect exchange mediated by a *bona fide* Vps21 GEF, Vps9 (B.T.L., C.L.B., and A.J.M., unpublished results). While this manuscript was under revision, similar results for Vps3 were reported by Ostrowicz et al. (2010).

The distinct nucleotide specificities of the Rab recognition modules within CORVET and HOPS are particularly striking. The CORVET subunits Vps3 and 8 appear to simply search for the presence or absence of Vps21-GTP. In contrast, the HOPS Rab recognition module contains one subunit, Vps41, that detects Ypt7-GTP and a second subunit, Vps39, that is insensitive to the nucleotide binding state of Ypt7. HOPS might therefore monitor not only the presence of Ypt7-GTP, but the *ratio* of Ypt7-GTP to Ypt7 GDP. The functional consequences of the divergent Rab-binding modalities of HOPS and CORVET are not yet understood.

As membrane traffic traverses successive endolysosomal organelles, the Rab5 ortholog Vps21 is replaced by the Rab7 ortholog Ypt7 (**Figure 2.9**). CORVET and HOPS, operating in concert with the GEFs Vps9 and Ccz1-Mon1, appear to control this Rab cascade (Peplowska et al., 2007; Rink et al., 2005; Vonderheit and Helenius, 2005). Vps11 appears to be a central scaffold upon which both HOPS and CORVET assemble. Deletion analyses of Vps11 (**Figure 2.5**) confirm the functional importance of the Vps11 CTD. The almost complete functional complementation *in trans* of two Vps11 truncation mutants (-735Δ and -926Δ) by a C-terminal

(736-1029) fragment of Vps11 – which contains a binding site or sites for the C-termini of Vps3 and Vps39 – underscores the modularity of this region. Vps11 may be a simple structural scaffold or it could have a more dynamic role in linking Rab signaling to Vps-C outputs, including the SNARE machinery that mediates fusion at the endosome and vacuole. In either case, the Vps11 CTD is now the prime candidate for the location at which switching between the HOPS and CORVET Vps-C configurations might occur. Consistent with the idea that the Vps11 CTD is a key element in this cascade, the C-terminal RING domain of Vps11 appears to function predominantly in fusion at the vacuole (**Figure 2.7**). Moreover, we recently isolated new *vps11* alleles bearing mutations solely in the Vps11 CTD and exhibiting selective defects in traffic through late endosomes, to the vacuole, or both (D.P.N., E. Fawcett, and A.J.M., unpublished results). We are now working to understand how Rab signaling through Vps-C complexes drives fusion and other "output" processes (Nickerson et al., 2009), and how Vps-C complexes signal in time and space to transport cargoes derived from early endosomes, the late Golgi, autophagosomes, and CVT vesicles through the endolysosomal system.

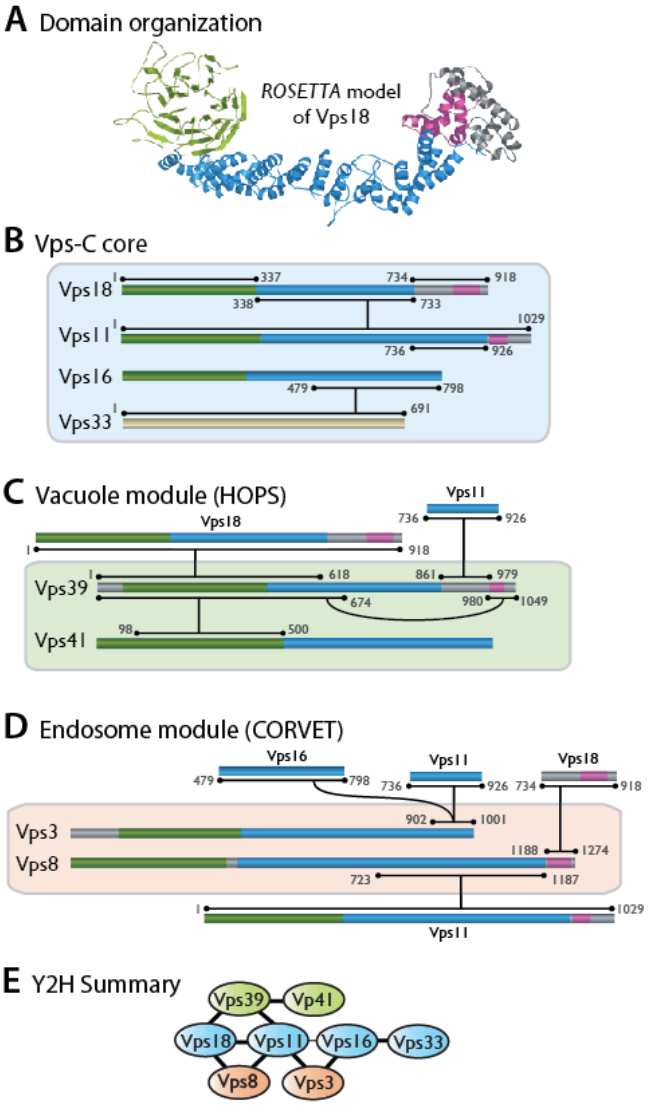

Figure 2.1. Vps-C domain structure and intersubunit interactions detected in Y2H
Structure predictions are color-coded consistent with the predicted structure of Vps18 (A). Predicted β-propellers are shaded green. Predicted α-solenoids are shaded blue. RING or RING-like motifs are shaded pink. (B-D) Summary of Y2H interactions. Horizontal bars at each end of an interaction line delineate the minimal region of each protein sufficient to support a Y2H interaction, with numbers denoting the termini of these regions. In many cases larger segments also supported each interaction (for more information see (Plemel et al., 2012)). (E) Summary of the overall interaction topology. The thinner line between Vps11 and Vps16 denotes a weak interaction not observed in all experiments.

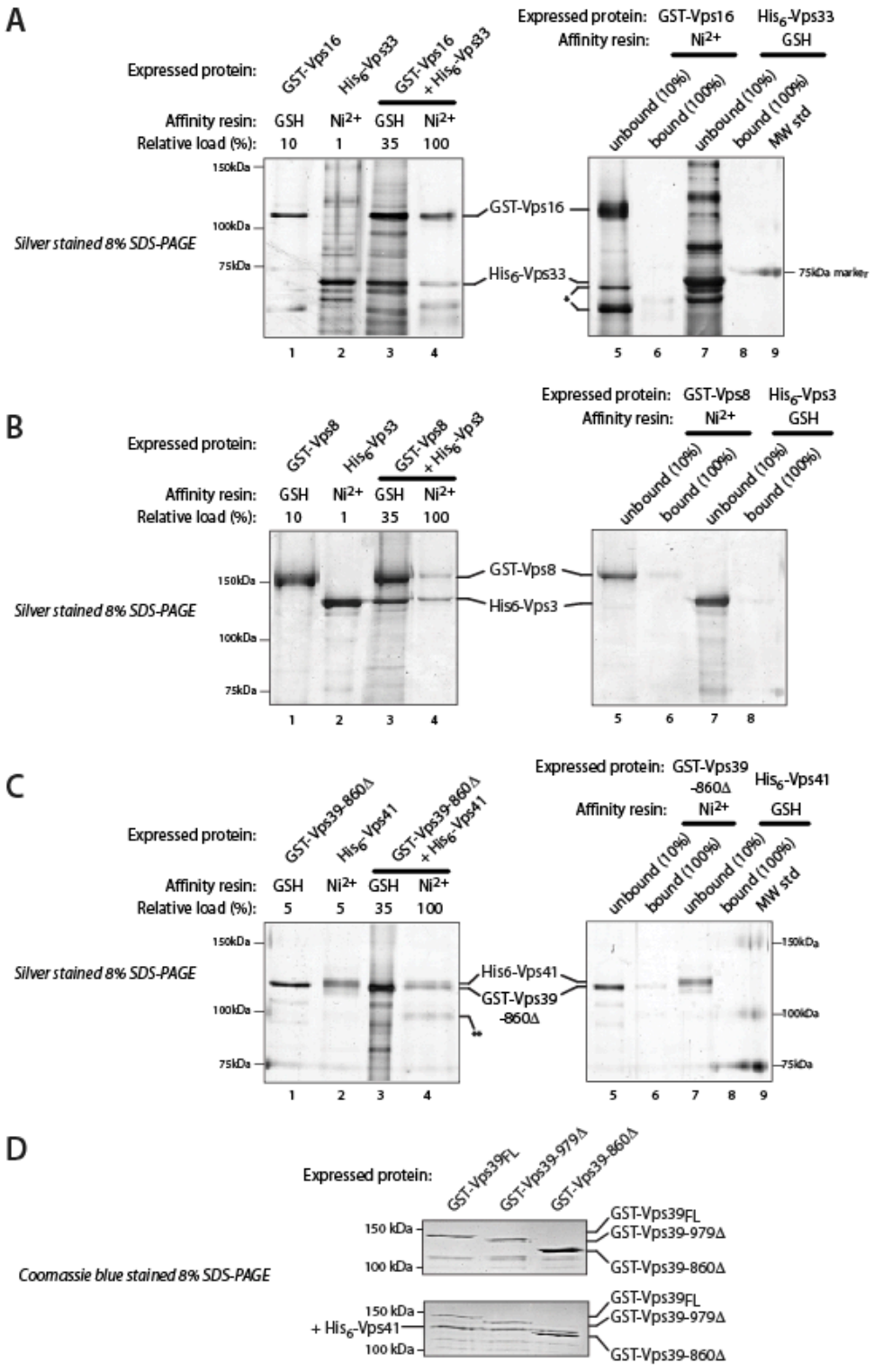

Figure 2.2. Purification of Vps-C sub-complexes
(A-C) The indicated subunits were expressed individually or in pairs in insect cells and isolated by affinity chromatography. In each panel, the gel on the left shows isolation of a sub-complex,

while the gel on the right shows pulldown specificity controls. Lanes 1 and 2: GST-tagged or His6-tagged subunits were expressed individually and purified on either Ni2+-NTA resin (Ni2+) or glutathione-agarose (GSH) resin. Lanes 3 and 4: pairs of GST- and His6-tagged subunits were co-expressed, captured on GSH resin and eluted with reduced glutathione (lanes 3), and then re-captured on Ni2+ resin (lanes 4). Lanes 5-8: pulldown specificity controls showing that Ni2+-NTA beads retain little or no GST fusion protein, and that glutathione-sepharose beads (GSH) retain little or no His6 fusion protein when these proteins are expressed individually (i.e., in the absence of an interacting partner whose tag can bind the affinity resin). Lanes 6 and 8: material retained on the noncognate affinity beads. Lanes 5 and 7: unbound (flow through) material. The SDS-PAGE gels were silver-stained. (D) Co-purification of His6-tagged Vps41 associated with GST-Vps39 or GST-Vps39 truncation mutants.

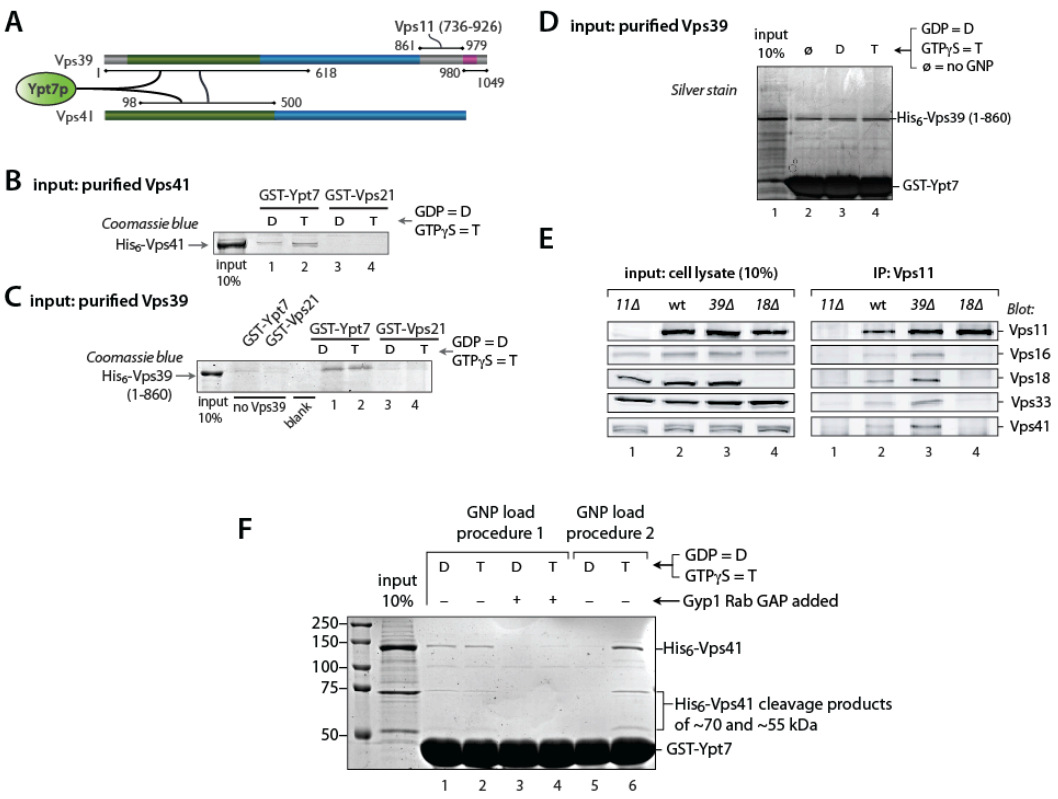

Figure 2.3. HOPS subunits Vps39 and Vps41 form an integrated Ypt7 binding module
(A) Summary of key Vps39 and Vps41 interactions. (B) Direct binding of Vps41 to Ypt7. Pulldowns were performed using purified recombinant His6-Vps41 and beads decorated with either GST-Ypt7 or GST-Vps21. The Rabs were nucleotide-loaded by procedure 2 (see Methods). (C) Direct binding of Vps39 to Ypt7. Pulldowns were performed using purified recombinant His6-Vps39-860Δ and beads decorated with either GST-Ypt7 or GST-Vps21. The Rabs were nucleotide-loaded by Procedure 2 (see Materials and Methods). (D) Vps39 binds Ypt7 without nucleotide selectivity. GST-Ypt7 was nucleotide-stripped by Procedure 2 (Methods), then loaded with GDP, GTPγS, or no nucleotide. Beads decorated with the resulting GST-Ypt7 were then used to pull down His6-Vps39 (1-860). No differences in binding efficiency were observed. (F) Addition of the Rab GAP Gyp1 to the binding reactions (lanes 3 and 4) abrogates Vps41 binding, indicating that the binding under Procedure 1 is mainly on GTP-Ypt7, not GNP-exchanged GTPγS-Ypt7. Procedure 2, used in the present study, yields unambiguous selectivity for GTPγS-loaded Ypt7.

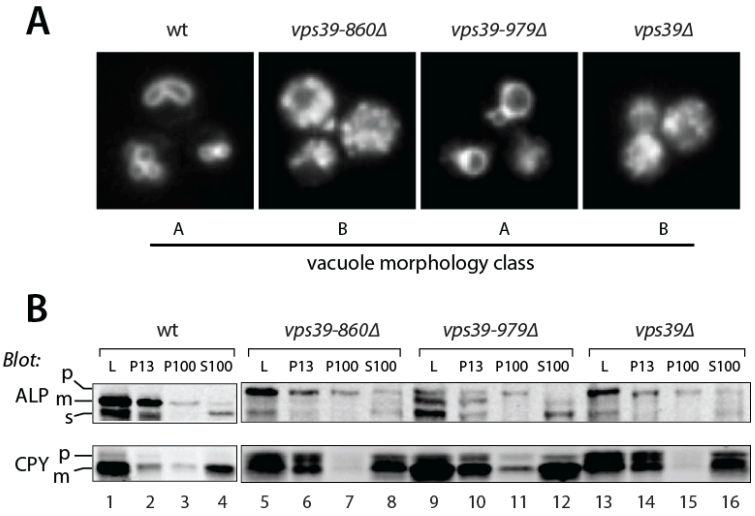

Figure 2.4. In vivo phenotypes of Vps39 C-terminal truncation mutants
(A) Vacuole morphology phenotypes of vps39 mutant cells. Vacuoles were labeled by pulse-chase with the tracer dye FM4-64 and examined by fluorescence microscopy. (B) Differential centrifugation analyses of ALP and CPY maturation and subcellular localization in vps39 mutant cells. L, cell lysate; P13 and P100, 13,000 × g and 100,000 × g pellets; S100, 100,000 × g supernatant. Vacuoles are found almost entirely in the P13 fraction. Small vesicles and Golgi membranes are found in the P100. Soluble proteins and complexes (including CPY and the soluble ALP cleavage product, sALP, released from the lumens of vacuoles that have ruptured during fractionation) are found in the S100. For each strain, 50 OD600xml were lysed and subjected to differential centrifugation (see Materials and Methods), and the fractions were analyzed by immunoblotting with monoclonal antibodies against ALP (Pho8) or CPY (Prc1). The cell lysate load fraction (L) corresponds to 20% of the other fractions. p=proenzyme, m=mature enzyme, s=soluble.

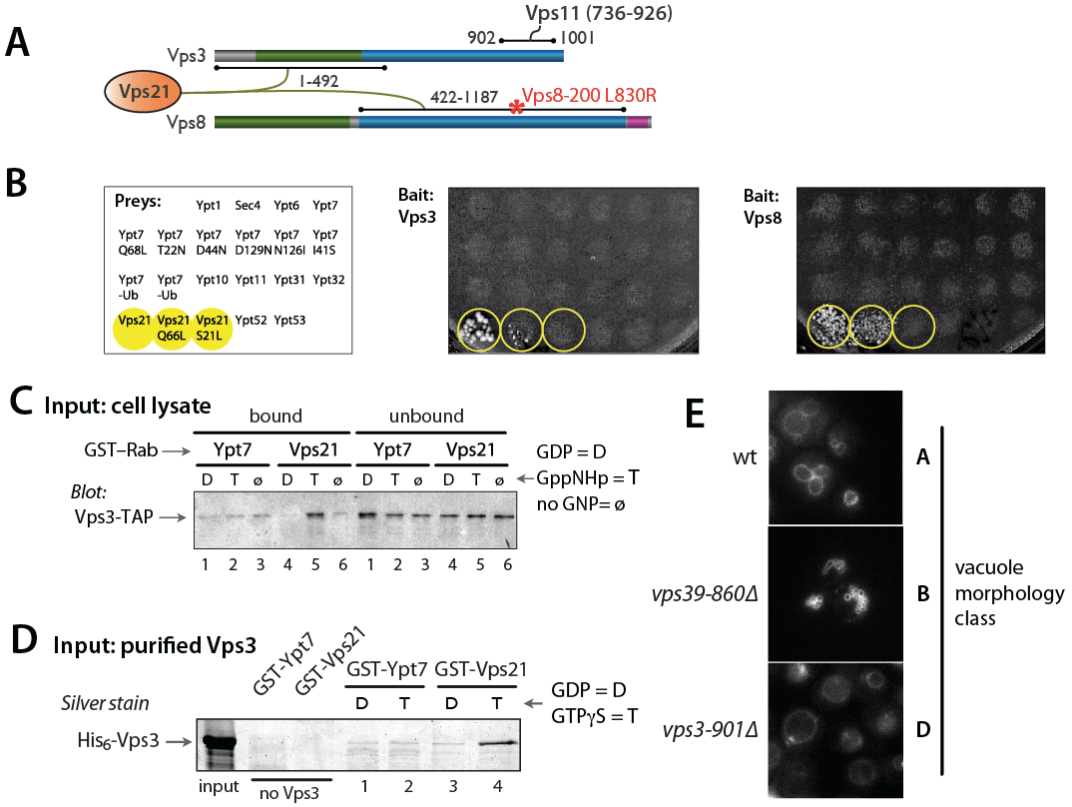

Figure 2.5 CORVET subunits Vps3 and Vps8 are a Vps21 interaction module
(A) Summary of Vps3 and Vps8 Y2H interactions. The position of the L830R mutation in the VPS8-200 mutant is indicated. (B) Vps3 and Vps8 interact with Vps21-GTP in Y2H miniarray experiments. The prey strains are indicated in the left panel, and were mated with strains containing either Vps3 (middle panel) or Vps8 (right panel) bait constructs. Yeast colony growth on synthetic medium (–Trp, –Leu, –His, +3-AT) indicates a positive Y2H interaction. Note that Vps3 and Vps8 interacted with Vps21 and the GTP-biased mutant Vps21-Q66L, but did not interact with any Rab other than Vps21, and did not interact with the GDP-biased Vps21-S21L mutant. (C) Native Vps3 in yeast cell lysates is selectively retained on a Vps21-GTP affinity resin. Note that most Vps3 in cell lysates is found within the CORVET complex. A similar pulldown, employing purified Vps3 rather than a cell lysate, is shown in Figure 3.5D. Cell lysates were prepared as described previously (Brett et al., 2008). TAP-tagged Vps3 was identified by immunoblotting with peroxidase-antiperoxidase (Upstate, Inc). (D) Vps3 binds directly to Vps21-GTP. GST pulldown experiments were performed using purified recombinant His6-Vps3 and beads decorated with GST-Ypt7 or GST-Vps21 loaded with GDP or GTPγS by Procedure 2 (Methods). (E) In vivo vacuole morphology of strains carrying Vps3 and Vps39 truncations that cannot interact with the Vps11 CTD. Vacuoles were stained using an FM4-64 pulse-chase (Methods).

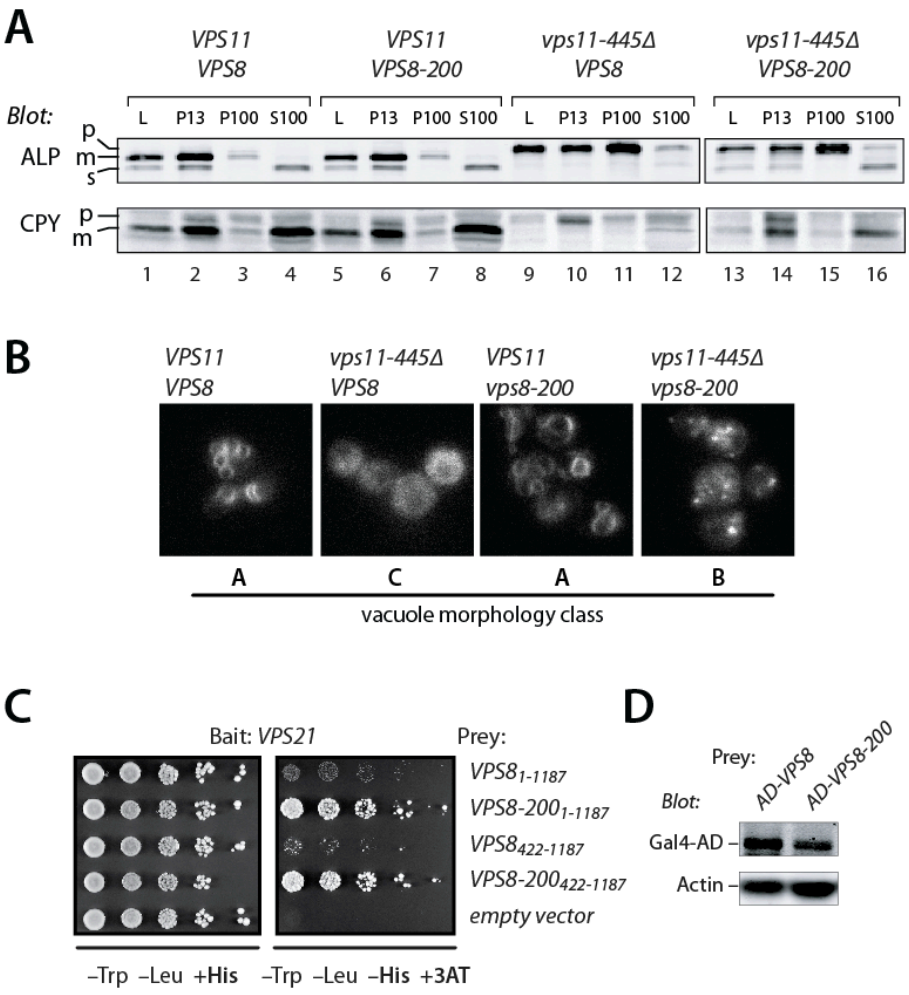

Figure 2.6. Genetic suppression reveals functional interactions between Vps8 and Vps21
(A) Differential centrifugation analysis of ALP and CPY maturation and subcellular localization in cells carrying vps11-445Δ and VPS8-200 alleles. (B) Vacuole morphology phenotypes of vps11-445Δ and VPS8-200 mutant cells. Vacuoles were visualized by pulse-chase with the fluorescent dye FM4-64 and examined by fluorescence microscopy. Assays were performed as in Fig. 3H. (C) Vps8-200 is a hyperactive Vps21 interactor in Y2H assays. More robust growth on media lacking His and supplemented with 3-aminotriazole (3AT) indicates a stronger Y2H interaction. Limiting dilution analysis is shown for each Y2H reporter strain, with serial 5-fold dilutions plated from left to right. (C) Differences in protein expression do not explain enhanced Y2H interactions between Vps8-200 and Vps21. Immunoblot analysis of the AD-Vps8 and AD-Vps8-200 Y2H prey constructs used in **Figure 2.6D** show that AD-Vps8-200 is expressed at identical or lower levels compared to AD-Vps8. The immunoblots were also probed with anti-actin as a gel loading control.

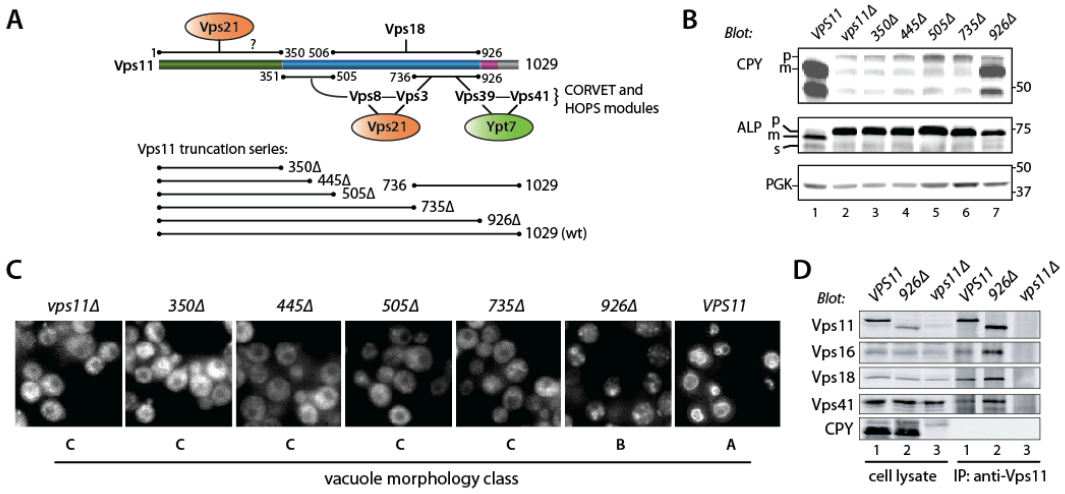

Figure 2.7. Multiple functional domains reside within the Vps11 CTD
(A) Map of Vps11 interactions. (B) CPY and ALP maturation phenotypes of cells harboring C-terminally truncated forms of Vps11. Accumulation of pro (p) forms of CPY and ALP indicate trafficking defects. (C) Vacuole morphology of vps11 truncation mutants. Vacuoles were stained with the vital fluorescent dye FM4-64 by pulse-chase labeling. The cartoon shows Vps11 interactions and a summary of the Vps11 truncation series. (D) Co-immunoprecipitation reveals an intact HOPS complex in vps11-926 cells. Lysates of the indicated mutant cells were immunoprecipitated with Vps11 antibodies under nondenaturing conditions and the eluates were analyzed by immunoblotting. Cell lysate lanes contain 10% load relative to IP eluate.

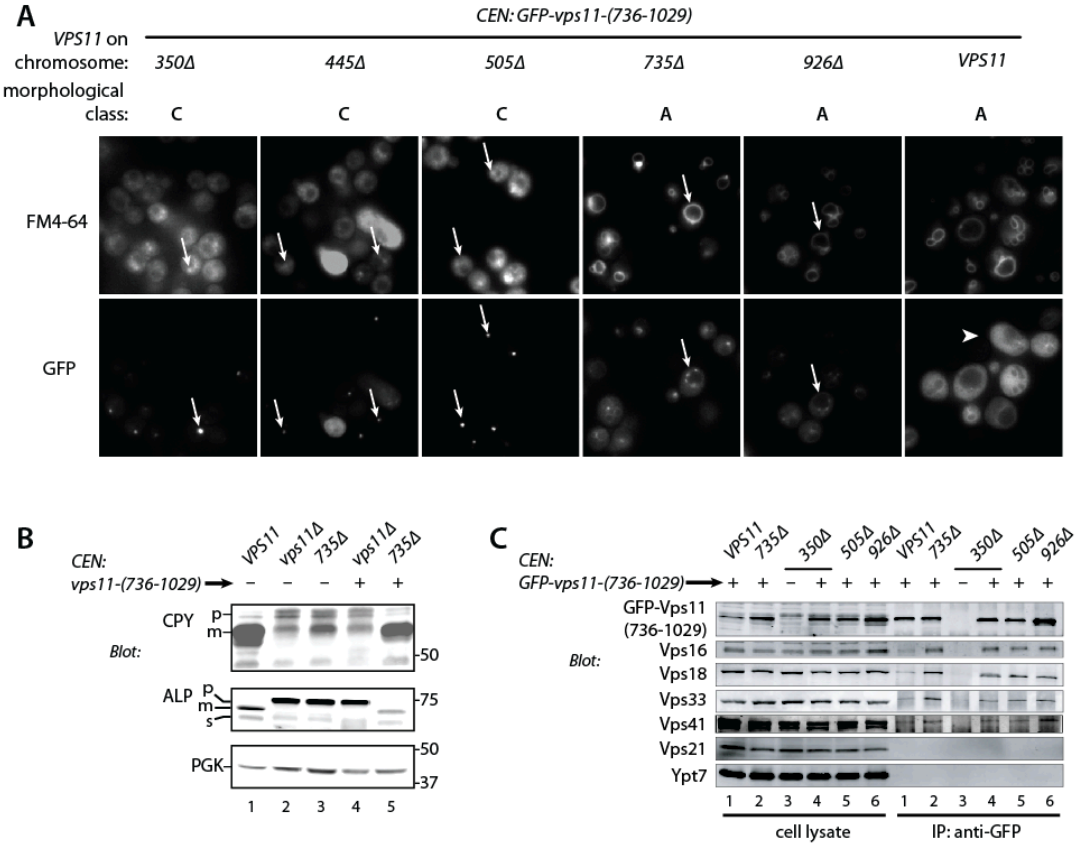

Figure 2.8. Split-Vps11 expressed as N- and C- terminal fragments is functional
(A) Vacuole morphology of vps11 truncation mutants co-expressing GFP-Vps11-(736-1029). Vacuoles were stained with the vital fluorescent dye FM4-64 by pulse-chase labeling (top row) The localization of GFP-Vps11-(736-1029) in the same cells is also shown (bottom row). GFP-Vps11-(736-1029) localizes to puncta in Vps11-350Δ, -445Δ, and -505Δ mutant cells, and at the vacuole rim in the Vps11-735Δ and -926Δ mutant cells (arrows). In contrast, GFP-Vps11-(736-1029) localizes to the cytoplasm in cells containing full-length Vps11 (arrowhead). (B) CPY and ALP maturation in Vps11 truncation mutants co-expressing GFP-Vps11-(736-1029). Note rescue of the 735Δ mutant (lane 5). (C) Co-immunoprecipitation of HOPS subunits with GFP-Vps11-(736-1029). Lysates from the indicated mutants, with or without GFP-Vps11-(736-1029) expression, were immunoprecipitated with anti-GFP. Cell lysate lanes contain 10% load relative to IP eluate. Note that HOPS subunits co-purify with low efficiency when full-length Vps11 is present (lanes 1). No HOPS subunits co-purify when GFP-Vps11-(736-1029) is not expressed (lanes 3).

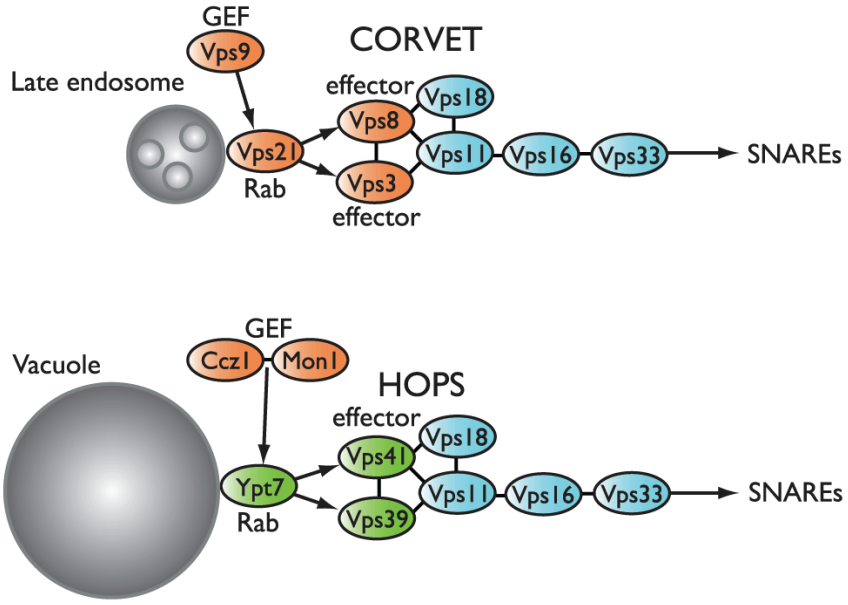

Figure 2.9. Interactions of HOPS and CORVET subunits
The subunit interaction topology summarized in this diagram integrates both biochemical and Y2H data. The similar diagram in **Figure 2.1** summarizes only Y2H interactions.

Chapter Three — Sec1/Munc18 protein Vps33 binds to SNARE domains and the quaternary SNARE complex[2]

3.1 –Introduction

Fusion, the final step of membrane trafficking between cellular compartments, requires the coordinated action of multiple conserved protein families including SNAREs (soluble N-ethylmaleimide-sensitive factor attachment protein receptor), Rab small G proteins, tethering proteins, and SNARE cofactors including the SM (Sec1/Munc18) proteins. A typical docking and fusion sequence entails activation of Rab proteins and recruitment of tethering factors. After tethering, three Q-SNARE domains (designated Qa, Qb, Qc) and one R-SNARE assemble into a coiled-coil *trans*-complex spanning the docked membranes. *Trans*-SNARE complex assembly is thought to drive membranes together, initiating merger of the apposed bilayers and intermixing of lumenal contents. Following fusion, the universal factors Sec17/α-SNAP (soluble *N*-ethylmaleimide-sensitive factor attachment protein) and Sec18/NSF (*N*-ethylmaleimide-sensitive factor) disassemble *cis*-SNARE complexes (for review see (Zhao et al., 2007)).

Despite intense efforts, the roles of SM proteins in these processes are incompletely understood. Genetic ablation or biochemical interference with SM function typically results in cessation of traffic through one or more pathways (Sudhof and Rothman, 2009). *In vitro,* SM proteins stimulate fusion of liposomes reconstituted with SNARE proteins (Scott et al., 2004; Shen et al., 2007). At the biochemical level, SM proteins have divergent modes of association

[2] **Chapter 3** was adapted with permission from Lobingier B.T. and Merz A.J, 2012. MBOC Dec; 23(23): 4611-22. http://www.molbiolcell.org/content/23/23/4611.long

with SNAREs (Carr and Rizo, 2010). It remains unclear how these biochemical properties are linked to the nearly absolute requirement for SM function that prevails *in vivo*.

SM proteins differ in their ability to bind cognate Qa SNAREs. Sly1 interacts with its cognate Qa SNARE by binding a N-terminal motif called the N-peptide (Peng and Gallwitz, 2002; Peng and Gallwitz, 2004; Yamaguchi et al., 2002). Vps45 and Munc18 also bind their cognate Qa SNAREs through interactions involving the N-peptide. Primarily, this interaction is with the "closed" conformation of the Qa SNARE, in which the tri-helical N-terminal H_{abc} domain folds back onto the SNARE domain (Dulubova et al., 2002). In these cases, the SM protein touches the N-peptide, the H_{abc} domain, and the SNARE domain. Although it has been hypothesized that N-peptide engagement might allosterically activate SM proteins, recent work suggests that a major function of N-peptide binding is simple recruitment of the SM to the fusion site (Rathore et al., 2010; Shen et al., 2010). In contrast, other SM proteins including Sec1 and, as shown in the present study, Vps33, do not engage their cognate Qa SNAREs with high affinity. Furthermore, these Qa SNAREs lack the N-peptide consensus sequence (Hu et al., 2007). The primary affinity of Sec1 is for the SNARE core complex, and it has lesser affinities for individual SNAREs (Morgera et al., 2011; Togneri et al., 2006). In lieu of N-peptide binding, these SMs are probably recruited to SNAREs through alternative mechanisms. For example, Sec1 binds the Sec6 subunit of the exocyst tethering complex, suggesting that exocyst positions Sec1 at sites of exocytosis (Morgera et al., 2011). Another Sec1-binding protein, Mso1, also interacts with the Qa-SNARE Sso1 and contributes to correct Sec1 localization (Knop et al., 2005).

Relative to other SM proteins, the endolysosomal SM Vps33 is poorly understood. Direct biochemical characterization of Vps33 has proven challenging due to its critical roles within at

least two Vps-C tethering complexes, HOPS (homotypic fusion and protein sorting) and CORVET (class C core vacuole/endosome tethering; for review see (Nickerson et al., 2009)). *In vivo* and *in vitro* studies indicate that HOPS promotes tethering, docking, and fusion at the terminal lysosomal vacuole and further suggest that HOPS may proofread *trans*-SNARE complexes and shield *trans*-complexes from disassembly (Hickey and Wickner, 2010; Starai et al., 2008; Stroupe et al., 2009; Xu et al., 2010a). The specific contributions of the six HOPS subunits to each of these functions are not understood.

It has been unclear whether previously reported interactions between HOPS and SNAREs are mediated directly by Vps33, or by the other five HOPS subunits. Cell-free assays demonstrated that the H_{abc} domain of the Qa SNARE Vam3 promotes HOPS recruitment to the vacuole. However, mutational analyses suggested that Vps18, not Vps33, is necessary for HOPS binding to Vam3 (Laage and Ungermann, 2001). Moreover, overproduced Vps33 in yeast cell lysates binds the Vam3 SNARE domain but not the N-terminal domain (Dulubova et al., 2001). In apparent contrast to these studies, an interaction between Vps33 and the Vam3 H_{abc} domain was postulated to occur (Pieren et al., 2010). Most recently, purified Vps33 was reported to bind preassembled 3Q and 3Q:R SNARE complexes but not individual SNAREs (Kramer and Ungermann, 2011). Purified HOPS was also reported to have affinity for the N-terminal PX-domain of Vam7 and weaker binding to Vam3 and Nyv1 (Stroupe et al., 2006). In the present study we re-examined the SNARE binding properties of Vps33, both in isolation and in the context of the native HOPS complex. Our findings unify much of the previous literature on interactions between SNAREs, HOPS, and the SM protein Vps33 and suggest a working model for HOPS-SNARE interactions.

3.2 –Materials and Methods

Strain and plasmid construction.

Briefly, *VPS33* was deleted from SEY6210 BHY10 and BY4742 *pep4*Δ. Vectors for expressing Vps33 under its native promoter were PCR-amplified from *VPS33-ttx-GFP*$_{A207K}$ (TEV, thrombin, and factor X recognition sites) and incorporated by homologous recombination into pRS416 vector (Wang et al., 2002). Point mutations in *VPS33* were introduced through homologous recombination, rescued, verified by sequencing, and transformed into SEY6210 BHY10 *vps33*Δ. For integration into BY4742 *pep4*Δ*vps33*Δ, wild-type and point mutants were PCR amplified from the pRS416 vectors and integrated into the chromosomal locus of *VPS33*. In brief, the GST-SNARE fusions were cloned in-frame with either a N- or C-terminal GST sequence separated by a short linker and TEV recognition site. GST-Vti1 was cloned as described (Stroupe et al., 2006). Full length Vam7 was cloned as described (Schwartz and Merz, 2009). Bos1 was cloned as described (Stone et al., 1997). N-terminally His_6-tagged SNARE fusions were cloned into pHIS-parallel1 vector. Vam7 SNARE domain was cloned into a pRSF-1b backbone in frame with a N-terminal His_6-GFP separated with a short linker and TEV recognition site. Vti1 was cloned into the pRSF-1b vector with a N-terminal His_7-MBP tag separated with a short linker and TEV recognition site. Vps33 was cloned for expression in the insect cell baculovirus system as described (Brett et al., 2008).

Protein expression.

Vps33. Insect cells expressing GST-Vps33 were lysed by sonication or high pressure disruption in buffer A (50 mM HEPES, 400 mM NaCl, 10% glycerol, 5 mM 2-mercaptoethanol, 5 mM EDTA, 0.5 % TritonX-100, pH 7.4) with protease inhibitors, and clarified lysate was bound to GSH 4B resin for 2 h at 4˚ C. The resin was washed extensively and the buffer was changed

step-wise into IEX binding buffer (20 mM Tris, 150 mM NaCl, 10% (w/v) glycerol, 5 mM 2-mercaptoethanol, pH 8.0). GST-Vps33 was eluted from GSH resin with 20 mM glutathione in IEX binding buffer and incubated with TEV protease at 4˚ C for 16-22 h. Cleaved Vps33 was further purified over UnoQ and Superdex200 columns, exchanged into Storage Buffer (20 mM HEPES, 200 mM NaCl, 10% (w/v) glycerol, 5 mM 2-mercaptoethanol) and snap frozen in liquid nitrogen.

SNAREs. SNARE proteins were expressed in *E. coli* that harbored a pRIL codon-bias correction plasmid. Cells were inoculated at 0.05 OD_{600}, grown to 1.0-1.2 OD_{600} in Terrific Broth, and expression was induced with 100 µM IPTG for overnight expression at 21˚ C (His_6-Nyv1 and His_7-MBP-Vti1, GST-Vam3$_{SNARE}$ domain and truncations, GST-Nyv1$_{SNARE}$ domain and truncations, His_6-Bos1, His_6-Bet1, His_6-Sec22), 500 µM IPTG for 4-5 h at 30˚ C (His_6-GFP-Vam7 SNARE), or 1mM IPTG for 3 h at 37˚ C (Vam3$_{1-264}$-GST). Full length Vam7 was expressed and purified as previously described (Schwartz and Merz, 2009). Cells expressing His-tagged SNAREs were lysed by sonication in Buffer A without EDTA and supplemented with 20 mM imidazole and protease inhibitors. Clarified lysates were prepared by centrifugation at 18,500 × g for 25 m at 4˚ C and incubated with Ni-NTA HP resin (GE Healthcare) for 10 m at 4˚ C. The bound material was washed extensively and His-tagged SNAREs were eluted with Storage Buffer (20 mM HEPES, 200 mM NaCl, 10% glycerol, 5 mM 2-mercaptoethanol, pH 7.4) supplemented with 400 mM imidazole, pH 7.4. His-tagged SNAREs were buffer exchanged into storage buffer without imidazole using PD-10 desalting columns (GE Healthcare) and snap frozen in liquid nitrogen. Cells expressing GST-tagged SNAREs were lysed by sonication in Storage Buffer supplemented with 5mM EDTA and protease inhibitors and clarified lysate was snap frozen in liquid nitrogen.

Pulldowns.

GST-SNARE proteins were bound to GSH 4B (GE Healthcare) by incubating clarified lysate with the resin for 2 h at 4˚C with rocking and washed extensively. For pulldowns on SNARE complexes, a five-fold molar excess of purified Vti1, Vam7, and Nyv1 were incubated with Vam3 pre-bound to GSH 4B for 16-22 h at 4˚ C with rocking. Golgi SNARE complexes were prepared in a similar manner with GST-Sed5 SNARE domain pre-bound to GSH 4B resin and the purified cytoplasmic domains of the other three SNAREs incubated at five-fold molar excess for 16-22 h at 4˚ C with rocking. In all cases, resins were washed extensively before to pulldown. Prior to pulldown, purified Vps33 was incubated with GSH 4B resin for 1 h at 23˚ C to remove residual uncleaved material. Pulldowns with recombinant Vps33 were performed in SNARE Assay buffer (20 mM HEPES, 200 mM NaCl, 5 mM 2-mercaptoethanol, 0.5% Triton, pH 7.4). Pulldowns with yeast lysate were performed as previously described (Angers and Merz, 2009). Briefly, lysis was performed in Yeast Lysis buffer (20 mM HEPES, 50 mM KOAc, 200 mM Sorbitol, 2 mM PIC) supplemented with protease inhibitors. Detergent lysates from ~450 $OD_{600\ nm}$ × mL of cells were incubated with resins pre-bound to GST-fusion proteins for 2 h at 4˚ C, washed three times with Yeast Lysis buffer, and eluted by incubating the resins with Yeast Lysis buffer supplemented with 20mM reduced glutathione, pH 7.4 final for 10 min at 4˚ C. Analysis was performed by SDS-PAGE and western blot. Antibodies were prepared as previously described (Angers and Merz, 2009). All pulldowns were repeated a minimum of three times; representative results are shown.

Quantification of Saturation Binding.

Minimal SNARE complexes were formed on GSH resin using the SNARE domain of $Vam3_{182-264}$-GST, the SNARE domain of Vam7 (His_6-GFP-$Vam7_{190-317}$), the cytoplasmic domains of Vti1

(His_7-MBP-$Vti1_{1-194}$) and Nyv1 (His_6-$Nyv1_{1-231}$). Increasing concentrations of Vps33 (0.1 μM to 10 μM) were incubated with minimal SNARE complex for 2 h at 30˚ C in SNARE Assay Buffer, washed three times, and eluted by incubating the resins with binding buffer supplemented with 20mM reduced glutathione, pH 7.4 final for 10 min at RT. Samples were separated by SDS-PAGE, detected with SYPRO-Ruby (Invitrogen), and imaged using a Gel Doc XR+ (Bio-Rad). The data from three experiments was plotted as fractional saturation of Vps33 binding to the minimal SNARE complexes relative to the total concentration of Vps33 in the reaction. K_d was estimated by nonlinear fitting of a single-site binding model to the data (GraphPad Prism 5).

Growth Assays. Strains were grown 16-22 h at 24˚ C and three dilutions were prepared (1.0, 0.05, and 0.0025 $OD_{600\ nm}$). Strains were plated on SC-URA or YPD plates, with or without 5mM $ZnCl_2$, and grown for 48 h at the indicated temperature.

Protein Sorting and vacuole morphology.

Yeast strains were grown 16-22 h at 24˚ C, and back diluted to 0.2 $OD_{600\ nm}$ × mL. Yeast were then grown at 30˚ C to 0.8-1.0 $OD_{600\ nm}$, and cell pellets were washed in 10 mM NaN_3. Cell pellets were resuspended in SDS-PAGE sample buffer. Samples were boiled for 15 min and then vortex-mixed with glass beads for 3 min. Samples were subjected to SDS-PAGE and western blots were performed as described (Plemel et al., 2011). Vacuoles were imaged by FM4-64 (Invitrogen) pulse-chase as described (Plemel et al., 2011).

Subcellular Fractionation.

Yeast strains were grown at 30˚ C to ~1.0 $OD_{600\ nm}$. Cells were centrifuged and washed for 10 min. at room temperature with 100mM Tris-Cl, pH 9.4 and 10 mM 2-mercaptoethanol. Cells were centrifuged and resuspended in spheroplasting buffer (50mM Tris-Cl, pH 7.9, 8% YPD, 1M sorbitol) with Zymolyase 20T (Seikagaku, Tokyo, Japan) that was further purified by cation

exchange chromatography prior to use. Cells were spheroplasted for 25 min. at 30˚ C, harvested by sedimentation, and resuspended in SF/IP buffer (20mM, 200mM Soribitol, 100mM NaCl, pH 7.4) supplemented with protease inhibitors. Spheroplasts were lysed by Dounce homogenization and clarified by centrifugation at 1000 × g. Lysates were subsequently centrifuged at 13,000 × g for 15 min to obtain pellet (P13) and supernatant (S13) fractions. The S13 fraction was centrifuged for 45 min at 100,000 × g to obtain pellet (P100) and cytosol (S100) fractions. Samples were incubated with SDS-loading buffer for 7 min at 95˚ C and analyzed by SDS-PAGE and western blot. Subcellular fractionations were repeated a minimum of three times, and representative western blots are reported.

Immunoprecipitation.

Cells were grown and spheroplasted as described for subcellular fractionation. The S1 fraction was incubated with 0.5% TritonX-100, on ice, for 10 min and clarified by centrifugation at 20,000 × g for 15 min. ~450 $OD_{600\ nm}$ × mL of lysate was incubated with Protein A-Sepharose resin (Pierce Chemical) covalently coupled to affinity-purified rabbit polycolonal GFP antiserum for 2 h at 4˚ C. Resins were washed five times SF/IP buffer and eluted by incubating the resin with SDS-loading buffer for 7 min. at 95˚ C. Immunoprecipitations were repeated a minimum of three times, and representative western blots are shown.

3.3 –Results

HOPS has multiple binding sites for the Qa SNARE Vam3

To evaluate interactions between the Qa SNARE Vam3 and native HOPS, we expressed and purified portions of Vam3 fused C-terminally to GST (**Figure 3.1A**). Affinity-capture experiments were then performed using lysates from wild-type cells or lysates from deletion

mutants lacking specific HOPS subunits. HOPS from wild-type cell lysates bound the full Vam3 cytoplasmic domain and the H_{abc} domain (**Figure 3.1B**). HOPS derived from lysates lacking the Rab-binding subunits Vps39 or Vps41 still bound Vam3 H_{abc}, indicating that Vps39 and Vps41 are not required for the Vam3-HOPS interaction (**Figure 3.2**). Surprisingly, in the absence of Vps33 (*vps33*Δ), HOPS still bound the Vam3 H_{abc} domain, indicating that a HOPS subunit other than Vps33 mediates H_{abc} binding. A partial loss of HOPS binding to the full Vam3 cytoplasmic domain in the absence of Vps33 suggested the hypothesis that Vps33 might act cooperatively with other HOPS subunits in binding to Vam3 containing both the H_{abc} and SNARE domains.

In *vps16*Δ null mutants, Vps33 cannot associate with the remainder of HOPS (**Figure 3.1A**) (Rieder and Emr, 1997). In pulldowns from *vps16*Δ cell lysates, Vps33 and HOPS had distinct binding profiles: Vps33 was retained on the Vam3 SNARE domain, while the remainder of HOPS was retained on the Vam3 H_{abc} domain. Deletion of either Vps11 or Vps18 strongly reduced pulldown of the remaining subunits with the Vam3 H_{abc} from yeast detergent lysate (**Figure 3.2**). In addition to the interaction between HOPS and the Vam3 H_{abc} domain, we detected weak interactions between HOPS and the Vam3 SNARE domain in the absence of Vps33 (lane 6 of **Figure 3.2B**). While this might be non-specific binding, a recent report of interactions between the HOPS subunits Vps16 and Vps18 and vacuole SNAREs raises the possibility that HOPS subunits other than Vps33 contact SNARE domains (Kramer and Ungermann, 2011).

To test whether Vps33 directly binds the Vam3 SNARE domain, we expressed and purified *S. cerevisiae* Vps33 from insect cells (**Figure 3.1C**). In binding experiments the purified Vps33 recapitulated results obtained with yeast cell lysates: Vps33 bound Vam3 directly through its SNARE domain (**Figure 3.1D**). Using the binding conditions for the yeast lysate pulldowns

(2 h at 4˚ C), purified Vps33 exhibited slight binding to the plasma membrane Qa SNARE Sso1 (**Figure 3.1D**). With optimized binding conditions for purified Vps33 (2 h at 30˚ C), the Vam3-Vps33 interaction was more efficient and there was no detectable binding to Sso1 or to two other non-cognate SNAREs, Sed5 and Sec22 (**Figure 3.2B,D**, **3.3, and 3.4**). Taken together, the data indicate that HOPS has at least two Vam3-binding sites. Vps11 and Vps18 are necessary for binding the Vam3 H_{abc} domain, while Vps33 binds the Vam3 SNARE domain. This working model is supported by the present results and most previous experiments addressing Vam3-HOPS interactions. We have so far been unable to detect binding of isolated Vps33, native or purified, to the Vam3 N-terminal H_{abc} domain (Pieren et al., 2010).

Vps33 binds vacuolar Qa, Qc, and R SNAREs and the quaternary SNARE complex

Interactions between SM proteins and individual non-Qa SNAREs are reported for Sly1, Vps45, Sec1, and Munc18 (Morgera et al., 2011; Peng and Gallwitz, 2004; Xu et al., 2010b). To test whether purified Vps33 directly binds vacuole SNAREs other than Vam3 (Qa), we prepared GST fusions to the cytoplasmic domains of Vti1 (Qb), Vam7 (Qc), and Nyv1 (R). We found (**Figures 3.3 and 3.6A**) that purified Vps33 bound Vam3, Vam7, and Nyv1, but not Vti1 or GST alone. Since Vps33 binds Vam3 through its SNARE domain, we tested whether purified Vps33 could also bind SNARE domains of Vam7 and Nyv1, and observed direct binding to these domains (**Figure 3.6B**). We further tested whether Vps33 is responsible for the reported interaction between HOPS and the N-terminal PX domain of Vam7 (Stroupe et al., 2006). Although purified Vps33 bound full-length Vam7 and Vam7 SNARE domain, Vps33 did not bind to the Vam7 PX domain (**Figure 3.4**). It was previously reported that Vps33 could bind the late endosomal Qa-SNARE Pep12 (Subramanian et al., 2004). While little of the HOPS in a

wild-type cell lysate was retained on Pep12 when compared to Vam3, purified Vps33 was retained equally on Pep12-GST and Vam3-GST resins (**Figure 3.5A and B**).

Direct SM binding to SNARE complexes is reported for Sec1, Vps45, and metazoan Munc18 (Carpp et al., 2006; Togneri et al., 2006; Xu et al., 2010b). To test whether Vps33 binds SNARE complexes, quaternary complexes containing the cytoplasmic domains of Vti1, Vam7, and Nyv1 were assembled on solid supports bearing the Vam3-GST. Importantly, Vps33 bound quaternary 3Q:R SNARE complexes, and was retained on SNARE complexes more efficiently than on any individual SNARE (**Figure 3.3, 3.4 and 3.6A and D**). To evaluate the selectivity of Vps33 binding to the vacuole SNARE complex, we assembled Golgi quaternary SNARE complexes containing the GST-Sed5 SNARE domain and cytoplasmic domains of Bos1, Bet1, and Sec22. Vps33 bound selectively to vacuole versus Golgi SNARE complex (**Figure 3.6C**).

The vacuole has two resident R-SNAREs. Nyv1 is thought to play a primary role in homotypic vacuole fusion, while Ykt6 functions in heterotypic fusion (Dilcher et al., 2001; Ungermann et al., 1999). To examine the ability of Vps33 to directly bind to Nyv1 or Ykt6, GST fusions to their full cytoplasmic domains were prepared. Sec22, a Golgi R-SNARE, was used as negative control. Vps33 was retained on Ykt6 to a greater degree than the negative controls, though less efficiently than on Nyv1 (**Figure 3.6D**). Purified Vps33 bound vacuolar SNARE complexes containing Nyv1 or Ykt6 with comparable efficiency.

To compare the relative affinities of Vps33 for an individual SNARE domain or the quaternary SNARE complex, we examined Vps33 binding to the SNARE domain of Vam3 or a minimal SNARE complex lacking the N-terminal domains of Vam3 and Vam7. Using a higher concentration of Vps33 (5.0 μM in **Figure 3.6E** compared to 0.25 μM in **Figures 3.6A, B, C, and F**), we were readily able to detect binding of Vps33 to the minimal SNARE complex using

Coomassie blue-stained polyacrylamide gels (**Figure 3.6E**). Less Vps33 was retained by the Vam3 SNARE domain compared to the minimal SNARE complex, consistent with the interaction between Vps33 and the Vam3 SNARE domain being of lower affinity (**Figure 3.6E**). By assaying binding over a range of Vps33 concentrations, we estimated the dissociation constant for Vps33 and the minimal SNARE complex as ~2.8 ± 0.2 μM (**Figure 3.6F**). This low micromolar apparent K_d falls between affinities reported for SNARE complex binding by Sec1 (~0.3 μM) and Munc18 (~6 μM) (Togneri et al., 2006; Xu et al., 2010b). We were unable to measure an apparent dissociation constant for Vps33 and individual SNAREs due to the lower affinity of these interactions and instability of Vps33 at higher concentrations. Despite their relatively lower affinity, the interactions between Vps33 and monomeric SNARE domains are selective (**Figures 3.1D, 3.3, 3.6A, B, C and D**), and it is plausible that interactions between Vps33 and individual SNAREs contribute to the SNARE assembly cycle *in vivo* (see Discussion).

Vps33 binding sites within Qa and R SNARE domains

SNARE domains share a conserved architecture with repeating hydrophobic packing layers and a central "zero" layer comprising polar (Q) and ionic (R) residues (Fasshauer et al., 1998). Negative numbering denotes packing layers N-terminal to the zero-layer while positive numbers are ascribed to the C-terminal (membrane-proximal) layers. Alignments of SNARE domains show substantial conservation of packing layers -8 to +8, but for clarity we have used the layer-based numbering system for our truncations outside of this region. To map the interaction of Vps33 with Vam3 (Qa), we assayed binding of purified Vps33 to truncated Vam3 SNARE domains. When truncating from the N-terminal side of the Vam3 SNARE domain, Vps33 binding was lost upon truncation from layer -7 to layer -5 (**Figure 3.7A**). In the C-terminal

truncation series (starting from the equivalent of layer +9), Vps33 binding decreased as the SNARE domain was truncated from layer +5 to +3, and Vps33 binding was lost when Vam3 was truncated to layer -5. Thus, the determinants for Vps33 binding reside within Vam3 SNARE layers -7 to +5. While it is possible that sequential truncations to the Vam3 SNARE domain alter the conformation or presentation of the SNARE motif, like other Qa SNARE domains, the Vam3 SNARE domain is largely unstructured in solution (Dulubova et al., 2001). Thus we define the outside boundaries of Vps33 binding site in Vam3 (i.e., the region bounded by layers -7 to +5) using only those truncation constructs that showed no loss of Vps33 binding.

Munc18 interacts with the SNARE domain of the R-SNARE synaptobrevin at the C-terminal juxtamembrane region, making contacts within layers +8 to +9 (Xu et al., 2010b). We asked whether truncation of the equivalent region of the vacuole R-SNARE Nyv1 would reduce Vps33 binding. Vps33 binding decreased when Nyv1 was truncated at its C-terminus to layer +9, and decreased further upon truncation from layer +7 to layer +5 (**Figure 3.7B**). We infer that residues required for Vps33 binding lie within the membrane-proximal region of the Nyv1 SNARE domain.

Phenotypic analyses of Vps33 point mutations

To further investigate the role of Vps33 in vacuole maintenance and fusion, we constructed *VPS33* alleles encoding missense mutations that alter conserved amino acids and that have been identified as causing phenotypic defects in Vps33 or other SM proteins (Dascher et al., 1991; Gissen et al., 2004; Hashizume et al., 2009; Li et al., 2007; Sevrioukov et al., 1999; Suzuki et al., 2003). Evolutionary conservation of the targeted amino acid positions was verified using published and in-house sequence alignments ((Gissen et al., 2004; Pieren et al., 2010); **Table 3.1**). Only an Ile residue mutated in a human patient with Hermansky-Pudlak syndrome falls at a

position not identical to yeast Vps33. Instead of Ile, yeast Vps33 has Phe at the equivalent position (Suzuki et al., 2003). In addition to the yeast Vps33 analog of the mouse buff (*bf)* mutation, D300E, we also tested a glycine substitution at the same position (D300G).

Yeast vacuole morphology is classified as A (wild-type), B (partially fragmented), C (severely fragmented), D (enlarged), and E (accumulation of a novel compartment adjacent to the vacuole) (Raymond et al., 1992). Loss of Vps33 causes vacuolar cargo missorting, class C vacuole morphology, and a failure to grow at non-permissive temperature (37˚ C) (Banta et al., 1990). Based on these parameters, the phenotypic defects of the ten Vps33 point mutations examined here ranged from no detected deficiency to the equivalent of a *vps33*Δ null mutant. The results from growth, trafficking, vacuole morphology, and Vps33-GFP localization assays are summarized in **Table 3.2** and described below. Based on the results from these assays, the ten mutants fall into four categories, referred to here as classes A, A´, B and C.

Four of the ten mutants had a novel collection of phenotypic defects intermediate to class A and class B here referred to as class A´. While D88K, I278N, D300G, and T553I resembled the wild type strain in growth at 30˚ C and 37˚ C, these alleles showed slow or no growth at 37˚ C on media supplemented with 5 mM $ZnCl_2$ (**Figure 3.8A**). Yeast with a wild-type copy of Vps33 showed no defect when grown under the same conditions. Furthermore, class A´ mutants had identifiable defects in trafficking of both CPY and ALP (**Figure 3.8B**). Although the vacuole morphology of class A´ mutants appeared similar to the wild type, Vps33-GFP localization was cytoplasmic rather than punctate in these mutants, as described below.

We saw no observable defects with three alleles associated with disease phenotypes in Vps33 orthologs: L75P, D300E, and F305L. Two of these encoded analogs of disease mutations in human *VPS33B* and *VPS33A* that cause ARC (arthrogryposis, renal dysfunction, and

cholestasis) and HPS (Hermansky-Pudlak syndrome), respectively (Gissen et al., 2004; Suzuki et al., 2003). For the HPS mutations, the lack of conservation of I256 with yeast Vps33 suggests a rationale for the lack of defect the F305L mutation in yeast. It is less clear why L75P has no effect in yeast despite the L30P mutation in human VPS33B causing multi-system disorders, although the L30P/L75P mutation falls within a region of Vps33 that is less well conserved. The amino acid mutated in the *buff* mouse is conserved in *S. cerevisiae* Vps33, but we observed no phenotypic defects from the analogous D300E mutation (Suzuki et al., 2003). We did observe phenotypic defects with a D300G mutation, indicating that the importance of this residue, if not its precise sensitivity to mutation, is conserved between mouse VPS33A and yeast Vps33.

Defects in Growth and Cargo Sorting

GFP-tagged Vps33 mutants were expressed in a *vps33*Δ background from single-copy plasmids under the native *VPS33* promoter. As some *vps33* mutants are temperature sensitive for growth (Banta et al., 1990), we asked whether any of the ten mutants produced similar sensitivity (**Figure 3.8A**). The *vps33*Δ mutant and two class C mutations, R281A and E653A, failed to grow at 37˚C. Defects in vacuole biogenesis cause sensitivity to extracellular Zn^{2+}, likely due to a failure to sequester metal ions within the vacuole (Subramanian et al., 2004). To test for more subtle defects in vacuole function, we stressed the cells by growing them in the presence of Zn^{2+} (**Figure 3.8A**). While the majority of Vps33 mutants had no growth defects at 37˚ C, several grew slowly or lost viability when grown at 37˚ C in the presence of 5 mM $ZnCl_2$: the class A´ mutants D88K, I278N, D300G, and T553I (**Figure 3.8A**). This was not a universal effect of growth at 37˚ C in the presence of Zn^{2+}, as strains containing wild-type Vps33 or the class A Vps33 mutants L75P, D300E, or F305L mutations grew normally. The class C mutations R281A

and E653A lost viability when grown 30˚ C with Zn^{2+}. The class B mutant and *carnation* analog G297V had strong growth defects at 37° C and at 30˚ C in the presence of Zn^{2+} (**Figure 3.8A**).

Carboxypeptidase Y (CPY) traffics from the Golgi to the vacuole via endosomes, while alkaline phosphatase (ALP) traffics directly from the Golgi to the vacuole. As CPY and ALP take independent routes to the vacuole, it is possible to selectively impair one pathway while leaving the other unaltered (Bowers and Stevens, 2005). Defects in trafficking to the vacuole result in accumulation of proenzymes (p) relative to active mature (m) forms. To further characterize the *vps33* alleles, detergent lysates from cells grown at 30˚ C were analyzed for Vps33 protein levels and defects in cargo transport (**Figure 3.8B**). While Vps33 levels were similar in each of the ten strains, ALP and CPY maturation defects varied greatly among the mutants (**Figure 3.8B**). Consistent with the growth data, strains with a wild-type copy of *VPS33* or class A mutations had normal levels of mature ALP and CPY. Partial accumulation of proALP and proCPY were noted in class A´ strains. Vps33-G297V, the sole class B mutant, had an intermediate cargo maturation phenotype: most of its ALP accumulated in the pro-form but there was partial maturation of CPY. Strains lacking a copy of Vps33, or carrying class C Vps33 mutant alleles R281A or E653A, failed to mature both CPY and ALP.

Defects in Vacuole Morphology and Vps33-GFP Localization

We next examined vacuole morphology and Vps33 localization in each of the mutants. The vacuole was visualized by pulse-chase labeling with the endocytic tracer FM4-64. In a strain carrying wild-type *VPS33*, vacuoles had normal (class A) morphology and Vps33-GFP accumulated in punctae adjacent to the vacuole, as expected (**Figure 3.9**; (Jun et al., 2006; Wang et al., 2002)). In accord with data from growth and trafficking assays, vacuole morphology and Vps33-GFP localization in L75P, D300E, F305L mutants were indistinguishable from wild-type

Vps33. In strains lacking Vps33, extreme fragmentation of the vacuole (class C morphology) was observed (Banta et al., 1990). Strains carrying the R281A or E653A mutations, which phenocopied the *vps33*Δ null in growth and cargo maturation assays, had class C morphology and lacked clearly identifiable Vps33-GFP punctae. The G297V mutation had partially fragmented, or class B, vacuole morphology without clear Vps33-GFP punctae. The class A´ mutants (D88K, I278N, D300G, and T553I) had normal, class A vacuole morphology. Surprisingly, in these four class A´ strains, the fluorescent Vps33-GFP punctae observed in wild-type cells were absent. Instead, Vps33-GFP had a diffuse cytosolic localization.

Class A´ Vps33 mutants show loss of in vivo binding to the HOPS complex

Despite their normal vacuole morphology, the four class A´ mutants (D88K, I278N, D300G, T553I) had growth defects under stressful conditions (37 ˚C and 5 mM $ZnCl_2$) and impaired cargo trafficking under standard conditions (30˚ C). To further characterize these mutants, Vps33-GFP alleles from different phenotypic classes (D88K, R281A, G297V, and D300G) were chromosomally integrated under the native *VPS33* promoter in a protease-deficient *pep4*Δ background. Examination of the chromosomal integrants revealed defects identical to phenotypes from plasmid-borne *vps33* alleles (**Figure 3.10**).

To test whether loss of Vps33-GFP punctae in the class A´ mutants was due to altered Vps33 association with membranes, we performed subcellular fractionation. Lysates of spheroplasted cells were centrifuged at 13,000 × g to obtain pellets (P13) highly enriched for vacuole membranes. The 13,000 × g supernatants (S13) were then centrifuged at 100,000 × g to yield a P100 fraction (enriched in endosomes, vesicles, and Golgi), and S100 cytosol. In wild-type cells, HOPS sedimented predominantly with the vacuole-enriched P13 fraction, with a smaller amount remaining in the S100 cytosol (**Figure 3.11A**). In strains carrying the class A´

mutations D88K or D300G, however, Vps33 shifted from the P13 to the S100 cytosol. Importantly, the other HOPS subunits remained in the vacuolar P13 (**Figure 3.11B**). Together with microscopy, these subcellular fractionation experiments confirm that in the D88K and D300G mutants, and likely in all the class A´ mutants, Vps33—but not the remainder of HOPS—shifts from mainly vacuolar to mainly cytosolic.

In previous studies, Vps33 stably associated with HOPS in co-immunoprecipitations (Rieder and Emr, 1997; Seals et al., 2000). Based on the above data, we predicted that the Vps33 mutations D88K or D300G would abrogate the Vps33-HOPS interaction. Co-immunoprecipitation from detergent lysates verified the stable association of wild type Vps33 with HOPS (**Figure 3.11C**). In contrast, co-immunoprecipitation from lysates from D88K or D300G mutant cells revealed a loss of association between Vps33 and HOPS. These results suggest that the altered Vps33 localization in class A´ mutants results from reduced steady state association of Vps33 with HOPS. Together with the growth and cargo trafficking defects, the class A´ mutants underscore the importance of proper steady state recruitment of Vps33 to the vacuole and vacuole fusion machinery (see Discussion).

3.4 –Discussion

A central challenge in developing general models for Sec1/Munc18 action is to reconcile the apparently divergent modes of SNARE association reported for the four SM subfamilies. Here, we have shown that Vps33 interacts with SNAREs and SNARE complexes in a manner closely analogous to Sec1 (Morgera et al., 2011; Togneri et al., 2006). Specifically, Vps33 interacts with individual SNARE domains and, with significantly greater affinity, quaternary SNARE complexes. Furthermore, we found that HOPS binds the Vam3 N-terminal domain through an

SM-independent mechanism that requires Vps11 and Vps18 but not Vps33. This is in contrast to the SM proteins Sly1, Vps45, and Munc18, which have high affinity interaction sites for their cognate Qa SNAREs. We also identified Vps33 mutants that exhibit a collection of phenotypic defects referred to here as class A´, including the loss of vacuole-associated Vps33 and reduced steady-state Vps33-HOPS interactions.

Although isolated Vps33 can bind SNAREs and SNARE complexes *in vitro*, recruitment of HOPS to membranes still occurs when Vps33 is absent. HOPS recruitment to docking junctions is enhanced by affinities of the HOPS complex for the Rab Ypt7 (Brett et al., 2008; Brocker et al., 2012; Plemel et al., 2011; Price et al., 2000), for specific lipids on the vacuole (Boeddinghaus et al., 2002; Fratti and Wickner, 2007), and for the N-terminal regions of the Qa and Qc SNAREs, Vam3 and Vam7 (Sato et al., 2000; Stroupe et al., 2006). Taken together, the available data suggest a model in which HOPS coordinates SNARE binding through its interactions with the N-terminal domains of the Qa and Qc SNAREs. This positions Vps33 to interact with the fusion-active SNARE domains of Qa, Qc, and R SNAREs, and finally with the SNARE core complex (**Figure 3.12**).

Consistent with this emerging picture, we identified four class A´ mutations in Vps33 that result in a change in the localization of Vps33, but not the remainder of HOPS, from the vacuole to the cytoplasm. Strains carrying class A´ alleles have reduced viability and cargo trafficking defects. It is tempting to speculate, given the loss of association between HOPS and the Vps33 class A´ mutants D88K or D300G, that the phenotypic defects of the class A´ mutants are due to a loss of HOPS-promoted recruitment of Vps33 to the vacuole. However, further characterization of these Vps33 alleles will be required to rule out the possibility that class A´ alleles have secondary defects that contribute to the observed phenotypes.

As with the interactions between Vps33 and individual SNAREs reported here, each of the other SM subfamilies has been reported to interact with non-Qa SNAREs and SNARE domains. Sly1 binds SNARE domains of Qb (Bos1 and Gos1) and Qc SNAREs (Bet1 and Sft1) (Peng and Gallwitz, 2004). The yeast endosomal SM Vps45 binds the SNARE domain of the R-SNARE Snc2 (Carpp et al., 2006). Munc18-1 binds the R-SNARE synaptobrevin and the Qa syntaxin 1A SNARE domain (Shi et al., 2011; Xu et al., 2010b). Sec1 binds the Qb-c SNARE Sec9, and the Qa SNARE Sso1 (Morgera et al., 2011). As interactions between SM proteins and individual SNARE domains are typically weak (6 to 20 μM), the functional *in vivo* significance of these interactions is still unclear (Morgera et al., 2011; Xu et al., 2010b). One model consistent with this pattern of interactions is that the SM protein makes similar contacts with a subset of SNARE domains when the SNAREs are unpaired or in the assembling SNARE complex bundle. The low affinities for individual SNAREs would be synergistic in the context of the SNARE complex, and these SNARE domain contacts could in turn provide a basis for the hypothesized activity of SM proteins towards the assembling *trans*-complex (Carr and Rizo, 2010; Sudhof and Rothman, 2009).

While nearly every SM protein has been reported to interact with individual SNARE domains, no clear pattern emerges as to which specific SNARE domains SM proteins contact. As some SM proteins must contact SNARE complexes with multiple Qa, Qb, Qc, and R SNARE compositions, it seems possible that a strict arrangement of SM-to-SNARE domain contacts would not be conserved while the general feature of interaction with at least two SNARE domains per SM would be maintained. A closely related question is whether SM proteins contribute to the specificity of fusion. We report here that Vps33 binds similarly to quaternary complexes with either of the physiologic R-SNAREs (Nyv1 and Ykt6), and binds the SNARE

domains of both endosomal and vacuole Qa-SNAREs (Vam3 and Pep12). In contrast, Vps33 shows high selectivity in binding to vacuole versus Golgi SNARE complexes and in binding cognate versus non-cognate individual SNAREs. This suggests, at least in principle, that SM proteins can contribute to the selectivity of membrane docking and fusion.

A recent study reported binding of Vps33 to 3Q and 3Q:R quaternary SNARE complexes, but not individual SNAREs (Kramer and Ungermann, 2011). As we observed stronger binding of Vps33 to SNARE complexes than to individual SNAREs, it is possible that differences in observed interactions reflect differences in experimental conditions. As 3Q complexes did not remain stably associated under our assay conditions, we did not examine their binding to Vps33. We emphasize that interactions between Vps33 and quaternary 3Q:R complexes were detected in both studies.

Our data suggest that compared to other SM proteins, Vps33 behaves in a manner most similar to Sec1. Both proteins can interact with isolated SNAREs but have greatest affinity for the SNARE complex. Moreover, both Vps33 and Sec1 interact with larger protein complexes (HOPS and exocyst), which in turn have additional affinities for SNAREs. In both cases, multi-subunit tethering complexes play an important role in recruitment of the cognate SM protein. We suggest that SM proteins fall into two classes based on a primary affinity for the Qa SNARE or SNARE complex. Class I SM proteins (including Munc18, Vps45, and Sly1) have a high affinity interaction site for the cognate Qa SNARE, and that cognate Qa SNARE contains the N-peptide consensus sequence. Class I SM proteins can be further divided into those which bind the closed conformation of the Qa SNARE (Munc18, Vps45), or do not (Sly1). Class II SM proteins (including Sec1 and Vps33) do not directly bind the N-peptide and, in fact, their cognate Qa SNAREs seem to lack the consensus N-peptide sequence (Hu et al., 2007). Instead, Sec1 and

Vps33 have primary affinity for the SNARE complex. Recently, it was suggested that the N-peptide of syntaxin-1 serves predominantly as a physical recruitment site for Munc18-1 (Rathore et al., 2010). In this model, class I SM proteins (Munc18, Vps45, and Sly1) are recruited through interactions with the N-peptide directly. Recruitment of Class II SM proteins (including Sec1 and Vps33) to unpaired SNAREs may be enhanced by tethering complexes such as HOPS and exocyst. Despite the divergence in SM protein affinity for cognate Qa SNARE, all SM proteins studied to date have the ability to bind unpaired SNARE domains. Furthermore, Munc18 and Vps45 have been reported to interact with the SNARE complex bundle, suggesting that the primary SNARE binding mode of Vps33 and Sec1—interaction with the SNARE complex bundle—is a shared feature of all SM proteins. This would suggest a unifying model in which the executive functions of SM proteins in docking and fusion are broadly conserved.

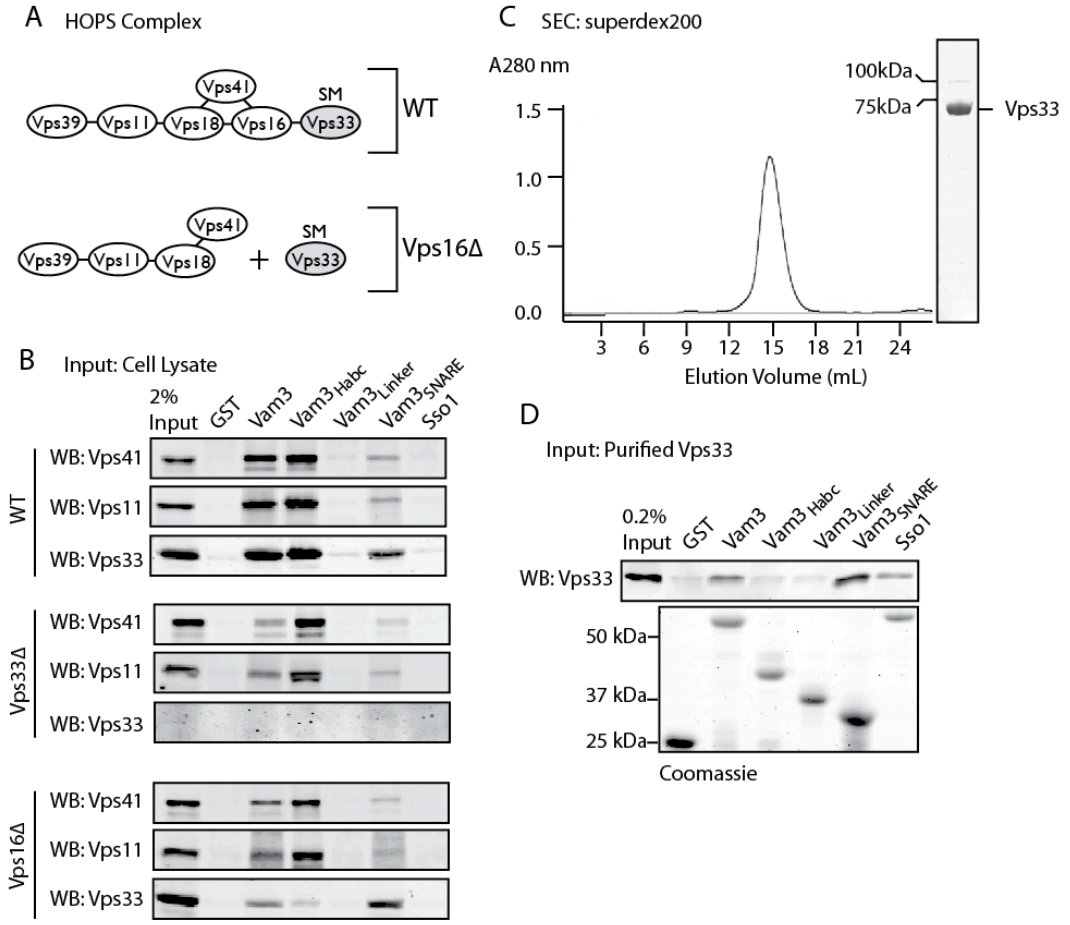

Figure 3.1. HOPS has multiple interaction sites for Vam3.
(A) Model of subunit interactions in HOPS of wild-type and a vps16Δ cells. In vps16Δ, Vps33 is separated from the remainder of HOPS. (B) Binding of native HOPS to GST-tagged Vam3 cytoplasmic domains. Equivalent loads (~3.5 μM) of each C-terminally GST-tagged fusion protein (25 to 100 μg depending on the MW) were incubated with GSH resin: Vam3 (1-264), H_{abc} (1-145), linker (116-186), and SNARE (182-264). GST and Sso1 (1-265) were negative controls. Coomassie blue stained gel of the of GST-fusions proteins shown in part D. Yeast detergent lysate was incubated with GST-fusion proteins for 2 h at 4˚ C, washed extensively, and eluted with 20mM glutathione. Samples were analyzed by SDS-PAGE and western blot (WB) for Vps41, Vps11 and Vps33. (C) Size exclusion chromatography shows that purified Vps33 migrates as expected for a monomer. Coomassie blue-stained SDS-PAGE of the pooled eluate. The faint band at 100 kDa is residual un-cleaved GST-Vps33, which was removed prior to pulldowns by pre-incubating purified Vps33 with GSH resin for 1 h at 23˚ C. (D) 1 μg (~25 nM) of purified Vps33 was incubated with Vam3 GST-constructs as in part B and analyzed by SDS-PAGE and western blot for Vps33.

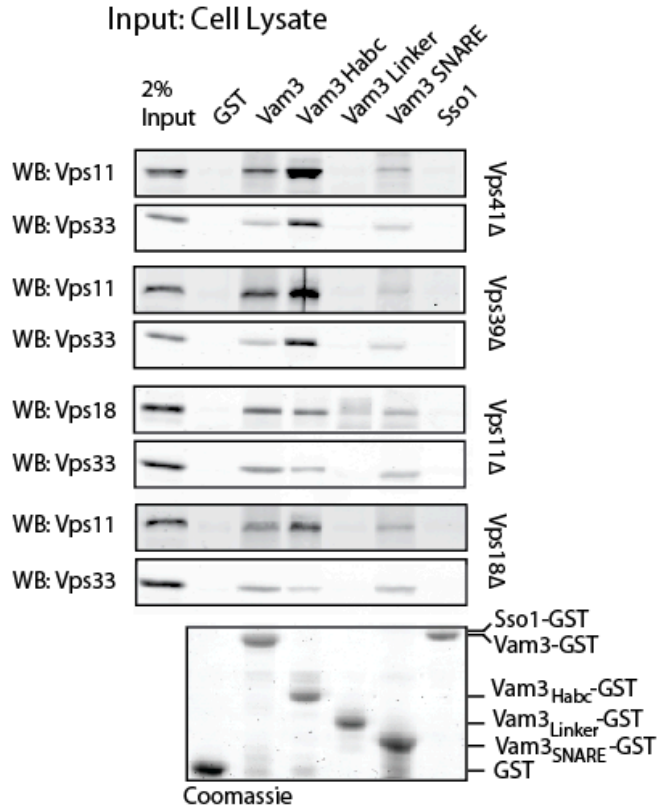

Figure 3.2. Interaction between HOPS and Vam3-Habc requires Vps11 and Vps18.
As in **Figure 3.1B**, the cytoplasmic domain of Vam3 (1-264), Habc domain (1-145), linker domain (116-186), and SNARE domain (182-264) were expressed as C-terminal GST fusions. GST and the exoctyic Qa SNARE, Sso1-GST (1-265), were negative controls. Coomassie stained gel of the of GST-fusions proteins shown. ~450 OD600 nm × mL of yeast detergent lysate were incubated with resins for 2 h at 4˚ C, washed three times with binding buffer, eluted, and samples were analyzed by SDS-PAGE and western blot (WB) for Vps11 or Vps18 and Vps33.

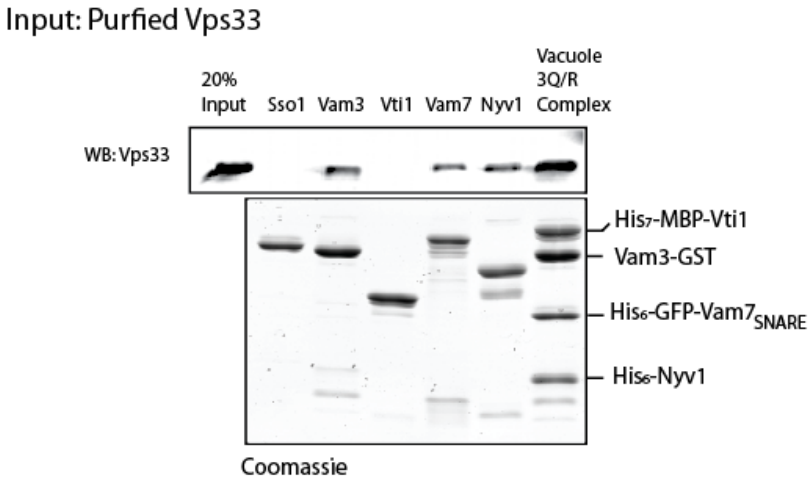

Figure 3.3. Vps33 binds vacuole Qa, Qc, and R SNAREs and the quaternary SNARE complex.
As in Figure 2A, the C-terminal GST fusions were made to the cytoplasmic domains of Vam3, Vti1, Vam7, and Nyv1. SNARE complexes were formed of cytoplasmic domain of Vam3. Sso1 was used as a negative control. ~30 µg (1 µM) of each GST-fusion protein were incubated with 10.5 µg (~0.25 µM) purified Vps33 for 2 h at 30˚ C, washed three times with binding buffer, and eluted with binding buffer supplemented with 10mM reduced glutathione, pH 7.4. Samples were analyzed by SDS-PAGE and western blot for Vps33.

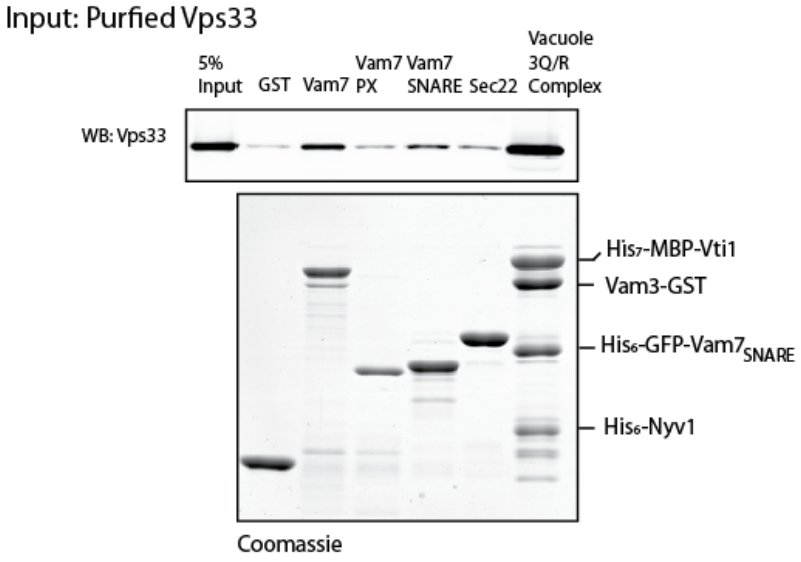

Figure 3.4. Vps33 binds Vam7 through its SNARE domain
GST-fusions to the Vam7 cytoplasmic domain, Vam7PX, Vam7SNARE, and the vacuole SNARE complex were used to pulldown purified Vps33. Sec22 and GST were used as negative controls. SNARE complexes were formed using purified Vam3-GST (1-264) bound to GSH resin and incubated overnight at 4˚ C with a five-fold excess of purified His7-MBP-Vti1 (1-194), His6-GFP-Vam7 SNARE (190-316), and His6-Nyv1 (1-231). 10.5 µg of purified Vps33 was incubated for 2 h at 30˚ C, washed three times with binding buffer, and eluted. Samples were separated by SDS-PAGE and analyzed by western blot for Vps33.

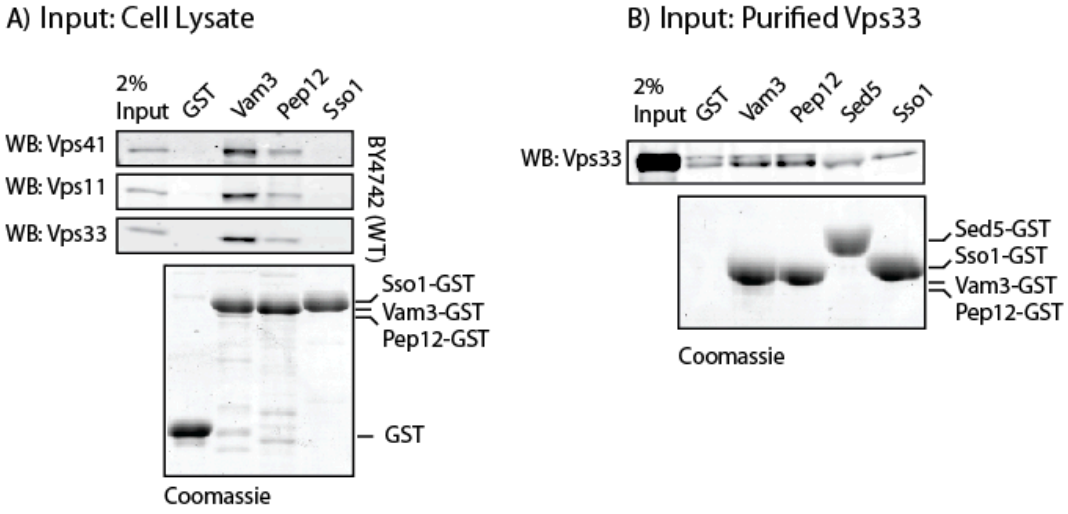

Figure 3.5. Vps33 binds Pep12.
(A) For pulldowns on Vam3 or Pep12, the cytoplasmic domain of Vam3 (1-264) or Pep12 (1-268) were expressed as C-terminal GST fusions. GST and the exocytic Qa SNARE, Sso1-GST (1-265), were negative controls. Coomassie stained gel of the of GST-fusions proteins shown. ~450 OD_{600} nm × mL of yeast detergent lysate were incubated with resins for 2 h at 4˚ C, washed three times with binding buffer, eluted, and samples were analyzed by SDS-PAGE and western blot (WB) for Vps41, Vps11 and Vps33. (B) The cytoplasmic domains of the Vam3 and Pep12 were fused to GST. C-terminal GST-fusions of Sed5 (1-319), Sso1 (1-265), and GST were used as negative controls. 1 µg of purified Vps33 was incubated resins pre-bound to GST-fusion proteins for 2 h at 4˚ C. Resins were washed, and bound fractions were eluted and analyzed by SDS-PAGE and western blot for Vps33.

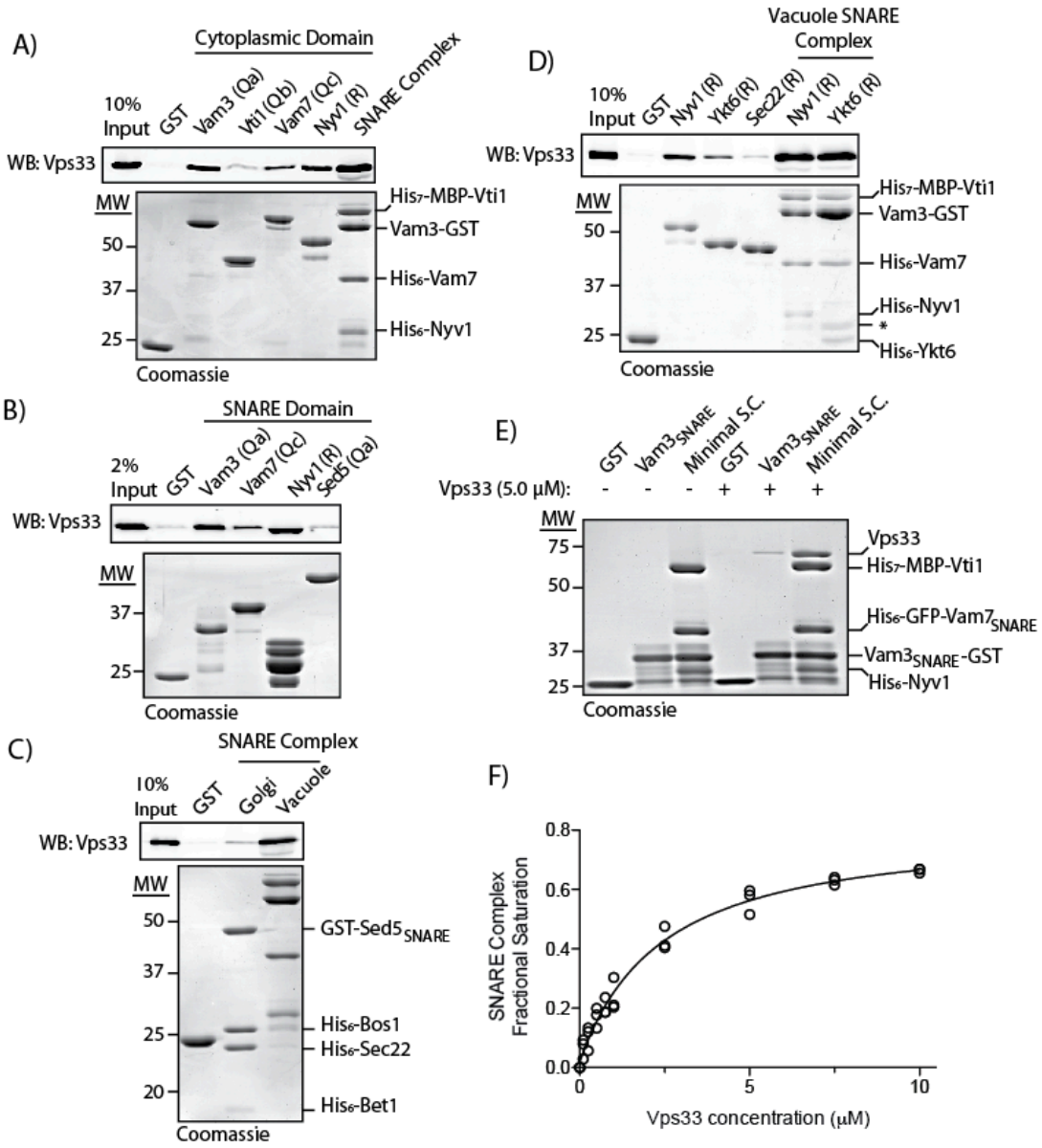

Figure 3.6. Purified Vps33 binds Qa, Qc, and R SNAREs, and vacuole SNARE complex
(A) Pulldown of purified Vps33 by cytoplasmic domains of vacuole SNAREs or quaternary vacuole SNARE complex. Equivalent loads of GST fusion proteins (~1 μM) were bound to GSH resin. Vacuole SNARE complexes were formed using 29 μg (~1 μM) purified Vam3-GST cytoplasmic and purified cytoplasmic domains of His7-MBP-Vti1, His6-Vam7, and His6-Nyv1. Purified Vps33 (10.5 μg, ~0.25 μM), was incubated for 2 h at 30˚ C with GST-fusion proteins, washed extensively, and eluted with 20 mM glutathione. Samples were separated by SDS-PAGE and analyzed by western blot for Vps33. (B) Pulldown of purified Vps33 by SNARE domains. 18 μg (~1 μM) of the GST-fusions to the SNARE domains of Vam3, Vam7, and Nyv1 were used to pull down purified Vps33. GST and SNARE domains of Sed5 were used as negative controls. (C) Comparison of purified Vps33 pulldown by Golgi or vacuole SNARE complexes. (D)

Pulldowns of purified Vps33 with GST-fusions to cytoplasmic domains of Nyv1 and Ykt6. Sec22 and GST were used as negative controls. SNARE complexes were formed as described for 3Q:R-Nyv1. For 3Q:R-Ykt6 complexes, a 2.5-fold greater amount of Vam3-GST was used to compensate for decreased SNARE complex formation with Ykt6. (E) Pulldown of 70 μg (~5 μM) Vps33 by GST, 12.8 μg (~2 μM) Vam3 SNARE domain (182-264), or ~2 μM minimal SNARE complex lacking the N-terminal domains of Vam3 and Vam7. (F) Binding curve for Vps33 to the minimal SNARE complex. A one-site binding model fit to data from three replicates results in an apparent Kd of 2.8 ± 0.2 μM (mean ± SEM; r2=0.98).

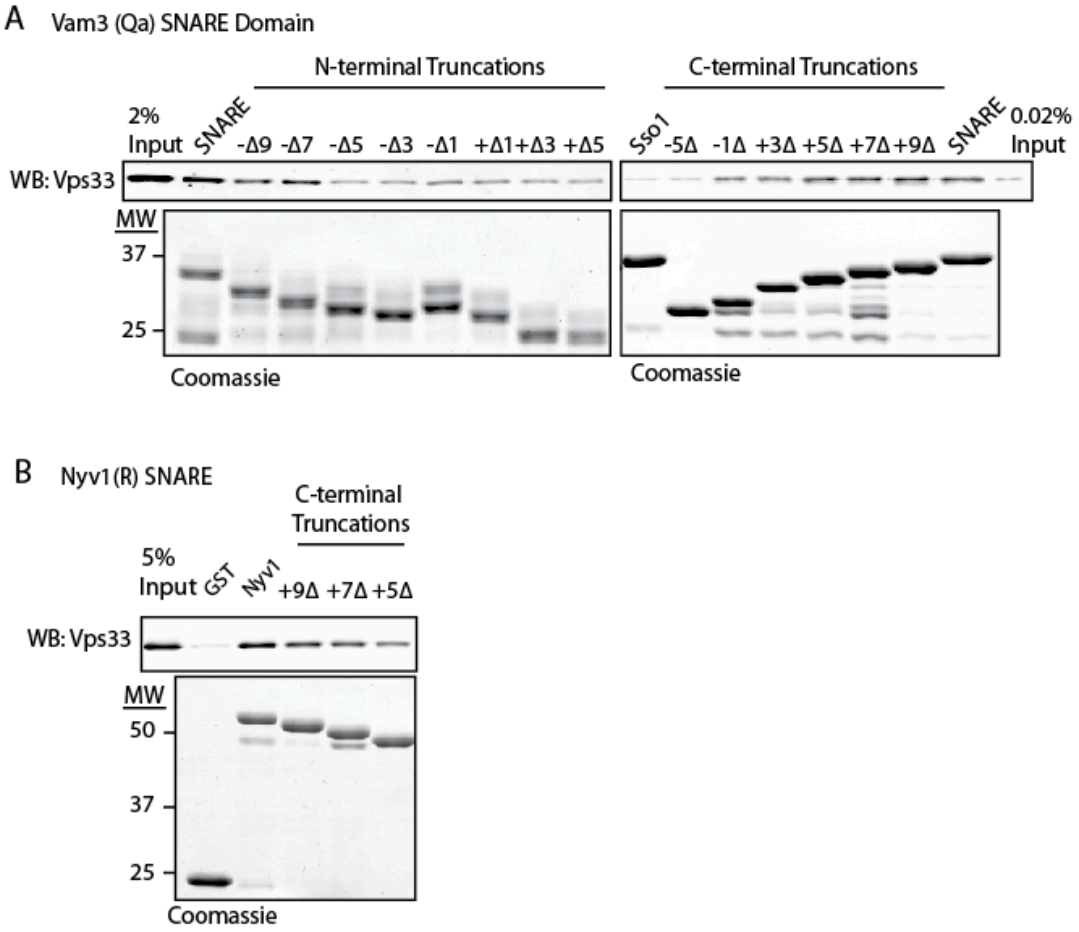

Figure 3.7. Mapping of Vps33 binding determinants on Vam3 and Nyv1 SNAREs
(A). Vam3 SNARE domain (182-264) was fused to GST at its C-terminus for a N-terminal truncations and the C-terminus for the N-terminal truncations. 18 µg (~1 µM) of GST-fusion protein was bound to GSH resin, incubated with 10.5 µg (~0.25 µM) of purified Vps33 for 2 h at 30˚C, washed three times with SNARE Assay buffer, and eluted with SA buffer supplemented with 20 mM glutathione. Eluates were separated by SDS-PAGE and analyzed by western blot for Vps33. (B) Nyv1 (1-231) cytoplasmic domain and the C-terminal truncation series were fused to GST at its N-terminus. 30 µg (~1 µM) of purified GST-fusion protein was incubated with GSH resin. 10.5 µg (~0.25 µM) of purified Vps33 was incubated with the GSH resin for 2 h at 30˚C, washed three times with binding buffer, and eluted. Bound fractions and 2% of the load relative to the bound were separated by SDS-PAGE and analyzed by western blotting for Vps33.

Table 1.

Vps33 Mutant	Species/ SM Family Member	Homolog/ Ortholog Mutation	Name	Phenotype	Paper
L75P	Human/ VPS33B	L30P	ARC syndrome	Multisystem disorder affecting the kidneys, liver, nervous system, and platelet function	Gissen et al., 2004
D88K	Yeast/ VPS33	D88K	Fusion Defect	Defect in content mixing and fusion	Pieren et al., 2010
I278N	Yeast/ SEC1	I249N	Sec1-36	Defects in growth and SNARE complex binding at restrictive temperature	Hashizume et al., 2009
R281A	Yeast/ SEC1	R252A	Sec1-78	No growth defect	Hashizume et al., 2009
G297V	Fly/ VPS33A	G249V	carnation	Defects in endocytic trafficking and pigment granules	Sevrioukov et al., 1999
D300E/ G	Mouse/ VPS33A	D251E	buff	Defects in melanosome morphology, hypopigmentation, and a mild platelet-storage pool deficiency; as the mice age, worsening motor defects, loss of Purkinje cells and reduction in size of the cerebellum	Suzuki et al., 2003; Chintala et al., 2009
F305L	Human/ VPS33A	I256L	HPS syndrome	Defects in the formation and maintenance of melanosomes, platlet-dense granules, and lyosomes result in albinism, bleeding disorder, and pulminary fibrosis	Suzuki et al., 2003
T553I	Yeast/ SLY1	T531I	Suppressor of Lethality of Ypt1	Suppressor of Lethality of Ypt1	Li et al., 2007
E653A	Yeast/ SEC1	E604A	Sec1-50	Defects in growth and SNARE complex binding at restrictive temperature	Hashizume et al., 2009

Table 2.

Vps33 Mutant	Growth at 30° C	Growth at 37° C	Growth at 37° C+5 mM $ZnCl_2$	Cargo Missorting at 30° C	Vacuole Morphology at 30° C
vps33Δ	√	No	No	Severe	C
WT	√	√	√	None	A
L75P	√	√	No	None	A
D88K	√	√	√	Detectable	A´
I278N	√	√	Slow	Detectable	A´
R281A	√	No	No	Severe	C
G297V	√	√	No	Moderate	B
D300E	√	√	√	None	A
D300G	√	√	No	Detectable	A´
F305L	√	√	√	None	A
T553I	√	√	Slow	Detectable	A´
E653A	√	No	No	Severe	C

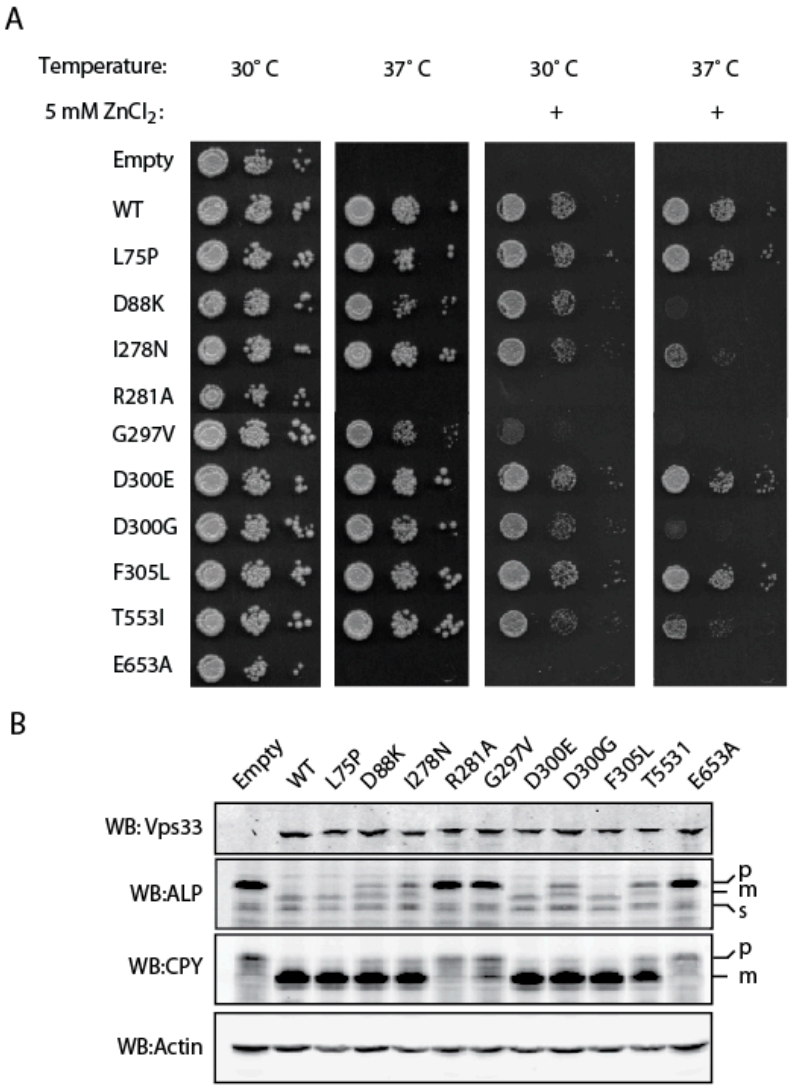

Figure 3.8. Characterization of Vps33 point mutants
(A) Cultures grown overnight at 24˚ C were plated onto SC-URA, YPD, or YPD+5mM ZnCl2 as 20-fold dilutions from 1.0 OD_{600} nm × mL. Plates were incubated for 48 h and imaged. B) Whole cell lysates were prepared from SEY6210 VPS33WT-ttx-GFPA207K and each of the mutant alleles. Cell lysates were separated by SDS-PAGE and analyzed by western blot.

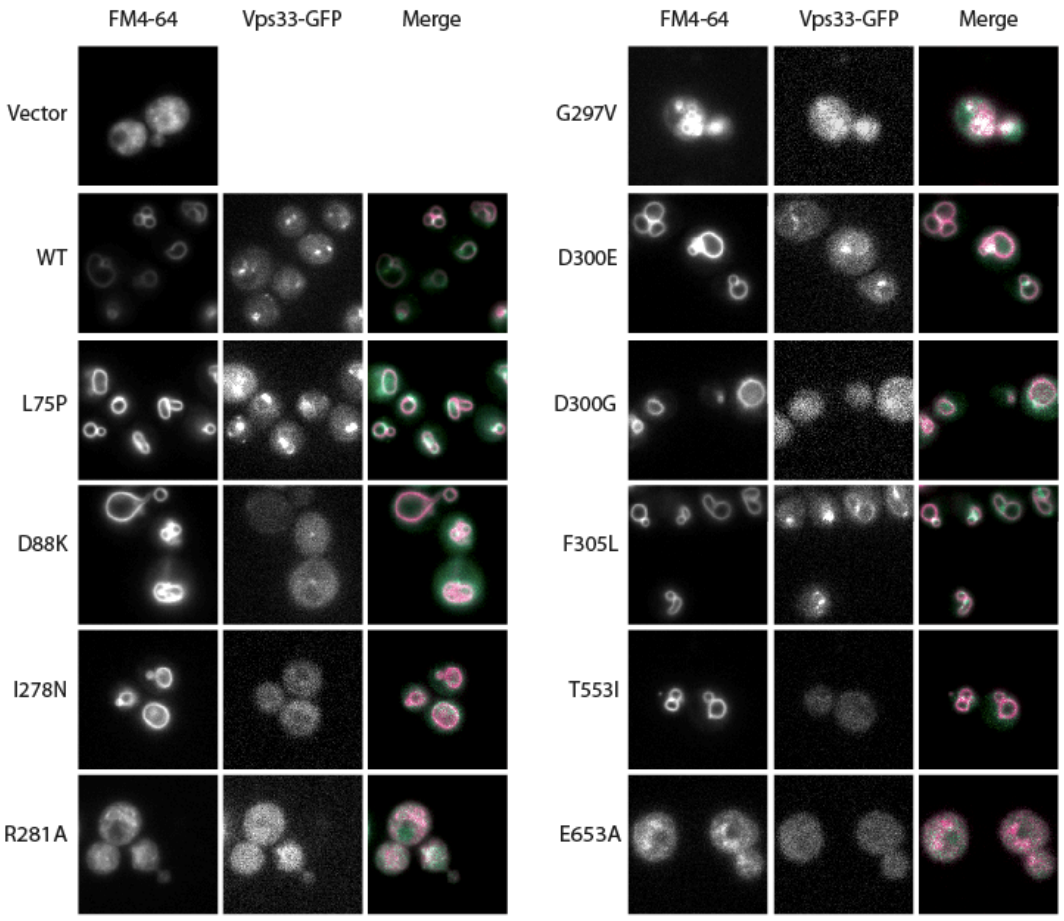

Figure 3.9. Vacuole morphology and Vps33-GFP localization
Strains were grown in minimal media to mid-log phase, and vacuoles were imaged by fluorescence microscopy after labeling with FM4-64

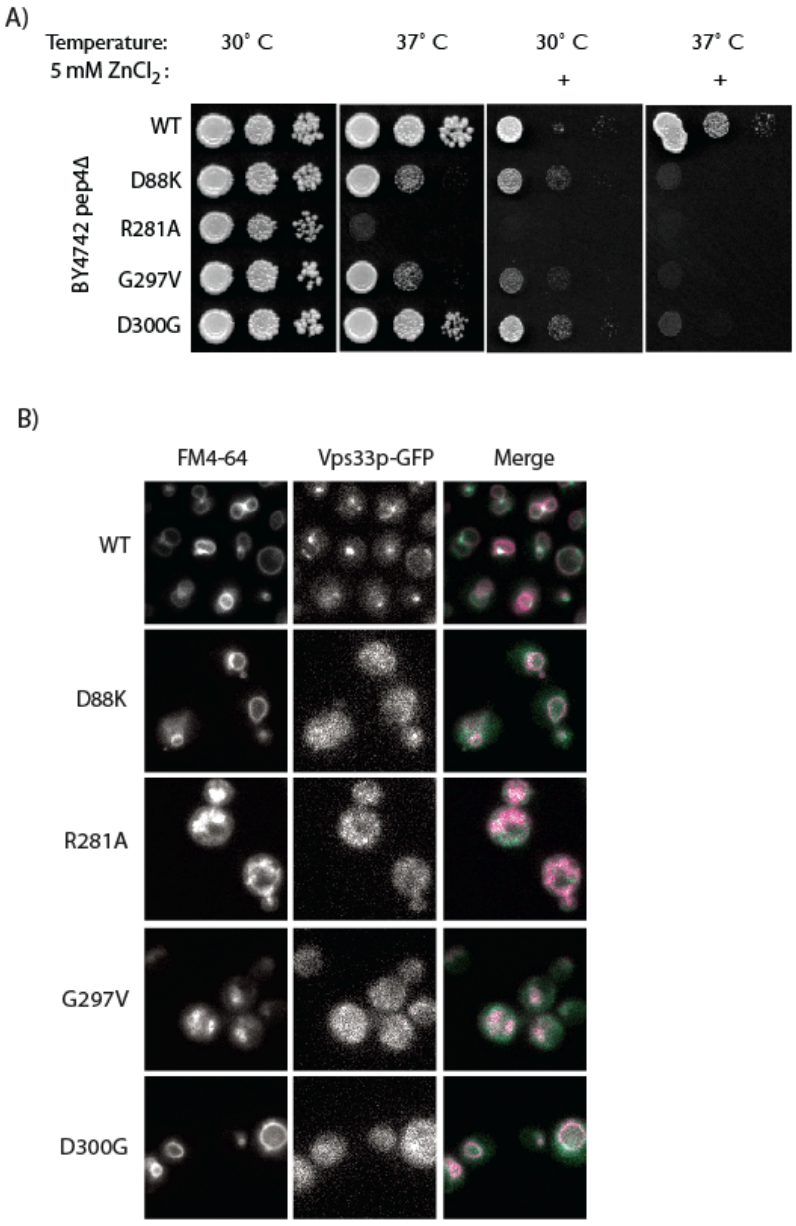

Figure 3.10. Characterization of chromosomal integrations of Vps33 point mutations
(A) Cultures grown overnight at 24˚ C were plated onto SC-URA, YPD, or YPD+5mM ZnCl2 as 20-fold dilutions from 1.0 OD_{600} nm × mL. Plates were incubated for 48 h and imaged. (B) Strains were grown in minimal media to late mid-log phase, and vacuoles were imaged by fluorescence microscopy after labeling with FM4-64.

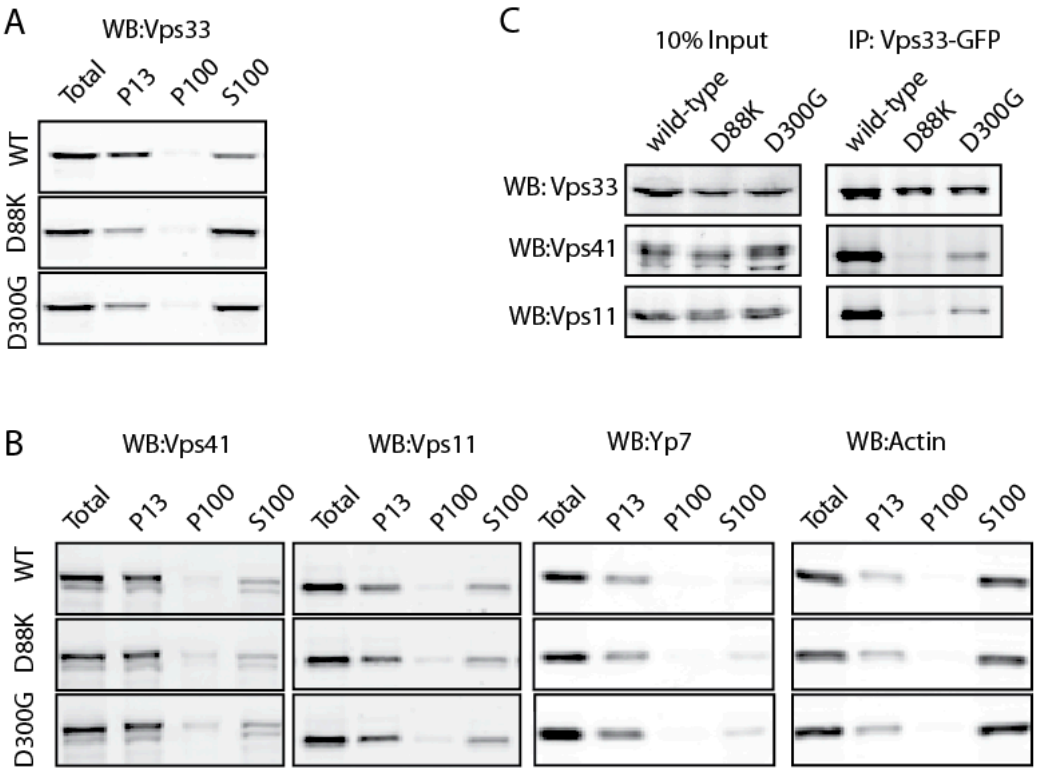

Figure 3.11. Vps33 mutations cause loss of steady state association with HOPS
(A) Subcellular fraction was performed using differential centrifugation with ~150 OD_{600} nm × mL. Spheroplasts were lysed and centrifuged to enrich for vacuoles (P13; 13,000 × g pellet); vesicles, endosomes and Golgi (P100; 100,000 × g pellet); and cytoplasm (S100; 100,000 × g supernatant). Fractions were separated by SDS-PAGE and analyzed by western blot for Vps33 (WB). (B) Subcellular fraction as in part A, with WB for HOPS subunits Vps41 and Vps11 and fractionation markers Ypt7 (found in the P13) and an actin subunit (found primarily in the S100). (C) Co-immunoprecipitation of HOPS complex with Vps33-GFP. Yeast detergent lysates from strains carrying a wild-type copy of Vps33-GFP, or the indicated Vps33 mutant, were incubated with Protein A resins covalently linked to an anti-GFP antibody. Input of the cell lysate is shown as 10% relative to eluate of the immunoprecipitation.

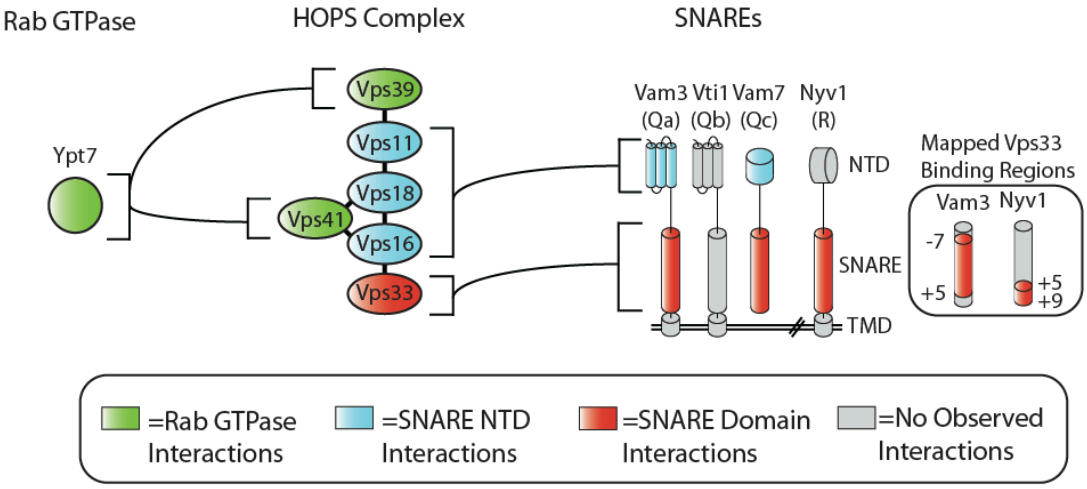

Figure 3.12. Summary of interactions between the Rab, HOPS, and SNAREs
Together with the published literature, our data suggest that several subunits of the HOPS complex coordinate binding of multiple SNARE domains. Vps33 directly binds the Qa, Qc, and R SNARE domains, while the N-terminal H_{abc} and PX domains of the Qa and Qc SNAREs are bound by other subunits within HOPS. Interactions of HOPS subunits Vps39 and Vps41 with the Rab Ypt7 have been demonstrated previously (Brett et al., 2008; Ostrowicz et al., 2010; Plemel et al., 2011)

Chapter Four — SM proteins cooperate with Sec17 to protect SNARE complexes from Sec18-mediated disassembly[3]

4.1 –Introduction

Intracellular trafficking must be regulated so that each organelle maintains its unique lipid and protein composition. The conserved protein machinery of membrane fusion plays a key role in ensuring trafficking fidelity (Wickner and Schekman, 2008). While some types of membrane fusion utilize additional proteins (e.g., neuronal exocytosis of synaptic vesicles), the fundamental process of cellular membrane fusion is conserved from yeast to humans (Sudhof and Rizo, 2011). At the core of this process are the universal factors Sec18/NSF (N-ethylmaleimide-sensitive factor) and Sec17/α-SNAP (soluble NSF attachment protein) and the compartment specific SNARE (SNAP receptors) and SM (Sec1/Munc18) proteins.

For membrane bilayers to fuse, SNARE proteins from apposed compartments must form a *trans*-SNARE complex (also called a SNAREpin). Formation of a four-helical complex between the SNARE domain from a R-SNARE (v-SNARE) and three SNARE domains from Q-SNAREs (t-SNAREs) is thought to drive bilayer fusion by coupling the free energy release of complex formation, via SNARE transmembrane domains, to deformation of the bilayers. After membrane fusion, Q- and R-SNAREs remain in a *cis*-SNARE complex in the newly fused compartment. For individual SNAREs of the *cis*-SNARE complex to participate in subsequent rounds of membrane fusion, the complex must be disassembled. The SNARE complex is first bound by the adapter protein Sec17/α-SNAP, which in turn recruits the AAA-family ATPase

[3] All experiments in **Chapter 4** were by performed by B.T.L with the exception of **Figure 4.3A**, which was contributed by Sheng-Ying Lo.

Sec18/NSF to disassemble the SNARE complex. While it is clear SM proteins play an essential role in SNARE-mediated membrane fusion, the mechanisms through which SM proteins act are still unclear and controversial (Rizo and Sudhof, 2012).

All four SM protein subfamilies (Sec1/Munc18, Sly1, Vps45, and Vps33) interact with SNAREs, and it is hypothesized that fusion-promoting abilities of SM proteins require their interaction with the *trans*-SNARE complex (Carr and Rizo, 2010). The best evidence to support this hypothesis is that many SM proteins have been shown to bind to the SNARE complex bundle, and it is likely that this is a conserved feature of SM proteins (Carr et al., 1999; Dulubova et al., 2007; Lobingier and Merz, 2012; Togneri et al., 2006; Xu et al., 2010b). Further evidence for a universal function for class I and class II SM proteins is offered by the observations that yeast Sec1 and metazoan Munc18 are able to accelerate the rate of *in vitro* SNARE-mediated liposome fusion (Scott et al., 2004; Shen et al., 2007). It is not currently clear how SM proteins accelerate the rate of *in vitro* membrane fusion, or if this is the essential role these proteins play in the cell.

A subset of SM proteins interacts with unpaired Qa SNAREs. Metazoan Munc18, human and yeast Vps45, and yeast Sly1 have strong affinities for their unpaired cognate Qa SNAREs, and are referred to here as class I SM proteins (Burkhardt et al., 2008; Carpp et al., 2006; Dulubova et al., 2002). This interaction involves a N-terminal motif in the Qa SNARE called the "N-peptide." Yeast Vps45, and metazoan Munc18 and Vps45, make contacts with the N-peptide while binding to an auto-inhibited form of the Qa SNARE in which the H_{abc} domain has folded back on the SNARE domain (Burkhardt et al., 2008; Furgason et al., 2009). Class II SM proteins, including yeast Sec1 and Vps33, have the greatest affinity for the four-helical SNARE complex bundle (Lobingier and Merz, 2012; Togneri et al., 2006). Interestingly, the cognate Qa SNAREs

of yeast Sec1 and Vps33 lack the N-peptide consensus sequence (Hu et al., 2007), and the crystal structure of Vps33 shows that this SM lacks an N-peptide binding pocket (Baker and Hughson, 2012).

In addition to the hypothesis that SM proteins function by directly accelerating membrane fusion, there is also support for the idea that SM proteins may have other, albeit potentially related, roles. It has been shown that the HOPS complex protects *trans*-SNARE complexes from Sec18-mediated disassembly *in vitro* (Xu et al., 2010a). Munc18, and its cofactor Munc13, allow SNARE-mediated lipsosome fusion occur in the presence of what would otherwise be inhibitory concentrations of NSF and α-SNAP (Ma et al., 2013). For both cases, it has been suggested that the synergy between the fusion promoting machinery (SM proteins, HOPS complex, Munc13) and SNARE disassembly machinery (Sec18/NSF and Sec17/α-SNAP) promote cognate, or on pathway, SNARE complex formation. Additional evidence for synergy among the universal factors Sec18/NSF and Sec17/α-SNAP and the compartment specific SNARE and SM proteins has been recognized by work with recent *in vitro* reconstitution assays of membrane fusion. These assays have shown that fusion proceeds most efficiently when SNARE disassembly machinery (Sec17/α-SNAP; Sec18/NSF) and SNARE assembly machinery (SM protein; Rab G proteins; effectors; tethers) work in tandem, and that addition of only SM proteins (or SM protein containing complexes) does not drive substantial amounts of membrane fusion (Ma et al., 2013; Ohya et al., 2009; Stroupe et al., 2009).

4.2 –Materials and Methods

Plasmid construction.

SNAREs and SM open reading frames were cloned as previously described (Lobingier and

Merz, 2012). In brief, the cytoplasmic domain of Vam3 (1-264) was cloned into pRSF-1b with no N-terminal tag and C-terminal GST separated from the SNARE by a TEV cleavage site. The full cytoplasmic domain of Sed5 (1-319), or a $Sed5_{SNARE}$ (170-319) construct lacking the N-peptide and Habc domain, were cloned into pGST-Parallel1. N-terminally His_6-tagged SNARE fusions were cloned into pHIS-Parallel1: Bos1 (1-222), Sec22 (1-188), Nyv1 (1-231). The SNARE domain of Vam7 (190-317) was fused in-frame to a His6-GFP-TEV sequence. Bet1 (1-123) and Vti1 (1-194) were cloned into pRSF-1b carrying an N-terminal His7-MBP tag. Full length Sly1 (1-667) was cloned for expression in pHIS-parallel1. Vps33 was cloned for expression in the insect cell/baculovirus system as described (Brett et al., 2008; Lobingier and Merz, 2012).

Protein Expression.

Vps33 was expressed and purified from insect cells as described (Lobingier and Merz, 2012). All other proteins were expressed in *E. coli* that harbored a pRIL codon-bias correction plasmid with the exception of Bos1. Bos1 was expressed in Rosetta2 pLys cells. Cells were inoculated at 0.05 OD_{600}, grown to 1.0-1.2 OD_{600} in Terrific Broth, and expression was induced with 100 μM IPTG for overnight expression at 21˚ C (His_6-Sly1, His_6-Nyv1 and His_7-MBP-Vti1, GST-$Sed5_{SNARE}$, His_6-Bos1, His_6-Bet1, His_6-Sec22), 500 μM IPTG for 4-5 h at 30˚ C (His_6-GFP-$Vam7_{SNARE}$), or 1 mM IPTG for 3 h at 37˚ C (Vam3-GST and GST-Sed5).

Protein Purification.

Cells expressing His-tagged proteins were lysed by sonication in Buffer A (50 mM HEPES, 200 mM NaCl, 10% w/v glycerol, 5 mM 2-meracptoethanol, 25 mM imidazole, 0.5 % TritonX-100, pH 7.4) supplemented with protease inhibitors. Cell lysates were clarified by centrifugation for 25 min at 18,500 × g at 4˚ C. The supernatant was incubated with Ni-NTA HP resin (GE

Heathcare) for 10 min at 4˚ C. The resins were washed extensively in Buffer A followed by washes in Buffer B (20 mM HEPES, 200 mM NaCl, 10 % w/v glycerol, 2 mM 2-mercaptoethanol, 35 mM imidazole, pH 7.4). His-tagged proteins were eluted from the resin with Buffer B supplemented with 400 mM imidazole, and then exchanged into Storage Buffer (20 mM HEPES, 200 mM NaCl, 10 % w/v glycerol, 2 mM 2-mercaptoethanol, pH 7.4) and snap frozen in liquid nitrogen. Cells containing the GST-tagged SNAREs were lysed in Storage Buffer supplemented with protease inhibitors and 5 mM EDTA, and the clarified lysate was frozen in liquid nitrogen.

Pulldowns.

SNARE complexes were formed by binding 125pmol of GST-SNARE (5.8 μg of GST-$Sed5_{SNARE}$ or 7.1 μg of Vam3-GST) to glutathione sepharose 4B resin (GE Healthcare) for 2 h at 4˚ C. Resins were wash twice with SM Assay Buffer (20 mM HEPES, 150 mM NaCl, 2 mM 2-mercaptoethanol, 0.05% (w/v) Anapoe-X-100 (also called Triton-X-100; Affymetrix), pH 7.4). A minimum of a five-fold molar excess of Qb-, Qc-, and R-SNAREs were incubated overnight at 4˚ C with the GST-SNARE. Unbound SNAREs were separated from SNARE complexes by washing the resins with SM assay buffer twice at 4˚ C and twice at 24˚ C (room temperature). Sec17, the SM protein, or both were added at the indicated concentration to binding reactions with a final concentration of the SNARE complex at 500 nM. Pulldowns were performed at the indicated temperature for 1 h, the resins were washed three times, and eluted with SM assay buffer supplemented with 20 mM reduced glutathione, pH 7.4. For the assays examining the temperature dependence of protein binding to SNARE complexes, pulldowns were performed in thin-walled tubes in a MJ Mini thermocycler (Bio Rad). The conditions and concentrations were identical to all other pulldowns reported in this paper, except that the samples were not rocked

during binding. We observed no change in the efficiency of binding between the two methods at the same temperatures. Samples were boiled in SDS-loading buffer, and separated on 12% SDS-PAGE gels (for experiments using Sly1) or 8% SDS-PAGE gels (for experiments using Vps33).

Imaging and Quantification.

Unless otherwise indicated, all gels shown in the paper were stained with Coomassie brilliant blue and imaged on a 4490 transmission scanner (Epson). All experiments were repeated three times or more; representative gels are shown. Protein quantification on polyacrylamide gels was performed using SYPRO-Ruby stain (Invitrogen), and the gels were imaged using a Gel Doc XR+ (Bio-Rad). Data from three experiments (Sly1) or two experiments (Vps33) were plotted as fractional saturation of ligand binding to the SNARE complex relative the total concentration of ligand in solution. As indicated, some experiments with Vps33 were done twice rather than 3 or more times due to limitations in the amount of available protein. Binding EC_{50} values and Hill coefficients were estimated by nonlinear fitting (GraphPad Prism 5) of a single-site binding model with Hill coefficient to the data. Two-site models did not substantially improve the quality of the fits.

SNARE complex disassembly assays.

SM assays buffer was supplemented with 1 mM ATP, 2 mM $MgCl_2$. Unless otherwise noted, the SM protein and Sec17 were allowed to bind to SNARE complexes for 1 h at 30 ˚C before addition of Sec18. Disassembly reactions were then incubated for the indicated times and terminated by washing the samples in ice-cold SM Assay Buffer. Remaining resin-bound proteins were eluted with SM Assay Buffer containing 20 mM reduced glutathione, pH 7.4 at 24 ˚C (room temperature).

4.3 –Results

Sec17 enhances the affinity of SM proteins for the SNARE complex

We have recently reported that the class II SM protein Vps33 has the greatest affinity for the quaternary SNARE complex bundle (Lobingier and Merz, 2012). As Sec17/α-SNAP also binds to the core SNARE complex, we wanted to investigate whether Vps33 and Sec17 compete for common sites on the SNARE complex (Chang et al., 2012; Hanson et al., 1997; Hohl et al., 1998; Marz et al., 2003). Vacuolar SNARE core complexes were formed on a Vam3-GST (Qa-SNARE) on a glutathione-sepharose support. Unexpectedly, binding of Vps33 to vacuolar SNARE complex was dramatically enhanced in the presence of Sec17 (**Figure 4.1A**). Using Sypro-Ruby staining, the amount of Vps33 and Sec17 bound to SNARE complexes under saturating conditions was quantified. We estimate a 1:3:1 stoichiometry of SNARE complex:Sec17:Vps33 (**Figure 4.1B**).

We next measured the EC_{50} of Vps33 binding in the absence and presence of Sec17, and found that Sec17 quadrupled the apparent affinity of Vps33 for the SNARE complex (**Figure 4.1C**). In GSH binding assays using previously established conditions (Lobingier and Merz, 2012), we obtain ~65 % saturation of vacuolar SNARE complex with 10 μM Vps33. Using a reduced amount of SNARE complex, we obtained 90 % saturation with the same amount of Vps33. The EC_{50} for Vps33 binding to the SNARE complex in this system as 1.7 ± 0.1 μM. When we added Sec17 during the binding reaction, the EC_{90} for Vps33 was reduced to 2.5 μM. Fitting of a one-site binding model with Hill slope gave an EC_{50} of 0.4 ± 0.02 μM and Hill cofficient of 1.1 ± 0.1. Together, these data suggest several characteristics of these SM/Sec17/S.C. co-complexes in our assays: the presence of Sec17 on SNARE complexes resulted in more than a 4-fold enhancement in Vps33 binding; there is only one binding site for

an SM protein per Sec17-bound SNARE complex; there is little measurable cooperativity in SM protein binding.

As formation of a co-complex between SNAREs, Sec17, and SM protein is unprecedented, we wanted to test whether similar results might be obtained using a divergent SM protein and its cognate SNARE complex. We chose the SM protein Sly1, as it is a well-studied class I SM protein that associates strongly with the N-peptide but does not exhibit binding to the "closed" conformation of the Qa SNARE (Peng and Gallwitz, 2002; Peng and Gallwitz, 2004). To examine binding of Sly1 to the core SNARE complex, we used a truncated Sed5 (Qa SNARE) lacking its N-peptide and H_{abc} sequences. We found that very little Sly1 is retained on resins with SNARE complexes alone, and that Sly1 binding is dramatically enhanced by Sec17 (**Figure 4.2A**). As with Vps33, we found that the stoichiometry of these complexes was 1:3:1 SNARE complex:Sec17:Sly1 (**Figure 4.2B**). In fact, we detected little or no binding of Sly1 to Golgi SNARE complexes at Sly1 concentrations up to 15 μM (**Figure 4.2C**). When Sec17 was present, however, there was 90% saturation of SNARE complex at 10 μM Sly1 (EC_{50} 1.5 ± 0.1 μM, Hill coefficient 1.1 ± 0.04). Thus, for both SM proteins examined, Vps33 and Sly1, binding to SNARE core complexes is strongly enhanced by Sec17. Furthermore, the binding of Sly1 to SNARE complexes was strongly dependent on the Sec17 concentration (**Figure 4.2D**). Importantly, Sec17 does not associate with a binary complex of full-length Sed5 and Sly1, which is mediated through the Sed5 N-peptide (**Figure 4.2D**).

SM protein makes contacts with the SNARE complex and Sec17

The experiments presented so far suggest that the SMs Vps33 and Sly1 have greater affinity for a Sec17-bound SNARE complex than a SNARE complex alone. It is unclear, however, if the SM protein is contacting Sec17, the SNARE complex, or both. To test for a

direct affinity between SM proteins and Sec17, we bound GST-tagged SMs to GSH and tested its ability to bind Sec17, cognate SNARE complexes, or both (**Figure 4.3A**). We were not able to detect any binding between the Vps33 and Sec17 except when vacuolar SNARE complex was present. Thus, Vps33 and Sec17 do not have detectable affinity for each other in the absence of SNARE complexes. While we do detect come retention of Sec17 by GST-Sly1 in the absence of SNARE complexes, the addition of SNARE complexes increases the pulldown of Sec17, which is consistent with our other observations. Given that we see no association between His6-Sly1 bound by the Sed5 N-peptide and Sec17 (**Figure 4.2D**), we suggest that the observed retention of Sec17 by GST-Sly1 is a particular attribute of this GST-tagged protein.

As three copies of Sec17 bind each SNARE complex, it is possible that these SM proteins function in a manner analogous to Sec18 (**Figures 4.1B and 4.2B**). Sec18 has little affinity for SNARE complexes or for a single copy of Sec17, but has higher affinity for multiple copies of Sec17, especially when they are bound to the SNARE complex. To test this model, we assayed binding of each SM to cognate and non-cognate SNARE complexes (**Figure 4.3B**). If the SM contacts only Sec17 trimer bound to SNARE complexes, the SM protein should show no selectivity between cognate and non-cognate SNARE complexes bound to Sec17. We found that Sly1 shows strong selectivity for Sec17-bound cognate SNARE complexes (**Figure 4.3B**). Interestingly, while the amount of Sly1 retained by non-cognate SNARE complexes was minimal, it slightly increased when Sec17 was present. Together, the data strongly suggest that Sly1 makes contacts with both the SNARE complex and Sec17.

As with Sly1, we found that Vps33 showed strong specificity for Sec17-bound cognate SNARE complexes (**Figure 4.3C**), indicating that Vps33 makes contacts with the SNARE complex in the presence of Sec17. To test if Vps33 makes contacts with Sec17, we again

examined binding to non-cognate complexes. Again, while there was less retention of Vps33 by non-cognate complexes than cognate complexes, Vps33 to non-cognate complexes increased slightly when Sec17 was present. Together these data suggest that Vps33, like Sly1, makes contacts with both SNARE complex and SNARE-bound Sec17.

SM binding to SNARE complexes is temperature dependent

While characterizing the co-complex of SM, Sec17, and SNARE complex, we observed that the SM proteins had several interesting properties. For example, the rate at which Sly1 associated with the Sec17-bound SNARE complex was much slower than the rate that it associated with the Sed5 N-peptide **(Figure 4.4A**). At 90% saturating Sly1 concentrations (EC_{90}), we found that the half-time for maximal binding was 20 min for Sly1 associating with the Sec17-bound SNARE complex, but <1 min for Sly1 binding to the Sed5 N-peptide. Similarly, an EC_{90} of Sec17 reached maximal binding to the Golgi SNARE complex in under a minute. Interestingly, the rate at which maximal binding was reached was extremely temperature dependent for the SM protein. At an EC_{90} for Sly1, maximal binding occurs in ~1 h at 30˚ C, and 4 hours at 24˚ C (**Figure 4.4B**). Almost no binding of Sly1 to the Sec17-bound SNARE complex occurred at 4˚ C (**Figure 4.4.B**). It is important to note that the binding of Sec17 to the SNARE complex showed no large variations in binding efficiency across the tested temperatures (**Figure 4.4C**). To further examine the temperature dependence of binding, we quantified the binding of Sly1 to the Sed5 N-peptide or the Sec17-bound SNARE complex (**Figure 4.4D**). While we found that binding of the former was relatively temperature independent, the binding of Sly1 to the Sec17-bound SNARE complex dropped from 90% to 10% of complexes bound as the temperature was decreased from 30˚ C to 20˚ C. In contrast, a constant amount of Sly1 bound to the Sed5 N-peptide across the temperature range (**Figure 4.4D**).

A similar pattern was observed for Vps33. While Sec17 bound to the SNARE complex at 4˚ C, little Vps33 binding was detected at the same temperature (**Figure 4.4E and F**). Quantification of Vps33 binding to the SNARE complex, or the Sec17-bound SNARE complex, showed that both interactions are highly temperature dependent (**Figure 4.4F**). In the absence of Sec17 Vps33 shows greater binding to cognate SNARE complexes compared to Sly1. In binding reactions containing only Vps33 and cognate SNARE complex, the binding dropped from 60% to 20 % when the temperature was decreased ten degrees from 32.5˚ C to 22.5˚ C. The 10˚ C decrease in binding temperature reduced the Vps33 association to the Sec17-bound SNARE complex from 95% to 45%.

When comparing Vps33 to Sly1, we observed that retention of Sly1 on a Sec17-bound SNARE had a much steeper temperature dependence than Vps33 to its cognate Sec17-bound SNARE complex (**Figure 4.4D and F**). This is consistent with our observations that Vps33 could bind directly to the SNARE complex at 30˚ C, while Sly1 showed little binding at 30˚ C unless Sec17 was present. Minimal binding was observed between both SM proteins and their cognate Sec17-bound SNARE complexes at temperatures below 10˚ C. The unusual and extremely strong temperature dependence of Vps33 and Sly1 binding to SNARE complexes, and the slow on-rates of these binding reactions, raise the possibility that these SM proteins must undergo a significant conformational change to become competent for SNARE complex binding (see Discussion)

SM proteins shield cognate SNARE complexes from Sec18-mediated disassembly

The Vps33-containing HOPS complex can protect *trans*-SNARE complexes from Sec18 mediated disassembly, though it is not known which subunit(s) of HOPS are responsible for this activity (Xu et al., 2010a). Moreover, Munc18 and Munc13 promote membrane fusion in the

presence of otherwise inhibitory concentrations of NSF and α-SNAP (Ma et al., 2013). To examine if the SM could protect SNARE complexes from Sec18-mediated disassembly, we compared the rates of disassembly of the SNARE-Sec17-SM co-complex to a SNARE-Sec17 complex lacking the SM protein. We found that Sly1 and Vps33 reduced the rate of Sec18-mediated disassembly (**Figure 4.5A and B**).

4.4 –Discussion

A major mystery in the field is what essential mechanistic function(s) the SM protein performs during a membrane fusion event. It is clear from reconstitution of SNARE-mediated liposome fusion that SM proteins alone are sufficient to accelerate the rate of membrane fusion (Rathore et al., 2010; Scott et al., 2004; Shen et al., 2007; Shen et al., 2010). However, more recent reconstitution efforts show that the SM protein, or SM protein containing complex, do not drive membrane fusion alone, and synergize with additional factors including Rabs, tethers, and Sec17/ α-SNAP and Sec18/NSF (Ma et al., 2013; Ohya et al., 2009; Stroupe et al., 2009). It is likely that these differences in the ability of an SM protein to directly stimulate SNARE-mediate liposome fusion are due to differences starting conditions, protein concentrations, and lipid composition than inherent differences in molecular activity of the proteins involved. In the context of these studies, however, our data suggests that in addition to directly acting on the SNARE complexes to accelerate membrane fusion, the SM promotes membrane fusion indirectly by acting cooperatively with Sec17 to protect cognate SNARE complexes from disassembly.

Wholly unexpectedly, Sec17 enhances the ability of the SM protein to bind their cognate SNARE complex. As our data shows that both Sly1 and Vps33 retain their selectivity for cognate

SNARE complexes, we suggest a model in which the SM protein makes cooperative contacts with both Sec17 and the core SNARE complex bundle. Studies of the HOPS complex on isolated vacuoles showed that at steady state, the Vps33-containing HOPS complex and Sec17 are present on different populations of cis-SNARE complexes (Collins et al., 2005). Likely, the majority of SNARE complexes in these assays are *cis*-SNARE complexes. As our assays use only the soluble domains of the SNAREs, it is unclear if the co-complex of SM/S.C./Sec17 can form on *cis*- or *trans*-SNARE complexes in the cell. Furthermore, recent work has shown that N-terminal residues on α-SNAP penetrate the membrane, thereby increasing the apparent affinity of α-SNAP for the SNARE complex. It is not known if this would alter the formation of the co-complexes studied here (Winter et al., 2009). Further studies will be required to address these questions.

Vps33 was able to bind cognate SNARE complexes in our assays in the absence of Sec17, albeit less well than when Sec17 was present. Sly1, however, only associated with SNARE complexes in the presence of Sec17. As Sly1 showed selectivity for its Sec17-bound cognate SNARE complex, we infer that Sly1, like other SM proteins, directly contacts the SNARE complex. It is plausible that the lower relative affinity of Sly1 for the SNARE complex bundle is due to the removal of the high affinity localization domain in the N-terminus of Sed5, the N-peptide. As Sly1 binds the N-peptide of Sed5 with nanomolar affinity, it was necessary in our studies to remove the N-peptide to study binding of Sly1 to the SNARE complex bundle (Grabowski and Gallwitz, 1997). Further studies will be required to examine if Sly1 binds the SNARE bundle more readily when bound to the Sed5 N-peptide, either through an increased local concentration, allosteric activation, or both mechanisms.

In our assay system, the binding of SM proteins to the SNARE complex, or the Sec17-bound SNARE complex, is highly temperature dependent. As with the synergy of SM's and Sec17, this is a wholly unanticipated finding. Classically, the dependence of enzyme activity over a range of temperatures can be analyzed as an Arrhenius plot, and non-linearity in the plot has been correlated with a conformational change requiring a large activation energy. While we were examining steady-state protein binding and not enzymatic rate, an Arrhenius-style plot could still be used to examine protein binding across a range of temperatures. As we used near saturating concentrations for the SM protein (EC_{90}) binding to the Sec17-bound SNARE complex, we examined the linearity at temperatures below 27.5˚ C. We find that Vps33 binding to SNARE complexes and Vps33 or Sly1 binding to Sec17-bound complexes is non-linear. Importantly, Sec17 binding to the SNARE complex was linear across the temperature range studies, as was Sly1 binding to the N-peptide. This suggests that temperature dependent binding event did not involve the region of the SNARE complex bound by Sec17, or the portion of Sly1 that interacts with the Sed5 N-peptide. It is hypothesized that central cavity of the SM protein interacts with the SNARE complex, and that access to this cavity may require the SM protein to undergo a conformational change (Bar-On et al., 2011; Bracher and Weissenhorn, 2001). Our data is consistent such a model. It should be noted that we cannot formally exclude alternatives models in which the temperature dependent process involves regions of the SNARE complex that the SM protein, but not Sec17, binds.

We also report that the SM proteins Sly1 and Vps33 partially protect cognate SNARE complexes from Sec18-mediated disassembly, even when Sec17 is bound in 3:1 stoichiometry to the SNARE complex. This is not an absolute blockade of Sec18 activity, but rather a kinetic protection—SNARE complexes bound by a SM protein are disassembled more slowly than

complexes without a SM. Our data suggest two possible models for the mechanistic basis of the kinetic protection. In the first model, the SM protein competes directly competes for Sec18-binding sites on the SNARE complex, Sec17, or both. In an alternative model, the SM protein alters the conformation of the Sec17 trimer so that Sec17 cannot properly engage, and activate, the ATP-dependent mechanochemical cycle of Sec18.

It is unclear from our *in vitro* data if the SM proteins protect *trans*- or *cis*-SNARE complexes in the cell. For several reasons, it seems most likely that the functionally relevant target of SM protection would be the pre-fusion *trans*-SNARE complex. First, *trans*-SNARE complexes must fully zipper to drive membrane fusion, and premature disassembly by Sec18 would stop membrane fusion. Second, multiple rounds of membrane fusion require that the post-fusion *cis*-SNARE complex be disassembled. There is evidence that it the Vps33-containing HOPS complex protects trans-SNARE complexes from disassembly on isolated organelles and on liposomes (Xu et al., 2010a). It has also been shown that overexpression of NSF in fly causes cellular defects and a reduction in steady-state SNARE complexes, indicating that NSF activity is limiting *in vivo* (Babcock et al., 2004). Further studies will be required to see whether *trans*-SNARE complexes in are accessible to Sec18/NSF disassembly in the cell, and whether this is true for all systems or only for a subset of intracellular trafficking pathways.

SM-mediated protection of cognate *trans*-SNARE complexes from Sec18/NSF-mediated disassembly suggests a model by which SNARE complexes are kinetically proofread. In this model, the SM protein binds and protects only cognate SNARE complexes, resulting in non-cognate SNARE complexes being preferentially disassembled by NSF. In the simplest models of function, the SM protein might not even distinguish between *trans*- and *cis*-SNARE complexes. As the *trans*-SNARE complex is a much shorter-lived species in the cell than the *cis*-SNARE

complex, protection of the former could lead to productive fusion events while protection of the latter only delays disassembly (Sudhof and Rizo, 2011).

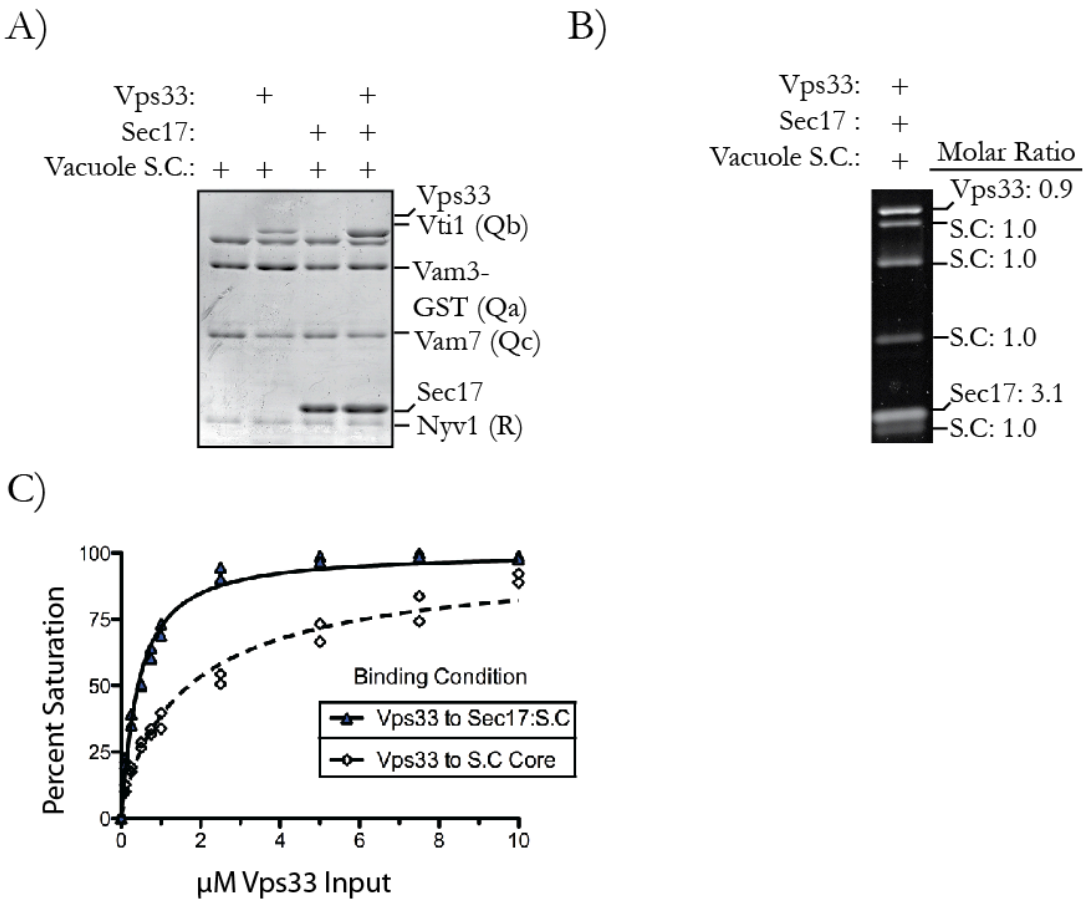

Figure 4.1. Sec17 enhances the affinity of Vps33 for the SNARE complex.
(A) 500 nM SNARE complex was formed on Vam3-GST. As indicated, 2.5 µM Vps33, 20 µM Sec17, or both proteins were added to SNARE complex for 1 h at 30 ˚C. Bound material was separated by SDS-PAGE and visualized with Coomassie Brilliant Blue. (B) 500 nM SNARE complex was formed was Vam3-GST. 2.5 µM Vps33 and 20 µM Sec17 were incubated for 1 h at 30˚ C. Bound material was separated by SDS-PAGE and visualized with SYPRO-Ruby. (C). 500 nM SNARE complex was formed on Vam3-GST. 20 µM Sec17, and the concentration of Vps33 indicated, was incubated for 1 h at 30 ˚C. Bound material was separated by SDS-PAGE and visualized with SYPRO-Ruby. Fractional saturation of total SNARE complex binding sites was plotted as a fraction of total Vps33 in the reaction. A one-site model with Hill coefficient was fit to the data using Graph Pad.

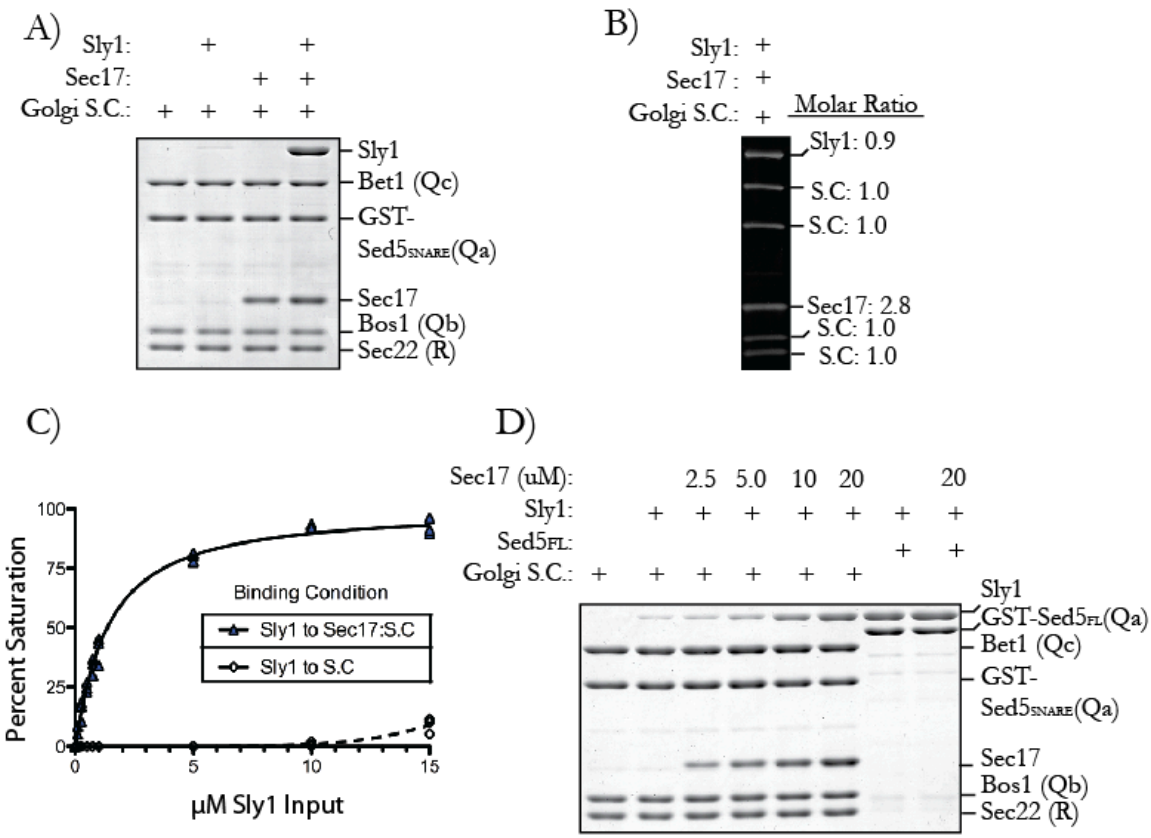

Figure 4.2. Sec17 enhances the affinity of Sly1for the SNARE complex.
(A) 500 nM SNARE complex was formed on GST-Sed5 lacking the N-peptide Habc domain ($Sed5_{SNARE}$). As indicated, 10 μM Sly1, 20 μM Sec17, or both proteins were added to SNARE complex for 1 h at 30 ˚C. Bound material was separated by SDS-PAGE and visualized with Coomassie Brilliant Blue. (B) 500 nM SNARE complex was formed was GST-$Sed5_{SNARE}$. 10 μM Sly1 and 20 μM Sec17 were incubated for 1 h at 30˚ C. Bound material was separated by SDS-PAGE and visualized with SYPRO-Ruby. (C). 500 nM SNARE complex was formed on GST-Sed5SNARE. 20 μM Sec17, and the concentration of Sly1 indicated, was incubated for 1 h at 30 ˚C. Bound material was separated by SDS-PAGE and visualized with SYPRO-Ruby. Fractional saturation of total SNARE complex binding sites was plotted as a fraction of total Sly1in the reaction. A one-site model with Hill coefficient was fit to the data using Graph Pad. (D) 500 nM SNARE complex was formed was GST-$Sed5_{SNARE}$. 500 nM GST-Sed5 containing the N-peptide sequence ($Sed5_{FL}$) was bound to GSH resin. 10 μM Sly1was incubated with the indicated amount of Sec17 for 1 h at 30 ˚C. Bound material was separated by SDS-PAGE and visualized with Coomassie Brilliant Blue.

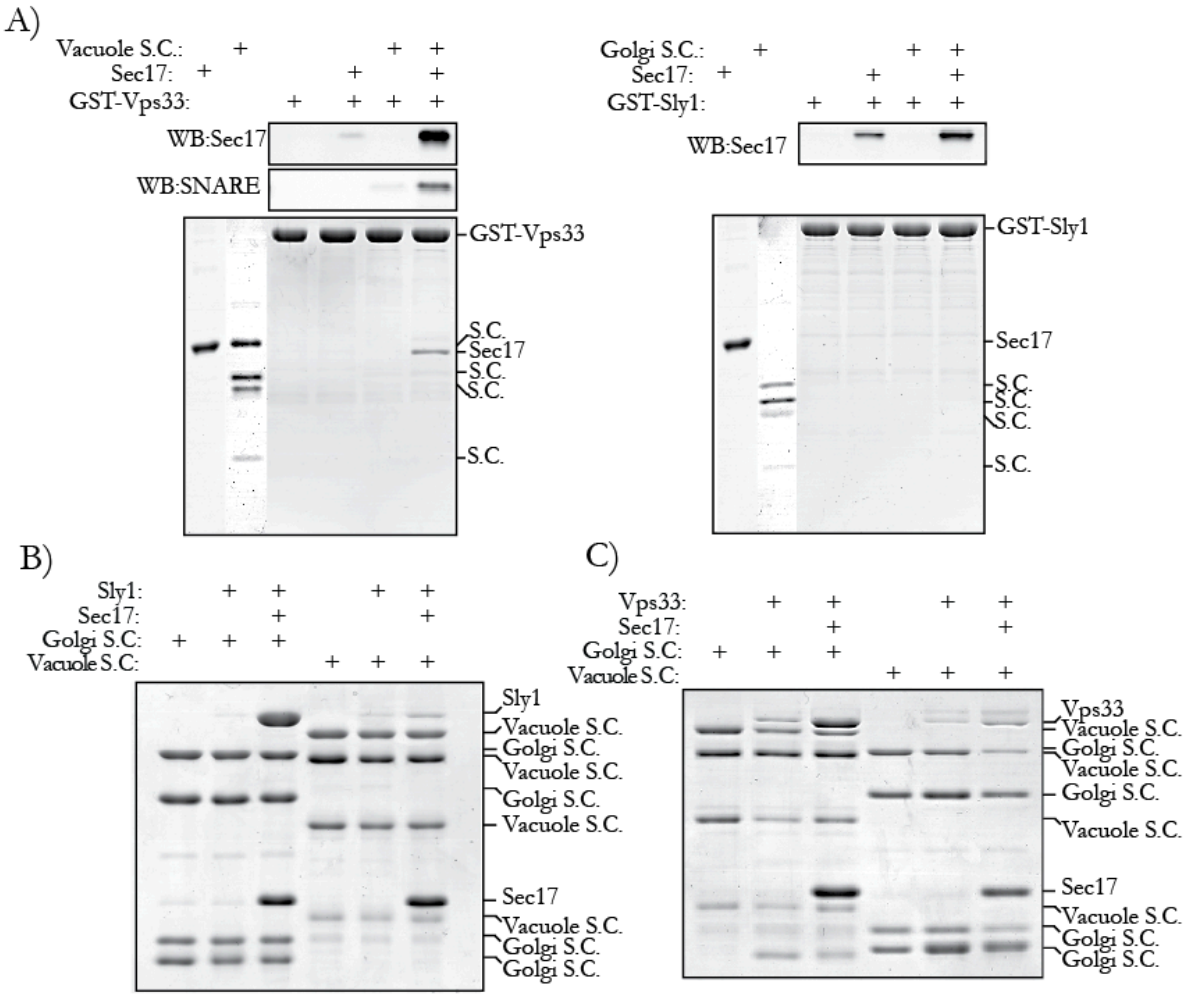

Figure 4.3. SM proteins show selectivity for Sec17-bound cogante SNARE complexes. (A) 500 nM GST-SM was bound to GSH resin, and incubated with 20 μM Sec17, SNARE complex, or both. Bound material was separated by SDS-PAGE and visualized with Coomassie Brilliant Blue or western blotting for Sec17 or a SNARE (Nyv1). (B) 500nM SNARE complex was formed on non-cognate GST-Sed5 lacking the N-peptide Habc domain ($Sed5_{SNARE}$) or Vam3-GST. As indicated, 10 μM Sly1, 20 μM Sec17, or both proteins were added to SNARE complex for 1 h at 30 ˚C. Bound material was separated by SDS-PAGE and visualized with Coomassie Brilliant Blue. (C) 500nM SNARE complex was formed on cognate Vam3-GST or non-cognate GST-Sed5 lacking the N-peptide Habc domain ($Sed5_{SNARE}$). As indicated, 2.5 μM Vps33, 20 μM Sec17, or both proteins were added to SNARE complex for 1 h at 30 ˚C. Bound material was separated by SDS-PAGE and visualized with Coomassie Brilliant Blue.

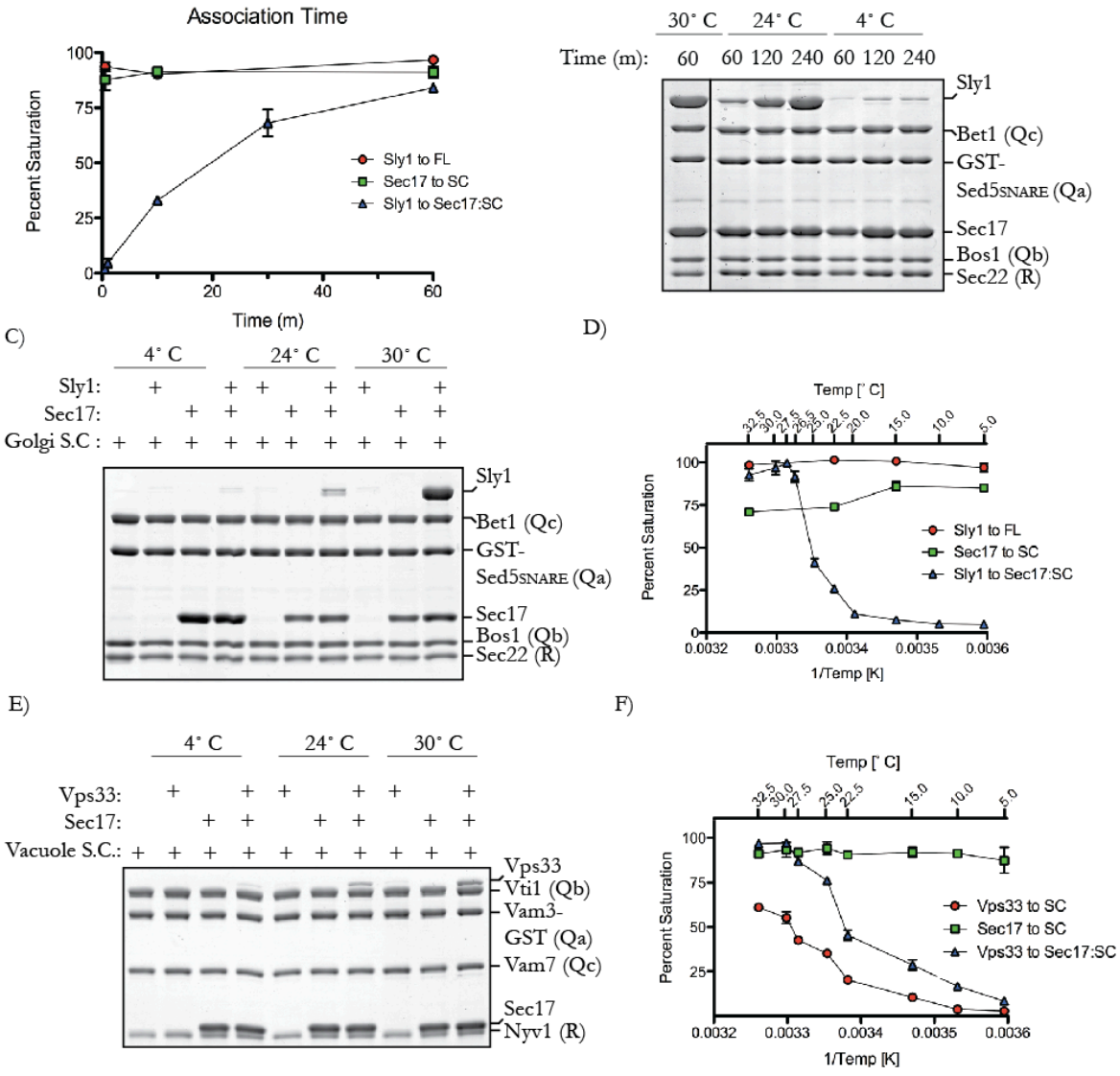

Figure 4.4. Binding of SM proteins to SNARE complexes is temperature dependent. (A) 500nM SNARE complex was formed on GST-Sed5 lacking the N-peptide Habc domain ($Sed5_{SNARE}$). 10 µM Sly1 and 20 µM Sec17 were incubated with the SNARE complex at 30˚ C for the indicated time. For Sec17 binding to the SNARE complex, an EC90 of 7 µM Sec17 was used in the binding assays. 500 nM GST-Sed5 containing the N-peptide sequence ($Sed5_{FL}$) was bound to GSH resin and incubated with 6 µM Sly1. Bound material was separated by SDS-PAGE and visualized with SYPRO-Ruby. (B) 500nM SNARE complex was formed on GST-Sed5 lacking the N-peptide Habc domain ($Sed5_{SNARE}$). 10 µM Sly1 and 20 µM Sec17 were incubated with the SNARE complex for the indicated time and temperature. Bound material was separated by SDS-PAGE and visualized with Coomassie Brilliant Blue. (C) 750 nM SNARE complex was formed on GST-Sed5 lacking the N-peptide Habc domain ($Sed5_{SNARE}$). As

indicated, 12 μM Sly1, 12 μM Sec17, or both proteins were added to SNARE complex for 2 h at the indicated temperature. (D) 500 nM SNARE complex was formed on GST-Sed5$_{SNARE}$. 20 μM Sec17, 10 μM Sly1 indicated, was incubated for 1 h at the indicated temperature. Bound material was separated by SDS-PAGE and visualized with SYPRO-Ruby. Fractional saturation of total SNARE complex binding sites was plotted against the inverse temperature. (E) 750 nM SNARE complex was formed on Vam3-GST. As indicated, 1 μM Vps33, 2 μM Sec17, or both proteins were added to SNARE complex for 2 h at the indicated temperature. Bound material was separated by SDS-PAGE and visualized with Coomassie Brilliant Blue. (F) 500 nM SNARE complex was formed on Vam3-GST. 20 μM Sec17, and the concentration of Vps33 indicated, was incubated for 1 h at 30 ˚C. Bound material was separated by SDS-PAGE and visualized with SYPRO-Ruby. Fractional saturation of total SNARE complex binding sites was plotted against the inverse temperature.

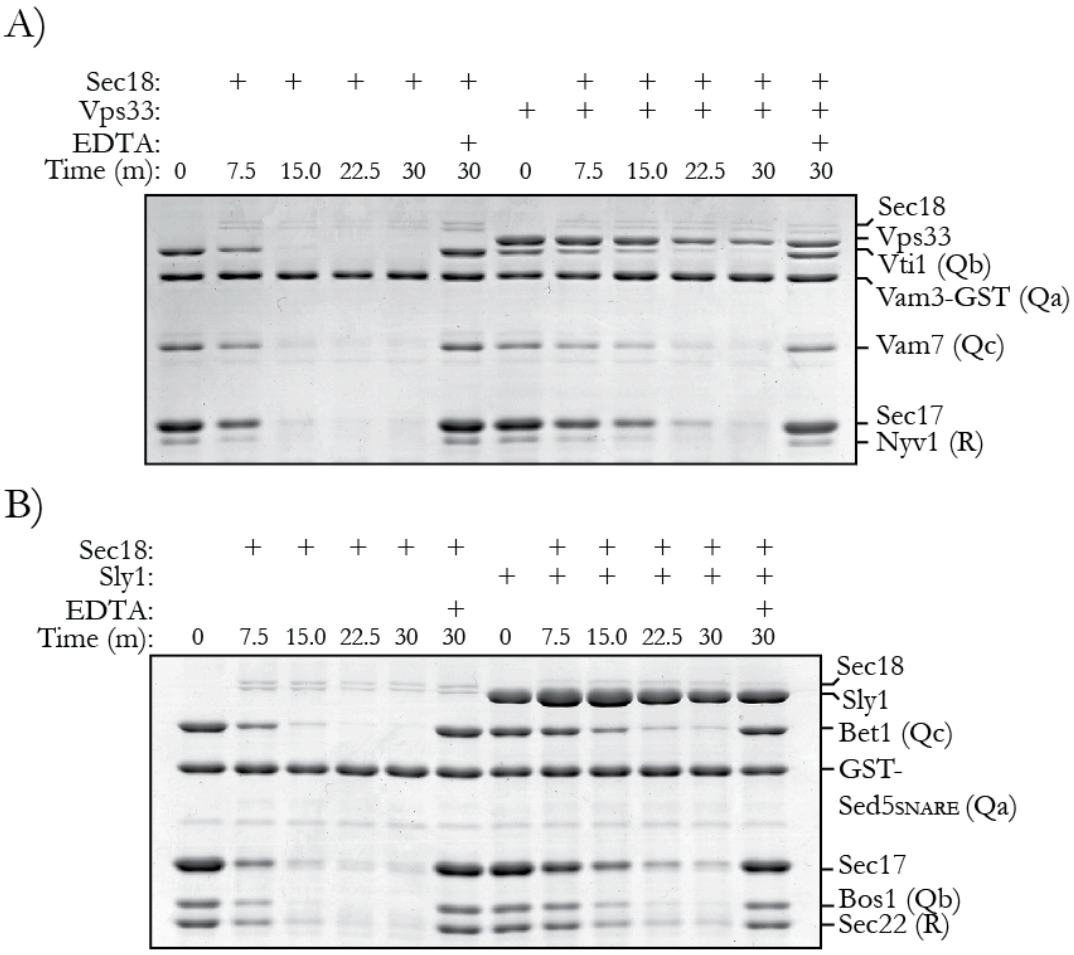

Figure 4.5. SM proteins protect cognate SNARE complexes from Sec18-mediated disassembly.
(A). 500 nM SNARE complex was formed on Vam3-GST. 20 μM Sec17 and 2.5 μM Vps33 were incubated for 1 h at 30 ˚C in SM Assay Buffer supplemented with 1 mM ATP and 2 mM MgCl2. For "EDTA", SM Assay Buffer was supplemented with 30 mM EDTA. 300 nM Sec18 was added as indicated, for the indicated period of time. Bound material was separated by SDS-PAGE and visualized with Coomassie Brilliant Blue. (B). 500 nM SNARE complex was formed on GST-Sed5$_{SNARE}$. 20 μM Sec17 and 10 μM Sly1 were incubated for 1 h at 30 ˚C in SM Assay Buffer supplemented with 1 mM ATP and 2 mM MgCl2. For "EDTA", SM Assay Buffer was supplemented with 30 mM EDTA. 300 nM Sec18 was added as indicated, for the indicated period of time. Bound material was separated by SDS-PAGE and visualized with Coomassie Brilliant Blue.

Chapter Five—Observations, Questions, and Future Directions

5.1–What are the roles of tethering complexes in membrane fusion?

The HOPS and CORVET hetero-hexameric complexes play an essential role in cargo trafficking through the late endosome and to the lysosomal-vacuole. The HOPS and CORVET complexes share four subunits, called the Vps C core, and loss of any of these four subunits stops all trafficking through the endo-lysosomal pathway. Loss of the HOPS- or CORVET-specific subunits causes less severe defects. Prior to staring my thesis, biochemical studies of the entire HOPS complex had suggested it had many properties: Rab binding, GEF activity, tethering, SNARE binding, and lipid interaction. It was not fully clear which subunits were contributing the observed biochemical properties. To better understand the roles that the HOPS and CORVET complexes play in membrane trafficking through the endo-lysosomal pathway, I used an ectopic system to express and purify each subunit and study their function individually and in combination. My specific biochemical observations from these studies (**Chapters 2, 3, and 4**) have contributed to the understanding of the many roles tethers play in membrane trafficking and fusion.

Using purified proteins, I showed that the HOPS complex has two unique sites for the Rab Ypt7: Vps41 and Vps39 (Brett et al., 2008; Plemel et al., 2011). Vps41 is an effector and binds to Ypt7 in its active, GTP-bound state. Surprisingly, while purified Vps39 selectively bound Ypt7, it showed no preference for Ypt7 in its GTP- or GDP-bound states. This was intriguing since Rab binding proteins tend to fall into categories of effectors (bind GTP-Rab) or

GEFs (bind GDP-Rab). Moreover, I showed that Vps39 does not have GEF activity toward Ypt7. While this was a negative result, it was a critical piece of data in changing the models of HOPS function that had dominated for several years. Later, the Ungerman lab also showed that Vps39 had no GEF activity toward Ypt7, and they demonstrated that the GEF is the Mon1/Ccz1 dimer (Nordmann et al., 2010). Interestingly, the correct interpretation had been suggested on the basis of elegant genetic experiments (Hoffman-Sommer et al., 2009; Kucharczyk et al., 2009; Wang et al., 2003a). I also showed that the HOPS complex has multiple SNARE binding sites (Lobingier and Merz, 2012). It can bind the SNARE domains of four of the five vacuole SNAREs through its subunit Vps33. The HOPS complex also has a binding site for the N-terminal regulatory domain of the Qa SNARE Vam3 as well as the previously identified binding site for the N-terminal regulatory domain of the Qc SNARE Vam7 (Lobingier and Merz, 2012; Stroupe et al., 2006).

Stepping back from the details of the protein interactions, there are several general points to take away from these binding studies. One of the standing questions in the field is how the proteins are coordinated between the two compartments prior to fusion. It is clear from *in vitro* studies that SNAREs alone are capable, if inefficient, at driving membrane fusion (McNew et al., 2000; Weber et al., 1998). It is thought proteins like Rabs, tethers, and SMs act cooperatively *in vivo* to allow SNAREs to function more effectively. The multiple Rab and SNARE affinities I have shown for the HOPS complex suggest a model in which SNARE pairing might be made more efficient: by engaging multiple Rabs and SNAREs in two different compartments at a distance greater than the SNAREs themselves are capable, the HOPS complex can increase the efficiency of SNARE pairing and thus membrane fusion itself. Furthermore, the HOPS complex integrates information from other signaling molecules. For example, the casein kinase Yck3

phosphorylates the HOPS subunit Vps41 to regulate its direct membrane association ability (Brett et al., 2008; Cabrera et al., 2009; Cabrera et al., 2010). Additionally, it is likely that a productive fusion event requires the function of at least three SNARE complexes (Shi et al., 2012). It is possible that temporal coordination between three SNARE complexes is critical for efficient membrane fusion, and the multiple SNARE avidities of the HOPS complex could provide such coordination. I am not the first to note that combining multiple avidities for Rabs, SNAREs, lipids could allow a MTC to act as integrator of proximity-based signals for membrane fusion (for reviews see: Nickerson et al., 2009; Yu and Hughson, 2010). Only when the correct conditions are present—in terms of the spatial localization of the correct lipids and proteins for a particular pathway—can a MTC bring together all of these pieces to drive regulated tethering, docking, and membrane fusion.

One of the more direct methods to test the model that a MTC functions by bringing together all the players of membrane fusion would be to design mutants that could interfere specifically with one or more of the many affinities. For example, would membrane fusion become less efficient, or fail entirely, if the Rab binding site in Vps39, but not Vps41, was non-functional? Crystal structures are needed to guide the design of such mutants, and efforts to obtain these structures are underway in multiple labs. A complementary approach could pair a new technology that allows specific proteins to be inducibly and rapidly targeted to the proteasome, and work from the Merz lab showing that at least one subunit of the HOPS complex can be fully functional when expressed as two separate polypeptides (Plemel et al., 2011). The new technology uses an E3 ligase and degron from plants that responds to auxin (Havens et al., 2012; Nishimura et al., 2009). This system has been translated into yeast, and proteins labeled with the degron are degraded in an auxin-dependent, proteasome-dependent manner. Certainly,

the degron can be used to tag and inducibly degrade entire subunits. As HOPS subunits can be split into two functional polypeptides, it could be possible to use the degron system to remove only one domain from the entire HOPS complex. This would allow a much more surgical test of the model above, as just the relevant domains but not the entire protein, could be removed.

5.2–Do all SM proteins share a fundamental SNARE interaction mode?

The role, or roles, of SM proteins in membrane fusion has been one of the most vexing questions over the last decade in the field of intracellular traffic. Although SM proteins share substantial structural homology, the apparently divergent observed SNARE binding modes of SM proteins have caused many in the field to question if SM proteins share a universal mechanism of action. In the broadest terms, my data suggest that the universal SNARE binding mode for SM proteins is to the SNARE complex; in the cell, it is likely the primary target of SM protein action is the *trans*-SNARE complex (Lobingier and Merz, 2012; Carr and Rizo, 2010). In more detailed terms, my data suggests that SM proteins can be separated into two subclasses that differ in their abilities to interact with single SNAREs but share the property of SNARE complex binding.

At least three major SNARE binding modes had been observed for SM proteins (see **Introduction**). What I have shown is that Vps33, like Sec1, has the strongest affinity for the SNARE complex (Lobingier and Merz, 2012). We have suggested the hypothesis that there are two subclasses of SM proteins based on sequence and on a function. The subclasses differ in the ability to bind to a motif in the NTD of the Qa SNARE, but share the ability to bind to the SNARE complex bundle. Class I SM proteins (Sly1, Vps45, and Munc18), and their cognate Qa SNAREs, have the N-peptide consensus sequence and binding pocket, and all have been shown

to interact with the N-peptide. The Qa SNARE of the Class II SM proteins (Sec1 and Vps33) lack the N-peptide consensus sequence. Moreover, the crystal structure of Vps33 lacks an N-peptide binding pocket (Baker et al., 2012).

What is the functional purpose the N-peptide when it is present and what, if any, other proteins replace this function when the N-peptide is absent? Although it has been suggested that N-peptide binding is central to the catalytic function of the neuronal SM Munc-18, we and others have suggested that the N-peptide has a simpler function: to recruit the SM protein to SNAREs (Shen et al., 2010). Importantly, I have shown that the HOPS complex plays an important role recruiting Vps33 to the vacuole, and others have shown that the exocyst complex recruits the SM protein Sec1 sites of exocytosis (Morgera et al., 2012). I have shown that there are moderate cellular defects when the HOPS complex recruits Vps33 less efficiently. We have suggested a model in which MTCs play the primary role SM protein recruitment in systems in which the N-peptide is lacking.

At least three of four SM protein subfamilies can bind the SNARE complex bundle: Sec1/Munc18, Vps33, and Vps45 (see **Introduction**). This had not been shown for the Sly1 subfamily. I show in **Chapter 4** that unlike Vps33, Sly1 has very little affinity for the SNARE complex bundle in the absence of Sec17. However, I also found that Sly1 can discriminate between cognate and noncognate SNARE complexes decorated with Sec17, indicating that Sly1 directly contacts the SNARE complex. Why is the affinity of Sly1 for the SNARE complex weaker than for other SMs? Unlike Sec1 and Vps33, Sly1 binds to the N-peptide and does so with low nanomolar affinity (Grabowski and Gallwitz, 1997). It is possible that since Sly1 binds the Sed5 N-peptide with nanomolar affinity, Sly1 would have a commensurately lesser affinity for the SNARE complex bundle. Another intriguing possibility is that the N-peptide

allosterically activates Sly1 for binding the SNARE complex and that my investigations—lacking the N-peptide in order to assay for SNARE complex binding—have removed a key factor (Arac et al., 2005). Adding a synthetically derived N-peptide in SNARE complex binding assays would allow for testing of this hypothesis. Alternatively, a FRET pair on Sly1 and the distal end of a SNARE domain could examine the occupancy of Sly1 on the SNARE complex bundle.

5.3–Does SM protein function require a conformational change?

The idea that SM proteins might undergo conformational change to become active is an old one in the field, but the existing data for it has been circumstantial. Three major lines of evidence have been offered to suggest that SM proteins might undergo a conformational change. First, the central cavity of the SM protein (which is thought to be where SNARE complexes bind) varies in the size of its opening between crystal structures of different SM proteins (Bracher and Weissenhorn, 2001). Second, mutations in Sly1 (the suppressor of lethality ypt1) allow it to bypass the need for the Rab Ypt1 (Dascher et al., 1991). It has been inferred, from the positions of these residues in a packing helix on the surface of the SM, that these mutations allow the SM protein to enter the "open" conformation without the normal regulation of the Rab. Finally, molecular dynamics simulation of SM protein Munc18 has suggested that it can change conformation: specifically, a change to the size of the opening to the central cavity that represents the SM transitioning to conformation that is competent to bind SNARE complexes (Bar-On et al., 2011).

My data on the temperature dependence of SM protein binding is consistent with the idea SM protein needs to undergo a conformational change to bind the SNARE complex. To recap:

the binding of a SM protein to a SNARE complex, or a SNARE complex bound to Sec17, is optimal at ~30 ˚C, and is reduced by 90% of maximum when the temperature is reduced to by ten degrees to 20 ˚C. A classic method in enzymology is to graph activity vs temperature as an Arrhenius plot. Steep temperature transitions, and non-linearity in an Arrhenius plot, have been argued to often be indicative of an activity that is dependent on a highly cooperative conformational change of the enzyme (Biosca et al., 1983; Massey et al., 1966; Roe et al., 1985). While I am assaying protein association and not an enzyme rate, it is possible to examine my data with the same underlying principle of an Arrhenius plot: steep temperature dependence of protein activity can suggest a large energy barrier to activation. It is clear from my data that the plot of SM protein binding vs. temperature is non-linear, which suggests that the SM protein might need to undergo a conformational change—one that is energetically unfavorable at lower temperatures—to bind SNARE complexes. Importantly, there is no temperature dependence of Sec17 binding to SNARE complexes, or the SM protein Sly1 binding to the N-peptide of the SNARE Sed5. These two controls suggest that the temperature dependent process occurs within the SM protein, and involves its binding to SNARE complex. Furthermore, I also observe strong temperature dependence in Vps33 binding to SNARE complexes or Sec17-bound SNARE complexes. As observed with the Golgi SNARE complexes, Sec17 showed no temperature dependence in the binding the vacuole SNARE complexes. Interestingly, the temperature dependence was not as sharp for Vps33 as for Sly1. As I can readily observe Vps33 binding to the SNARE complex in absence of Sec17, but cannot for Sly1, it is possible that Vps33 more readily undergoes the conformational change that is a prerequisite for SNARE complex binding. It should be underscored, however, that my data cannot rule out the possibility that the SM protein binds a surface of the SNARE complex that Sec17 does not, and it is that part of the

SNARE complex—and not the SM protein—that undergoes the temperature dependent process in binding to the SM protein.

More directly testing the hypothesis that a SM protein undergoes a conformational change to promote membrane fusion, and the methods in which the conformal change is regulated *in vivo*, will be an important area of future study. One method of testing this hypothesis would be to use mutations known for "activating" SM proteins *in vivo* (the Rab-bypass mutants Sly1-15 or Sly1-20 or the dominant negative Vps45 W244R) (Carpp et al., 2006). As I have performed detailed kinetic studies of Sly1 and Vps33 association rates and temperature-dependent binding, it would be interesting to see if these mutants produce identical curves to the wild-type proteins. Also, it has been suggested that the N-peptide can induce conformational change in Sly1, and addition of a synthetic N-peptide in my binding studies could test this model. One hypothesis would be that these activated SMs could bind more quickly and at lower temperatures. There are many other techniques to assay for conformational change that could be brought to bear if a mutant or condition was found that had different binding properties: limited trypsin digestion, 1,8-ANS binding, and, near-UV CD could allow for comparison of the steady-state conformations of wild-type and mutant protein. Another method to test the hypothesis of conformational change could take advantage of data that shows phosphorylation of Munc18 limits its activity *in vivo*. In molecular dynamics simulations of Munc18, known phosphorylation sites (that negatively effect Munc18 function in the cell) are shown to reduce the frequency of Munc18 entering the "open" state (Bar-On et al., 2011). Similar phosphorylation sites have been found for Vps33 in a phospho-proteomics screen (S373 and S626) (Albuquerque et al., 2008). It could be very useful to test if phosphomimetics of these mutants alter the temperature dependence, or association rate, or Vps33 to SNARE complexes *in*

vitro. If these phosphomimetics did change the binding properties of Vps33, it could be very useful to look for defects in vacuolar function *in vivo* or vacuole fusion *in vitro.*

5.4–What are the functional implications of SM-mediated SNARE complex protection *in vivo*?

Unexpectedly, I discovered that two SM proteins (Vps33 and Sly1) act synergistically with Sec17 to bind to the SNARE complex, and that SM proteins partially protect SNARE complexes from Sec18/NSF mediated disassembly. These results were surprising for several reasons. First, SM proteins are considered to be part of the SNARE assembly machinery, and Sec17 part of the disassembly machinery. Prior to my results, SNARE assembly and disassembly was thought to be temporally sequential, and cooperativity between Sec17 and SM proteins would be unlikely. My data strongly suggest that the temporal separation of SNARE assembly and disassembly—that first SNAREs assemble without interference from Sec18, and then SNARE complexes are disassembled without interference from the SM protein—is not wholly accurate. Rather, my data suggest that the SNARE assembly machinery and disassembly machinery might be operating simultaneously in the cell, and that competition between the processes is involved in regulating the membrane fusion.

What are the functional implications if the SM protein can protect *trans*-SNARE complexes from Sec18-mediated disassembly in the cell? My data suggests that SM proteins can discriminate between cognate and non-cognate SNARE complexes. If this is the case *in vivo*, it suggests SNARE complexes could be proofread by the synergistic functioning of SM proteins with Sec17 and Sec18. Specifically, with SM proteins not binding and thus not offering protection, non-cognate complexes would be disassembled at a greater rate. The result of this

molecular selectivity for cognate SNARE complexes would be a process that could be described as passive proofreading. Is proofreading SNARE complexes necessary in the cell? It has been shown *in vitro* that SNARE proteins can assemble into non-cognate complexes but—in general—only cognate complexes can drive membrane fusion (McNew et al., 2000). The exception to this rule is that some R-SNAREs can drive fusion with non-cognate Q-SNARE complexes (Izawa et al., 2012). Thus, it is possible that improper R-SNARE to Q-SNARE pairing needs to be suppressed to stop vesicles from fusing with the wrong compartment. It has also been shown *in vitro* that cognate SNAREs can pair improperly: for example, non-parallel assembly (e.g., not all SNAREs aligned N- to C-terminal) or SNARE complexes made up of all Q-SNAREs (Fasshauer and Margittai, 2004). These types of SNARE complexes are non-productive for fusion. By protecting cognate and properly paired SNARE complexes, while leaving non-cognate complexes susceptible to Sec18-mediated disassembly, SM proteins could funnel SNARE assembly toward productive complexes and membrane fusion.

It will be important to understand the role of SM-mediated SNARE complex protection *in vivo*. For example, if the SM protein opposes Sec18 in SNARE complex disassembly, overexpression of either Sec18 or the SM protein could cause cellular defects, but that co-overexpression would rescue those defects. It is possible that excess SM protein might lead to overprotection of *cis*-SNARE complexes and reduce the number of individual SNAREs to drive membrane fusion, while overproduction of Sec18 might result excess disassembly of *trans*-SNARE complexes. Alternatively, a partial loss of function mutant of either the SM protein or Sec18 might cause cellular defects, while combining those mutants might restore function. As two SM proteins (Sly1 and Sec1) are essential genes, some types of genetic rescue experiments may require the activity of both proteins to be modified in tandem.

A key question concerns the type of SNARE complexes protected by SM proteins in vivo. Unregulated disassembly of the *trans*-complex is likely to be detrimental as premature disassembly could slow or stop membrane fusion. Can SM proteins protect the *trans*-SNARE complex from Sec18? There is evidence from flies that overexpression of NSF is toxic and this toxicity is correlated with reduced SNARE complex abundance (Babcock et al., 2004). This suggests that disruption of *trans*-SNARE complexes could cause cellular defects. It has been shown that the HOPS holocomplex—which contains the SM protein Vps33—can protect *trans*-SNARE complexes from Sec18-mediated disassembly during *in vitro* membrane fusion assays and that this protection is important for *in vitro* fusion (Xu et al., 2010). It was not clear from this study what part of HOPS was protecting SNARE complexes. Also, the mechanistic basis of this protection was not elucidated, and it has been unclear whether this feature of the HOPS complex was general or specific to yeast vacuole fusion. My data strongly suggests that Vps33 (the only HOPS subunit that binds the SNARE complex—**Chapter 3**) is the key factor in *trans*-SNARE complex protection, but this hypothesis needs to be subjected to additional scrutiny. The most direct method would be to establish a reconstitution system for membrane fusion in which long-lasting *trans*-SNARE complexes are formed using the 3Δ SNARE mutants developed in the Merz lab (Schwartz and Merz, 2009).

It is also worth considering if protection of the *cis*-SNARE complex from Sec18-mediated disassembly could be beneficial. As stated above, it is likely that the most important complex to protect from Sec18-mediated disassembly is the *trans*-SNARE complex. On the surface it seems surprising that protection of *cis*-SNARE complexes would be beneficial, as disassembly of *cis*-SNARE complexes is essential for membrane fusion. It is important to underscore that my results show SM proteins do not provide complete protection for SNARE

complexes, but rather a kinetic protection: SNARE complexes bound to Sec17 and SM proteins are disassembled by Sec18 more slowly than those without an SM protein. Furthermore, we observe that while the SM protein reduces the rate of SNARE complex disassembly, Sec18 eventually strips apart the SNARE complex. Unlike the SNAREs, the SM protein is not fully removed from the matrix-bound Qa SNARE. In the cell, SNAREs participate in many rounds of SNARE complex assembly and disassembly. Does the SM-bound Qa SNARE, post Sec18-mediated disassembly, allow reassembly of SNARE complexes at a different rate than Qa SNARE lacking an SM protein? This could be investigated by disassembling SNARE complexes with or without SM protein. The ATPase activity of Sec18 could be quenched by the addition of EDTA, and SNARE complex reassembly could be measured. Kinetic protection of *cis*-SNARE complexes has potentially interesting effects. For example, once *cis*-SNARE complexes are disassembled, the individual SNAREs are free to diffuse within the bilayer. Nominally, this could result wide spatial separation of the fusion machinery. In the cell, however, we know that fusion can proceed through "hot spots," in which the membrane fusion machinery has been concentrated (Wang et al., 2003b). It is possible that the SM, by opposing Sec18-mediated *cis*-SNARE complex disassembly, could increase the local concentration of fusion factors.

There are several methods through which this model could be tested. *In vivo*, the localization of fluorescently tagged SNAREs or HOPS components could be examined in a wild-type background or backgrounds in which Sec18 was overexpressed or SM function compromised. The prediction would be that in the non-wild-type backgrounds, the fluorescent puncta would disperse, or be reduced, if the SM protein played a critical role in concentrating the SNARE fusion machinery. *In vitro, cis*-SNARE complex formation could be tested in liposomes in the presence of Sec17/Sec18 with or without the SM protein. FRET assays for SNAREs in

membranes have been worked out in several systems, and could provide a way to monitor *cis*-SNARE associations. To prevent homotypic fusion, a 3Δ soluble SNARE could be used (Schwartz and Merz, 2009).

To test these hypotheses, we would ideally have a crystal structure of a SNARE complex bound to Sec17 and the SM protein. Mutations could be designed in Sec17 that either break its contact with the SNARE complex or contact with the SM protein. Similar mutations could be made in the SM protein that break the contacts with the SNARE complex or Sec17. These types of experiments could drive right to heart of SM protein function and the role of Sec17. Obviously, crystal structures can be very difficult to obtain, and co-complex structures can be more difficult still. I have several observations from my studies that could be useful in choosing the correct crystallization targets and conditions. The first point of consideration is stability of the co-complex. Trials with Sly1, Sec17, and the Golgi SNARE complex have shown that the affinities are in the mid-micromolar range (10 μM Sly1 and 20 μM Sec17; 500 nM SNARE complex). While the co-complexes will stably form on resins, they dissociate in solution. Increasing the affinity of Sec17 and Sly1 for the Golgi SNARE complex will be an important step in the stabilizing the co-complex. While optimization of buffer conditions and protein concentrations could help in co-complex stability, an intriguing option involves the work of the Hanson lab (Marz et al., 2003). They performed mutagenic scanning experiments on α-SNAP (Sec17) and found mutations that increase or decrease its affinity for the SNARE complex. If several of the affinity increasing mutations were combined in Sec17, it might stabilize the entire co-complex. E34K, E35K, E125A, E128A are four mutations in Sec17 that could be a very helpful starting point. Alternatively, it should be noted that the affinities of Vps33 and Sec17 for the vacuolar SNARE complex are several times greater than Sly1 and Sec17 for the Golgi

complex. It could be that the vacuole co-complex proves more amenable to gel filtration and crystallization.

5.5–What is the central function of SM proteins?

Many hypotheses have been suggested over years to explain why SM proteins are essential in the cell for SNARE-mediated membrane fusion. The most recent hypotheses take into account an observation of SM protein function *in vitro:* acceleration of SNARE-mediated liposome fusion. It should be noted, however, that reconstitution efforts of membrane fusion have produced a wide variety of results. Initially, SNAREs alone were shown to catalyze liposome fusion (Weber et al., 1998). For SM proteins to have an affect, SNARE concentration was decreased and a several hour pre-incubation with the SM protein was added (Scott et al., 2004; Shen et al., 2007). Furthermore, other proteins have been shown to accelerate SNARE-mediated liposome fusion. For example, the neuronal SNARE binding protein synaptotagmin has been shown to increases the rates of membrane fusion to a much greater degree than Munc18 or Sec1 (Wang et al., 2011). It more recent reconstitution efforts, Munc18 alone has no effect on the rate of membrane fusion, and addition of synaptotagmin with Munc18 is required for fusion (importantly, this group showed through mutational analysis that Munc18 was necessary for membrane fusion in these assays) (Ma et al., 2013). In fact, there are several reports that SM proteins have no effect on the rate of liposome fusion by themselves, but instead are a necessary part of a group of fusion promoting factors including tethering proteins, Rab effectors, and the SNARE disassembly machinery Sec17/alpha-SNAP and Sec18-NSF (Ohya et al., 2009; Stroupe et al., 2009).

These observations make it worth considering, at least momentarily, if data obtained from adding only SM proteins to SNARE-mediated liposome fusion assays are being correctly interpreted. Could an incomplete reconstitution that contained only SNAREs and SM proteins show, with the correct preincubation conditions, moderate increases in the rate of membrane fusion that are thermodynamic byproduct of SM proteins designed function to protect the *trans*-SNARE complex from disassembly? While this is possible, it is more likely that the SM protein has multiple functions that are derived from the same molecular feature; specifically, binding the *trans*-SNARE complex. Thus, contacting the *trans*-SNARE complex allows SNARE complex protection in addition to the previously proposed functions of SM proteins: 1) keeping the SNARE complexes aligned in a topological manner to promote membrane fusion; 2) helping to resolve the hemifusion intermediate (Carr and Rizo, 2010). What should be able to be determined is the relative importance of protecting the SNARE complex from disassembly. My data suggests that contacts between the SM protein and Sec17 are essential for its protection. Finding mutants in the SM that break its contact with Sec17, and not the SNARE complex, could be verified *in vitro* and then compared *in vivo* to defects that arise from a SM protein deletion.

Bibliography

Aballay, A., M. A. Barbieri, M. I. Colombo, G. N. Arenas, P. D. Stahl, and L. S. Mayorga. 1998. A phorbol ester-binding protein is required downstream of Rab5 in endosome fusion. *FEBS Lett.* 441:373-378.

Allan, B. B., B. D. Moyer, and W. E. Balch. 2000. Rab1 recruitment of p115 into a cis-SNARE complex: programming budding COPII vesicles for fusion. *Science.* 289:444-448.

Angers, C. G., and A. J. Merz. 2009. HOPS interacts with Apl5 at the vacuole membrane and is required for consumption of AP-3 transport vesicles. *Mol Biol Cell.* 20:4563-4574.

Angers, C. G., and A. J. Merz. 2011. New links between vesicle coats and Rab-mediated vesicle targeting. *Semin Cell Dev Biol.* 22:18-26.

Arac, D., Dulubova, I., Huryeva, I., Grishin, N.V., Rizo, J. 2005. Three-dimensional structure of the rSly1 N-terminal domain reveals a conformational change induced by binding to synaxtin 5. *J Mol Biol.* 46(2):589-601.

Babcock, M., G. T. Macleod, J. Leither, and L. Pallanck. 2004. Genetic analysis of soluble N-ethylmaleimide-sensitive factor attachment protein function in Drosophila reveals positive and negative secretory roles. *J Neurosci.* 24:3964-3973.

Baker, R.W., Hughson, J.F., 2012. Structure of Vps33, a Key Regulator of Membrane Fusion. *ASCB abstract.*

Banta, L. M., T. A. Vida, P. K. Herman, and S. D. Emr. 1990. Characterization of yeast Vps33p, a protein required for vacuolar protein sorting and vacuole biogenesis. *Mol Cell Biol.* 10:4638-4649.

Bar-On, D., E. Nachliel, M. Gutman, and U. Ashery. 2011. Dynamic conformational changes in munc18 prevent syntaxin binding. *PLoS Comput Biol.* 7:e1001097.

Barr, F., and D. G. Lambright. 2010. Rab GEFs and GAPs. *Curr Opin Cell Biol.* 22:461-470.

Behnia, R., and S. Munro. 2005. Organelle identity and the signposts for membrane traffic. *Nature.* 438:597-604.

Bentley, M., Y. Liang, K. Mullen, D. Xu, E. Sztul, and J. C. Hay. 2006. SNARE status regulates tether recruitment and function in homotypic COPII vesicle fusion. *J Biol Chem.* 281:38825-38833.

Binda, M., M. P. Peli-Gulli, G. Bonfils, N. Panchaud, J. Urban, T. W. Sturgill, R. Loewith, and C. De Virgilio. 2009. The Vam6 GEF controls TORC1 by activating the EGO complex. *Mol Cell.* 35:563-573.

Boeddinghaus, C., A. J. Merz, R. Laage, and C. Ungermann. 2002. A cycle of Vam7p release from and PtdIns 3-P-dependent rebinding to the yeast vacuole is required for homotypic vacuole fusion. *J Cell Biol.* 157:79-89.

Bonifacino, J. S., and B. S. Glick. 2004. The mechanisms of vesicle budding and fusion. *Cell.* 116:153-166.

Bowers, K., and T. H. Stevens. 2005. Protein transport from the late Golgi to the vacuole in the yeast Saccharomyces cerevisiae. *Biochim Biophys Acta.* 1744:438-454.

Bracher, A., A. Perrakis, T. Dresbach, H. Betz, and W. Weissenhorn. 2000. The X-ray crystal structure of neuronal Sec1 from squid sheds new light on the role of this protein in exocytosis. *Structure.* 8:685-694.

Bracher, A., and W. Weissenhorn. 2001. Crystal structures of neuronal squid Sec1 implicate inter-domain hinge movement in the release of t-SNAREs. *J Mol Biol.* 306:7-13.

Braun, P., M. Tasan, M. Dreze, M. Barrios-Rodiles, I. Lemmens, H. Yu, J. M. Sahalie, R. R.Murray, L. Roncari, A. S. de Smet, K. Venkatesan, J. F. Rual, J. Vandenhaute, M. E. Cusick, T. Pawson, D. E. Hill, J. Tavernier, J. L. Wrana, F. P. Roth, and M. Vidal. 2009. An experimentally derived confidence score for binary protein-protein interactions. *Nat Methods.* 6:91-97.

Brett, C. L., R. L. Plemel, B. T. Lobingier, M. Vignali, S. Fields, and A. J. Merz. 2008. Efficient termination of vacuolar Rab GTPase signaling requires coordinated action by a GAP and a protein kinase. *J Cell Biol.* 182:1141-1151.

Brocker, C., A. Kuhlee, C. Gatsogiannis, H. J. Kleine Balderhaar, C. Honscher, S. Engelbrecht-Vandre, C. Ungermann, and S. Raunser. 2012. Molecular architecture of the multisubunit homotypic fusion and vacuole protein sorting (HOPS) tethering complex. *Proc Natl Acad Sci U S A.* 109:1991-1996.

Brodsky, F. M. 2012. Diversity of clathrin function: new tricks for an old protein. *Annu Rev Cell Dev Biol.* 28:309-336.

Brohawn, S. G., N. C. Leksa, E. D. Spear, K. R. Rajashankar, and T. U. Schwartz. 2008. Structural evidence for common ancestry of the nuclear pore complex and vesicle coats. *Science.* 322:1369-1373.

Burkhardt, P., D. A. Hattendorf, W. I. Weis, and D. Fasshauer. 2008. Munc18a controls SNARE assembly through its interaction with the syntaxin N-peptide. *EMBO J.* 27:923-933.

Cai, Y., H. F. Chin, D. Lazarova, S. Menon, C. Fu, H. Cai, A. Sclafani, D. W. Rodgers, E. M. De La Cruz, S. Ferro-Novick, and K. M. Reinisch. 2008. The structural basis for activation of the Rab Ypt1p by the TRAPP membrane-tethering complexes. *Cell.* 133:1202-1213.

Cao, X., N. Ballew, and C. Barlowe. 1998. Initial docking of ER-derived vesicles requires Uso1p and Ypt1p but is independent of SNARE proteins. *EMBO J.* 17:2156-2165.

Carette, J. E., M. Raaben, A. C. Wong, A. S. Herbert, G. Obernosterer, N. Mulherkar, A. I. Kuehne, P. J. Kranzusch, A. M. Griffin, G. Ruthel, P. Dal Cin, J. M. Dye, S. P. Whelan, K. Chandran, and T. R. Brummelkamp. 2011. Ebola virus entry requires the cholesterol transporter Niemann-Pick C1. *Nature.* 477:340-343.

Carpp, L. N., L. F. Ciufo, S. G. Shanks, A. Boyd, and N. J. Bryant. 2006. The Sec1p/Munc18 protein Vps45p binds its cognate SNARE proteins via two distinct modes. *J Cell Biol.* 173:927-936.

Carr, C. M., E. Grote, M. Munson, F. M. Hughson, and P. J. Novick. 1999. Sec1p binds to SNARE complexes and concentrates at sites of secretion. *J Cell Biol.* 146:333-344.

Carr, C. M., and J. Rizo. 2010. At the junction of SNARE and SM protein function. *Curr Opin Cell Biol.* 22:488-495.

Chen, Y. C., S. V. Rajagopala, T. Stellberger, and P. Uetz. 2010. Exhaustive benchmarking of the yeast two-hybrid system. *Nat Methods.* 7:667-8; author reply 668.

Chivian, D., D. E. Kim, L. Malmstrom, J. Schonbrun, C. A. Rohl, and D. Baker. 2005. Prediction of CASP-6 structures using automated Robetta protocols. *Proteins.*

Chin, H. F., Y. Cai, S. Menon, S. Ferro-Novick, K. M. Reinisch, and E. M. De La Cruz. 2009. Kinetic analysis of the guanine nucleotide exchange activity of TRAPP, a multimeric Ypt1p exchange factor. *J Mol Biol.* 389:275-288.

Collins, K. M., N. L. Thorngren, R. A. Fratti, and W. T. Wickner. 2005. Sec17p and HOPS, in distinct SNARE complexes, mediate SNARE complex disruption or assembly for fusion. *EMBO J.* 24:1775-1786.

Conibear, E., and T. H. Stevens. 1998. Multiple sorting pathways between the late Golgi and the vacuole in yeast. *Biochim. Biophys. Acta.* 1404:211-230.

Darsow, T., G. Odorizzi, and S. D. Emr. 2000. Invertase fusion proteins for analysis of protein trafficking in yeast. *Methods Enzymol.* 327:95-106.

Dascher, C., R. Ossig, D. Gallwitz, and H. D. Schmitt. 1991. Identification and structure of four yeast genes (SLY) that are able to suppress the functional loss of YPT1, a member of the RAS superfamily. *Mol Cell Biol.* 11:872-885.

Dilcher, M., B. Kohler, and G. F. von Mollard. 2001. Genetic interactions with the yeast Q-SNARE VTI1 reveal novel functions for the R-SNARE YKT6. *J Biol Chem.* 276:34537-34544.

Drin, G., V. Morello, J. F. Casella, P. Gounon, and B. Antonny. 2008. Asymmetric tethering of flat and curved lipid membranes by a golgin. *Science.* 320:670-673.

Dulubova, I., T. Yamaguchi, Y. Wang, T. C. Sudhof, and J. Rizo. 2001. Vam3p structure reveals conserved and divergent properties of syntaxins. *Nat Struct Biol.* 8:258-264.

Dulubova, I., T. Yamaguchi, Y. Gao, S. W. Min, I. Huryeva, T. C. Sudhof, and J. Rizo. 2002. How Tlg2p/syntaxin 16 'snares' Vps45. *EMBO J.* 21:3620-3631.

Epp, N., R. Rethmeier, L. Kramer, and C. Ungermann. 2011. Membrane dynamics and fusion at late endosomes and vacuoles--Rab regulation, multisubunit tethering complexes and SNAREs. *Eur J Cell Biol.* 90:779-785.

Ernst, J. A., and A. T. Brunger. 2003. High resolution structure, stability, and synaptotagmin binding of a truncated neuronal SNARE complex. *J Biol Chem.* 278:8630-8636.

Fasshauer, D., and M. Margittai. 2004. A transient N-terminal interaction of SNAP-25 and syntaxin nucleates SNARE assembly. *J Biol Chem.* 279:7613-7621.

Fasshauer, D., R. B. Sutton, A. T. Brunger, and R. Jahn. 1998. Conserved structural features of the synaptic fusion complex: SNARE proteins reclassified as Q- and R-SNAREs. *Proc Natl Acad Sci U S A.* 95:15781-15786.

Fratti, R. A., and W. Wickner. 2007. Distinct targeting and fusion functions of the PX and SNARE domains of yeast vacuolar Vam7p. *J Biol Chem.* 282:13133-13138.

Furgason, M. L., C. MacDonald, S. G. Shanks, S. P. Ryder, N. J. Bryant, and M. Munson. 2009. The N-terminal peptide of the syntaxin Tlg2p modulates binding of its closed conformation to Vps45p. *Proc Natl Acad Sci U S A.* 106:14303-14308.

Gao, Y., S. Zorman, G. Gundersen, Z. Xi, L. Ma, G. Sirinakis, J. E. Rothman, and Y. Zhang. 2012. Single reconstituted neuronal SNARE complexes zipper in three distinct stages. *Science.* 337:1340-1343.

Gissen, P., C. A. Johnson, N. V. Morgan, J. M. Stapelbroek, T. Forshew, W. N. Cooper, P. J. McKiernan, L. W. Klomp, A. A. Morris, J. E. Wraith, P. McClean, S. A. Lynch, R. J. Thompson, B. Lo, O. W. Quarrell, M. Di Rocco, R. C. Trembath, H. Mandel, S. Wali, F. E. Karet, A. S. Knisely, R. H. Houwen, D. A. Kelly, and E. R. Maher. 2004. Mutations in VPS33B, encoding a regulator of SNARE-dependent membrane fusion, cause arthrogryposis-renal dysfunction-cholestasis (ARC) syndrome. *Nat Genet.* 36:400-404.

Grabowski, R., and D. Gallwitz. 1997. High-affinity binding of the yeast cis-Golgi t-SNARE, Sed5p, to wild-type and mutant Sly1p, a modulator of transport vesicle docking. *FEBS Lett.* 411:169-172.

Griff, I. C., R. Schekman, J. E. Rothman, and C. A. Kaiser. 1992. The yeast SEC17 gene product is functionally equivalent to mammalian alpha-SNAP protein. *J Biol Chem.* 267:12106-12115.

Grosshans, B. L., D. Ortiz, and P. Novick. 2006. Rabs and their effectors: achieving specificity in membrane traffic. *Proc. Natl. Acad. Sci. U S A.* 103:11821-11827.

Guo, W., D. Roth, C. Walch-Solimena, and P. Novick. 1999. The exocyst is an effector for Sec4p, targeting secretory vesicles to sites of exocytosis. *EMBO J.* 18:1071-1080.

Hama, H., G. G. Tall, and B. F. Horazdovsky. 1999. Vps9p is a guanine nucleotide exchange factor involved in vesicle-mediated vacuolar protein transport. *J. Biol. Chem.* 274:15284-15291.

Hanson, P. I., R. Roth, H. Morisaki, R. Jahn, and J. E. Heuser. 1997. Structure and conformational changes in NSF and its membrane receptor complexes visualized by quick-freeze/deep-etch electron microscopy. *Cell.* 90:523-535.

Hashizume, K., Y. S. Cheng, J. L. Hutton, C. H. Chiu, and C. M. Carr. 2009. Yeast Sec1p functions before and after vesicle docking. *Mol Biol Cell.* 20:4673-4685.

Havens, K. A., J. M. Guseman, S. S. Jang, E. Pierre-Jerome, N. Bolten, E. Klavins, and J. L. Nemhauser. 2012. A synthetic approach reveals extensive tunability of auxin signaling. *Plant Physiol.* 160:135-142.

Hayes, G. L., F. C. Brown, A. K. Haas, R. M. Nottingham, F. A. Barr, and S. R. Pfeffer. 2009. Multiple Rab GTPase binding sites in GCC185 suggest a model for vesicle tethering at the trans-Golgi. *Mol Biol Cell.* 20:209-217.

Hickey, C. M., and W. Wickner. 2010. HOPS initiates vacuole docking by tethering membranes before trans-SNARE complex assembly. *Mol Biol Cell.* 21:2297-2305.

Horazdovsky, B. F., C. R. Cowles, P. Mustol, M. Holmes, and S. D. Emr. 1996. A novel RING finger protein, Vps8p, functionally interacts with the small GTPase, Vps21p, to facilitate soluble vacuolar protein localization. *J. Biol. Chem.* 271:33607-33615.

Hu, J., W. A. Prinz, and T. A. Rapoport. 2011. Weaving the web of ER tubules. *Cell.* 147:1226-1231.

Hu, S. H., C. F. Latham, C. L. Gee, D. E. James, and J. L. Martin. 2007. Structure of the Munc18c/Syntaxin4 N-peptide complex defines universal features of the N-peptide binding mode of Sec1/Munc18 proteins. *Proc Natl Acad Sci U S A.* 104:8773-8778.

Izawa, R., T. Onoue, N. Furukawa, and J. Mima. 2012. Distinct contributions of vacuolar Qabc- and R-SNARE proteins to membrane fusion specificity. *J Biol Chem.* 287:3445-3453.

Jun, Y., N. Thorngren, V. J. Starai, R. A. Fratti, K. Collins, and W. Wickner. 2006. Reversible, cooperative reactions of yeast vacuole docking. *EMBO J.* 25:5260-5269.

Kaiser, C. A., and R. Schekman. 1990. Distinct sets of SEC genes govern transport vesicle formation and fusion early in the secretory pathway. *Cell.* 61:723-733.

Kim, D. E., D. Chivian, and D. Baker. 2004. Protein structure prediction and analysis using the Robetta server. *Nucleic Acids Res.* 32:W526-31.

Kinchen, J. M., and K. S. Ravichandran. 2010. Identification of two evolutionarily conserved genes regulating processing of engulfed apoptotic cells. *Nature.* 464:778- 782.

Knop, M., K. J. Miller, M. Mazza, D. Feng, M. Weber, S. Keranen, and J. Jantti. 2005. Molecular interactions position Mso1p, a novel PTB domain homologue, in the interface of the exocyst complex and the exocytic SNARE machinery in yeast. *Mol Biol Cell.* 16:4543-4556.

Koumandou, V. L., J. B. Dacks, R. M. Coulson, and M. C. Field. 2007. Control systems for membrane fusion in the ancestral eukaryote; evolution of tethering complexes and SM proteins. *BMC Evol Biol.* 7:29.

Kramer, L., and C. Ungermann. 2011. HOPS drives vacuole fusion by binding the vacuolar SNARE complex and the Vam7 PX domain via two distinct sites. *Mol Biol Cell.* 22:2601-2611.

Kraynack, B. A., A. Chan, E. Rosenthal, M. Essid, B. Umansky, M. G. Waters, and H. D. Schmitt. 2005. Dsl1p, Tip20p, and the novel Dsl3(Sec39) protein are required for the stability of the Q/t-SNARE complex at the endoplasmic reticulum in yeast. *Mol Biol Cell.* 16:3963-3977

Kucharczyk, R., M. Hoffman-Sommer, I. Piekarska, G. F. von Mollard, and J. Rytka. 2009. The Saccharomyces cerevisiae protein Ccz1p interacts with components of the endosomal fusion machinery. *FEMS Yeast Res.* 9:565-573.

Kucharczyk, R., S. Dupre, S. Avaro, R. Haguenauer-Tsapis, P. P. Slonimski, and J. Rytka. 2000. The novel protein Ccz1p required for vacuolar assembly in Saccharomyces cerevisiae functions in the same transport pathway as Ypt7p. *J. Cell Sci.* 113 Pt 23:4301-4311.

Kucharczyk, R., A. M. Kierzek, P. P. Slonimski, and J. Rytka. 2001. The Ccz1 protein interacts with Ypt7 GTPase during fusion of multiple transport intermediates with the vacuole in S. cerevisiae. *J. Cell Sci.* 114:3137-3145.

Laage, R., and C. Ungermann. 2001. The N-terminal domain of the t-SNARE Vam3p coordinates priming and docking in yeast vacuole fusion. *Mol Biol Cell.* 12:3375-3385.

Li, Y., H. D. Schmitt, D. Gallwitz, and R. W. Peng. 2007. Mutations of the SM protein Sly1 resulting in bypass of GTPase requirement in vesicular transport are confined to a short helical region. *FEBS Lett.* 581:5698-5702.

Lobingier, B. T., and A. J. Merz. 2012. Sec1/Munc18 protein Vps33 binds to SNARE domains and the quaternary SNARE complex. *Mol Biol Cell.* 23:4611-4622.

Ma, C., L. Su, A. B. Seven, Y. Xu, and J. Rizo. 2013. Reconstitution of the vital functions of Munc18 and Munc13 in neurotransmitter release. *Science.* 339:421-425.

Markgraf, D. F., F. Ahnert, H. Arlt, M. Mari, K. Peplowska, N. Epp, J. Griffith, F. Reggiori, and C. Ungermann. 2009. The CORVET subunit Vps8 cooperates with the Rab5 homolog Vps21 to induce clustering of late endosomal compartments. *Mol. Biol. Cell.* 20:5276-5289.

Marz, K. E., J. M. Lauer, and P. I. Hanson. 2003. Defining the SNARE complex binding surface of alpha-SNAP: implications for SNARE complex disassembly. *J Biol Chem.* 278:27000-27008.

Matveeva, E., and S. W. Whiteheart. 1998. The effects of SNAP/SNARE complexes on the ATPase of NSF. *FEBS Lett.* 435:211-214.

McNew, J. A., F. Parlati, R. Fukuda, R. J. Johnston, K. Paz, F. Paumet, T. H. Sollner, and J. E. Rothman. 2000. Compartmental specificity of cellular membrane fusion encoded in SNARE proteins. *Nature.* 407:153-159.

McNew, J. A., T. Weber, D. M. Engelman, T. H. Sollner, and J. E. Rothman. 1999. The length of the flexible SNAREpin juxtamembrane region is a critical determinant of SNARE-dependent fusion. *Mol Cell.* 4:415-421.

Meeusen, S. L., and J. Nunnari. 2005. How mitochondria fuse. *Curr Opin Cell Biol.* 17:389-394.

Mima, J., C. M. Hickey, H. Xu, Y. Jun, and W. Wickner. 2008. Reconstituted membrane fusion requires regulatory lipids, SNAREs and synergistic SNARE chaperones. *EMBO J.* 27:2031-2042.

Mizuno-Yamasaki, E., F. Rivera-Molina, and P. Novick. 2012. GTPase networks in membrane traffic. *Annu Rev Biochem.* 81:637-659.

Morgera, F., M. R. Sallah, M. L. Dubuke, P. Gandhi, D. N. Brewer, C. M. Carr, and M. Munson. 2011. Regulation of exocytosis by the exocyst subunit Sec6 and the SM protein Sec1. *Mol Biol Cell.*

Nakamura, N., A. Hirata, Y. Ohsumi, and Y. Wada. 1997. Vam2/Vps41p and Vam6/Vps39p are components of a protein complex on the vacuolar membranes and involved in the vacuolar assembly in the yeast Saccharomyces cerevisiae. *J. Biol. Chem.* 272:11344-11349.

Nickerson, D. P., C. L. Brett, and A. J. Merz. 2009. Vps-C complexes: gatekeepers of endolysosomal traffic. *Curr Opin Cell Biol.* 21:543-551.

Nishimura, K., T. Fukagawa, H. Takisawa, T. Kakimoto, and M. Kanemaki. 2009. An auxin-based degron system for the rapid depletion of proteins in nonplant cells. *Nat Methods.* 6:917-922.

Nordmann, M., M. Cabrera, A. Perz, C. Brocker, C. Ostrowicz, S. Engelbrecht-Vandre, and C.Ungermann. 2010. The Mon1-Ccz1 complex is the GEF of the late endosomal Rab7 homolog Ypt7. *Curr. Biol.* 20:1654-1659.

Odorizzi, G., M. Babst, and S. D. Emr. 1998. Fab1p PtdIns(3)P 5-kinase function essential for protein sorting in the multivesicular body. *Cell.* 95:847-858.

Ohya, T., M. Miaczynska, U. Coskun, B. Lommer, A. Runge, D. Drechsel, Y. Kalaidzidis, and M. Zerial. 2009. Reconstitution of Rab- and SNARE-dependent membrane fusion by synthetic endosomes. *Nature.* 459:1091-1097.

Ostrowicz, C. W., C. Brocker, F. Ahnert, M. Nordmann, J. Lachmann, K. Peplowska, A. Perz, K. Auffarth, S. Engelbrecht-Vandre, and C. Ungermann. 2010. Defined Subunit Arrangement and Rab Interactions Are Required for Functionality of the HOPS Tethering Complex. *Traffic*. 11(10):1334-46.

Pawelec, A., J. Arsic, and R. Kolling. 2010. Mapping of Vps21 and HOPS binding sites in Vps8 and effect of binding site mutants on endocytic trafficking. *Eukaryot Cell*. 9(4): 602–610.

Peng, R., and D. Gallwitz. 2002. Sly1 protein bound to Golgi syntaxin Sed5p allows assembly and contributes to specificity of SNARE fusion complexes. *J Cell Biol.* 157:645-655.

Peng, R., and D. Gallwitz. 2004. Multiple SNARE interactions of an SM protein: Sed5p/Sly1p binding is dispensable for transport. *EMBO J.* 23:3939-3949.

Peplowska, K., D. F. Markgraf, C. W. Ostrowicz, G. Bange, and C. Ungermann. 2007. The CORVET tethering complex interacts with the yeast Rab5 homolog Vps21 and is involved in endo-lysosomal biogenesis. *Dev Cell.* 12:739-750.

Perez-Victoria, F. J., and J. S. Bonifacino. 2009. Dual roles of the mammalian GARP complex in tethering and SNARE complex assembly at the trans-golgi network. *Mol Cell Biol.* 29:5251-5263.

Peterson, M. R., C. G. Burd, and S. D. Emr. 1999. Vac1p coordinates Rab and phosphatidylinositol 3-kinase signaling in Vps45p-dependent vesicle docking/fusion at the endosome. *Curr. Biol.* 9:159-162.

Peterson, M. R., and S. D. Emr. 2001. The class C Vps complex functions at multiple stages of the vacuolar transport pathway. *Traffic.* 2:476-486.

Pieren, M., A. Schmidt, and A. Mayer. 2010. The SM protein Vps33 and the t-SNARE H(abc) domain promote fusion pore opening. *Nat Struct Mol Biol.* 17:710-717.

Plemel, R. L., B. T. Lobingier, C. L. Brett, C. G. Angers, D. P. Nickerson, A. Paulsel, D. Sprague, and A. J. Merz. 2011. Subunit organization and Rab interactions of Vps-C protein complexes that control endolysosomal membrane traffic. *Mol Biol Cell.* 22:1353-1363.

Pobbati, A. V., A. Stein, and D. Fasshauer. 2006. N- to C-terminal SNARE complex assembly promotes rapid membrane fusion. *Science.* 313:673-676.

Popoff, V., F. Adolf, B. Brugger, and F. Wieland. 2011. COPI budding within the Golgi stack. *Cold Spring Harb Perspect Biol.* 3:a005231.

Poteryaev, D., S. Datta, K. Ackema, M. Zerial, and A. Spang. 2010. Identification of the switch in early-to-late endosome transition. *Cell.* 141:497-508.

Price, A., D. Seals, W. Wickner, and C. Ungermann. 2000. The docking stage of yeast vacuole fusion requires the transfer of proteins from a cis-SNARE complex to a Rab/Ypt protein. *J Cell Biol.* 148:1231-1238.

Pulipparacharuvil, S., M. A. Akbar, S. Ray, E. A. Sevrioukov, A. S. Haberman, J. Rohrer, and H. Kramer. 2005. Drosophila Vps16A is required for trafficking to lysosomes and biogenesis of pigment granules. *J. Cell Sci.* 118:3663-3673.

Puthenveedu, M. A., B. Lauffer, P. Temkin, R. Vistein, P. Carlton, K. Thorn, J. Taunton, O. D. Weiner, R. G. Parton, and M. von Zastrow. 2010. Sequence-dependent sorting of recycling proteins by actin-stabilized endosomal microdomains. *Cell.* 143:761-773.

Rathore, S. S., E. G. Bend, H. Yu, M. Hammarlund, E. M. Jorgensen, and J. Shen. 2010. Syntaxin N-terminal peptide motif is an initiation factor for the assembly of the SNARE-Sec1/Munc18 membrane fusion complex. *Proc Natl Acad Sci U S A.* 107:22399-22406.

Raymond, C. K., I. Howald-Stevenson, C. A. Vater, and T. H. Stevens. 1992. Morphological classification of the yeast vacuolar protein sorting mutants: evidence for a prevacuolar compartment in class E vps mutants. *Mol Biol Cell.* 3:1389-1402.

Rehling, P., T. Darsow, D. J. Katzmann, and S. D. Emr. 1999. Formation of AP-3 transport intermediates requires Vps41 function. *Nat Cell Biolog.* 1:346-353.

Ren, Y., C. K. Yip, A. Tripathi, D. Huie, P. D. Jeffrey, T. Walz, and F. M. Hughson. 2009. A structure-based mechanism for vesicle capture by the multisubunit tethering complex Dsl1. *Cell.* 139:1119-1129.

Rice, L. M., and A. T. Brunger. 1999. Crystal structure of the vesicular transport protein Sec17: implications for SNAP function in SNARE complex disassembly. *Mol Cell.* 4:85-95.

Rieder, S. E., and S. D. Emr. 1997. A novel RING finger protein complex essential for a late step in protein transport to the yeast vacuole. *Mol Biol Cell.* 8:2307-2327.

Rink, J., E. Ghigo, Y. Kalaidzidis, and M. Zerial. 2005. Rab conversion as a mechanism of progression from early to late endosomes. *Cell.* 122:735-749.

Rizo, J., and T. C. Sudhof. 2012. The Membrane Fusion Enigma: SNAREs, Sec1/Munc18 Proteins, and Their Accomplices-Guilty as Charged? *Annu Rev Cell Dev Biol.* 28:279-308.

Sato, T. K., P. Rehling, M. R. Peterson, and S. D. Emr. 2000. Class C Vps protein complex regulates vacuolar SNARE pairing and is required for vesicle docking/fusion. *Mol Cell.* 6:661-671.

Seals, D. F., G. Eitzen, N. Margolis, W. T. Wickner, and A. Price. 2000.A Ypt/Rab effector complex containing the Sec1 homolog Vps33p is required for homotypic vacuole fusion. *Proc. Natl. Acad. Sci. U S A.* 97:9402-9407.

Schafer, I. B., G. G. Hesketh, N. A. Bright, S. R. Gray, P. R. Pryor, P. R. Evans, J. P. Luzio, and D. J. Owen. 2012. The binding of Varp to VAMP7 traps VAMP7 in a closed, fusogenically inactive conformation. *Nat Struct Mol Biol.* 19:1300-1309.

Schwartz, M. L., and A. J. Merz. 2009. Capture and release of partially zipped trans-SNARE complexes on intact organelles. *J Cell Biol.* 185:535-549.

Scott, B. L., J. S. Van Komen, H. Irshad, S. Liu, K. A. Wilson, and J. A. McNew. 2004. Sec1p directly stimulates SNARE-mediated membrane fusion in vitro. *J Cell Biol.* 167:75-85.

Seals, D. F., G. Eitzen, N. Margolis, W. T. Wickner, and A. Price. 2000. A Ypt/Rab effector complex containing the Sec1 homolog Vps33p is required for homotypic vacuole fusion. *Proc Natl Acad Sci U S A.* 97:9402-9407.

Sevrioukov, E. A., J. P. He, N. Moghrabi, A. Sunio, and H. Kramer. 1999. A role for the deep orange and carnation eye color genes in lysosomal delivery in Drosophila. *Mol Cell.* 4:479-486.

Shen, J., S. S. Rathore, L. Khandan, and J. E. Rothman. 2010. SNARE bundle and syntaxin N-peptide constitute a minimal complement for Munc18-1 activation of membrane fusion. *J Cell Biol.* 190:55-63.

Shen, J., D. C. Tareste, F. Paumet, J. E. Rothman, and T. J. Melia. 2007. Selective activation of cognate SNAREpins by Sec1/Munc18 proteins. *Cell.* 128:183-195.

Shi, L., D. Kummel, J. Coleman, T. J. Melia, and C. G. Giraudo. 2011. Dual roles of Munc18-1 rely on distinct binding modes of the central cavity with Stx1A and SNARE complex. *Mol Biol Cell.* 22:4150-4160.

Shorter, J., M. B. Beard, J. Seemann, A. B. Dirac-Svejstrup, and G. Warren. 2002. Sequential tethering of Golgins and catalysis of SNAREpin assembly by the vesicle-tethering protein p115. *J Cell Biol.* 157:45-62.

Sivaram, M. V., J. A. Saporita, M. L. Furgason, A. J. Boettcher, and M. Munson. 2005. Dimerization of the exocyst protein Sec6p and its interaction with the t-SNARE Sec9p. *Biochemistry.* 44:6302-6311.

Solinger, J. A., and A. Spang. 2013. Tethering complexes in the endocytic pathway: CORVET and HOPS. *FEBS J.*

Sorensen, J. B., K. Wiederhold, E. M. Muller, I. Milosevic, G. Nagy, B. L. de Groot, H. Grubmuller, and D. Fasshauer. 2006. Sequential N- to C-terminal SNARE complex assembly drives priming and fusion of secretory vesicles. *EMBO J.* 25:955-966.

Srivastava, A., C. A. Woolford, and E. W. Jones. 2000. Pep3p/Pep5p complex: a putative docking factor at multiple steps of vesicular transport to the vacuole of Saccharomyces cerevisiae. *Genetics.* 156:105-122.

Starai, V. J., C. M. Hickey, and W. Wickner. 2008. HOPS proofreads the trans-SNARE complex for yeast vacuole fusion. *Mol Biol Cell.* 19:2500-2508.

Stone, S., M. Sacher, Y. Mao, C. Carr, P. Lyons, A. M. Quinn, and S. Ferro-Novick. 1997. Bet1p activates the v-SNARE Bos1p. *Mol Biol Cell.* 8:1175-1181.

Strop, P., S. E. Kaiser, M. Vrljic, and A. T. Brunger. 2008. The structure of the yeast plasma membrane SNARE complex reveals destabilizing water-filled cavities. *J Biol Chem.* 283:1113-1119.

Stroupe, C. 2012. The yeast vacuolar Rab GTPase Ypt7p has an activity beyond membrane recruitment of the homotypic fusion and protein sorting-Class C Vps complex. *Biochem J.* 443:205-211.

Stroupe, C., K. M. Collins, R. A. Fratti, and W. Wickner. 2006. Purification of active HOPS complex reveals its affinities for phosphoinositides and the SNARE Vam7p. *EMBO J.* 25:1579-1589.

Stroupe, C., C. M. Hickey, J. Mima, A. S. Burfeind, and W. Wickner. 2009. Minimal membrane docking requirements revealed by reconstitution of Rab GTPase-dependent membrane fusion from purified components. *Proc Natl Acad Sci U S A.* 106:17626-17633.

Subramanian, S., C. A. Woolford, and E. W. Jones. 2004. The Sec1/Munc18 protein, Vps33p, functions at the endosome and the vacuole of Saccharomyces cerevisiae. *Mol Biol Cell.* 15:2593-2605.

Sudhof, T. C., and J. Rizo. 2011. Synaptic vesicle exocytosis. *Cold Spring Harb Perspect Biol*. 3(12).

Sudhof, T. C., and J. E. Rothman. 2009. Membrane fusion: grappling with SNARE and SM proteins. *Science.* 323:474-477.

Suvorova, E. S., R. Duden, and V. V. Lupashin. 2002. The Sec34/Sec35p complex, a Ypt1p effector required for retrograde intra-Golgi trafficking, interacts with Golgi SNAREs and COPI vesicle coat proteins. *J Cell Biol.* 157:631-643.

Suzuki, T., N. Oiso, R. Gautam, E. K. Novak, J. J. Panthier, P. G. Suprabha, T. Vida, R. T. Swank, and R. A. Spritz. 2003. The mouse organellar biogenesis mutant buff results from a mutation in Vps33a, a homologue of yeast vps33 and Drosophila carnation. *Proc Natl Acad Sci U S A.* 100:1146-1150.

Temkin, P., B. Lauffer, S. Jager, P. Cimermancic, N. J. Krogan, and M. von Zastrow. 2011. SNX27 mediates retromer tubule entry and endosome-to-plasma membrane trafficking of signalling receptors. *Nat Cell Biol.* 13:715-721.

Togneri, J., Y. S. Cheng, M. Munson, F. M. Hughson, and C. M. Carr. 2006. Specific SNARE complex binding mode of the Sec1/Munc-18 protein, Sec1p. *Proc Natl Acad Sci U S A.* 103:17730-17735.

Tripathi, A., Y. Ren, P. D. Jeffrey, and F. M. Hughson. 2009. Structural characterization of Tip20p and Dsl1p, subunits of the Dsl1p vesicle tethering complex. *Nat Struct Mol Biol.* 16:114-123.

Uetz, P., L. Giot, G. Cagney, T. A. Mansfield, R. S. Judson, J. R. Knight, D. Lockshon, V. Narayan, M. Srinivasan, P. Pochart, A. Qureshi-Emili, Y. Li, B. Godwin, D. Conover, T. Kalbfleisch, G. Vijayadamodar, M. Yang, M. Johnston, S. Fields, and J. M.

Rothberg. 2000. A comprehensive analysis of protein-protein interactions in Saccharomyces cerevisiae. *Nature.* 403:623-627.

Ungermann, C., G. F. von Mollard, O. N. Jensen, N. Margolis, T. H. Stevens, and W. Wickner. 1999. Three v-SNAREs and two t-SNAREs, present in a pentameric cis-SNARE complex on isolated vacuoles, are essential for homotypic fusion. *J Cell Biol.* 145:1435-1442.

Venkatesan, K., J. F. Rual, A. Vazquez, U. Stelzl, I. Lemmens, T. Hirozane-Kishikawa, T. Hao, M. Zenkner, X. Xin, K. I. Goh, M. A. Yildirim, N. Simonis, K. Heinzmann, F. Gebreab, J. M. Sahalie, S. Cevik, C. Simon, A. S. de Smet, E. Dann, A. Smolyar, Vinayagam, H. Yu, D. Szeto, H. Borick, A. Dricot, N. Klitgord, R. R. Murray, C. Lin, M. Lalowski, J. Timm, K. Rau, C. Boone, P. Braun, M. E. Cusick, F. P. Roth, D. E. Hill, J. Tavernier, E. E. Wanker, A. L. Barabasi, and M. Vidal. 2009. An empirical framework for binary interactome mapping. *Nat Methods.* 6:83-90.

Verhage, M., A. S. Maia, J. J. Plomp, A. B. Brussaard, J. H. Heeroma, H. Vermeer, R. F. Toonen, R. E. Hammer, T. K. van den Berg, M. Missler, H. J. Geuze, and T. C. Sudhof. 2000. Synaptic assembly of the brain in the absence of neurotransmitter secretion. *Science.* 287:864-869.

Vonderheit, A., and A. Helenius. 2005. Rab7 associates with early endosomes to mediate sorting and transport of Semliki forest virus to late endosomes. *PLoS Biol.* 3:e233.

Wang, C. W., P. E. Stromhaug, E. J. Kauffman, L. S. Weisman, and D. J. Klionsky. 2003. Yeast homotypic vacuole fusion requires the Ccz1-Mon1 complex during the tethering/docking stage. *J. Cell Biol.* 163:973-985.

Wang, C. W., P. E. Stromhaug, J. Shima, and D. J. Klionsky. 2002. The Ccz1-Mon1 protein complex is required for the late step of multiple vacuole delivery pathways. *J. Biol. Chem.* 277:47917-47927.

Wang, L., A. J. Merz, K. M. Collins, and W. Wickner. 2003. Hierarchy of protein assembly at the vertex ring domain for yeast vacuole docking and fusion. *J Cell Biol.* 160:365-374.

Wang, L., E. S. Seeley, W. Wickner, and A. J. Merz. 2002. Vacuole fusion at a ring of vertex docking sites leaves membrane fragments within the organelle. *Cell.* 108:357-369.

Wickner, W. 2010. Membrane fusion: five lipids, four SNAREs, three chaperones, two nucleotides, and a Rab, all dancing in a ring on yeast vacuoles. *Annu Rev Cell Dev Biol.* 26:115-136.

Wickner, W., and R. Schekman. 2008. Membrane fusion. *Nat Struct Mol Biol.* 15:658-664.

Woolford, C. A., G. S. Bounoutas, S. E. Frew, and E. W. Jones. 1998. Genetic interaction with vps8-200 allows partial suppression of the vestigial vacuole phenotype caused by a pep5 mutation in Saccharomyces cerevisiae. *Genetics.* 148:71-83.

Winter, U., X. Chen, and D. Fasshauer. 2009. A conserved membrane attachment site in alpha-SNAP facilitates N-ethylmaleimide-sensitive factor (NSF)-driven SNARE complex disassembly. *J Biol Chem.* 284:31817-31826.

Wurmser, A. E., T. K. Sato, and S. D. Emr. 2000. New component of the vacuolar class C-Vps complex couples nucleotide exchange on the Ypt7 GTPase to SNARE-dependent docking and fusion. *J. Cell Biol.* 151

Xu, H., Y. Jun, J. Thompson, J. Yates, and W. Wickner. 2010a. HOPS prevents the disassembly of trans-SNARE complexes by Sec17p/Sec18p during membrane fusion. *EMBO J.* 29:1948-1960.

Xu, Y., L. Su, and J. Rizo. 2010b. Binding of Munc18-1 to synaptobrevin and to the SNARE four-helix bundle. *Biochemistry.* 49:1568-1576.

Yamaguchi, T., I. Dulubova, S. W. Min, X. Chen, J. Rizo, and T. C. Sudhof. 2002. Sly1 binds to Golgi and ER syntaxins via a conserved N-terminal peptide motif. *Dev Cell.* 2:295-305.

Yang, B., M. Steegmaier, L. C. J. Gonzalez, and R. H. Scheller. 2000. nSec1 binds a closed conformation of syntaxin1A. *J Cell Biol.* 148:247-252.

Ybe, J. A., F. M. Brodsky, K. Hofmann, K. Lin, S. H. Liu, L. Chen, T. N. Earnest, R. J. Fletterick, and P. K. Hwang. 1999. Clathrin self-assembly is mediated by a tandemly repeated superhelix. *Nature.* 399:371-375.

Yu, I. M., and F. M. Hughson. 2010. Tethering factors as organizers of intracellular vesicular traffic. *Annu Rev Cell Dev Biol.* 26:137-156.

Zanetti, G., K. B. Pahuja, S. Studer, S. Shim, and R. Schekman. 2012. COPII and the regulation of protein sorting in mammals. *Nat Cell Biol.* 14:20-28.

Zhao, C., E. C. Smith, and S. W. Whiteheart. 2012. Requirements for the catalytic cycle of the N-ethylmaleimide-Sensitive Factor (NSF). *Biochim Biophys Acta.* 1823:159-171.

Zhou, P., Z. P. Pang, X. Yang, Y. Zhang, C. Rosenmund, T. Bacaj, and T. C. Sudhof. 2013. Syntaxin-1 N-peptide and H(abc)-domain perform distinct essential functions in synaptic vesicle fusion. *EMBO J.* 32:159-171.

Zink, S., D. Wenzel, C. A. Wurm, and H. D. Schmitt. 2009. A link between ER tethering and COP-I vesicle uncoating. *Dev Cell.* 17:403-416.

Zwilling, D., A. Cypionka, W. H. Pohl, D. Fasshauer, P. J. Walla, M. C. Wahl, and R. Jahn. 2007. Early endosomal SNAREs form a structurally conserved SNARE complex and fuse liposomes with multiple topologies. *EMBO J.* 26:9-18.

Appendix A: Abbreviations

ALP – alkaline phosphatase
(sALP, soluble ALP; mALP, mature ALP; pALP, proALP)
ARC – Arthrogryposis renal dysfunction cholestasis
bf – mouse buff mutation
COG – conserved oligomeric Golgi
COP – coat protein complex
CORVET – class C core vacuole/endosome tethering
CPS– carboxypeptidase S
CPY – carboxypeptidase Y
CTD – carboxyterminal domain
GAP – GTPase activating protein
GARP – Golgi-associated retrograde protein
GDI – GDP dissociation inhibitor
GEF – guanine nucleotide exchange factor
GMAP210 – Golgi microtubule associated protein 210
GSH – glutathione sepharose resin
HPS – Hermansky-Pudlak syndrome
HOPS – homotypic fusion and vacuolar protein sorting
MTC – multi-subunit tethering complex
NSF – N-ethylmaleimide sensitive factor
PX – phox homology
RING – really interesting new gene
SC – synthetic complete
SM – Sec1/Munc18
SNAP – soluble n-ethylmaleimide sensitive factor attachment protein
SNARE – soluble n-ethylmaleimide sensitive factor attachment protein receptor
TAP– tandem affinity purification
TRAPPI – transport protein particle I
TTX – TEV (tobacco etch virus), thrombin, factor X

VPS-C – vacuole protein sorting – class C

Y2H – yeast-two hybrid

Table 3. Strains and plasmids used in this study

Name	Genotype	Reference/source
SEY6210	*MATa leu2-3,112 ura3-52 his3-200 trp1-901 lys2-801 suc2-9*	(Robinson *et al.*, 1988)
BHY10	SEY6210 *CPY-Invertase::LEU2* (pBHY11)	(Horazdovsky *et al.*, 1994)
BY4742	*MATa his3Δ1 leu2Δ0 lys2Δ0 ura3Δ0*	ATCC
BY4742 *vps11*Δ	BY4742; *vps11*Δ::KAN	Invitrogen
BY4742 *vps16*Δ	BY4742; *vps16*Δ::KAN	Invitrogen
BY4742 *vps18*Δ	BY4742; *vps18*Δ::KAN	Invitrogen
AMY1275	BY4742; *vps33*Δ::KAN	This work
BY4742 *vps39*Δ	BY4742; *vps39*Δ::KAN	Invitrogen
BY4742 *vps41*Δ	BY4742; *vps41*Δ::KAN	Invitrogen
BLY1	BHY10 *vps33*Δ*::KAN*	This work
BY4742 *pep4*Δ	BY4742 *pep4*Δ*::neo*	(Collins *et al*, 2007)
BLY2	BY4742 *pep4*Δ*::neo vps33*Δ*::KAN*	This work
BLY3	BHY10 *VPS33-ttx-GFP$_{A207K}$::NAT*	This work
BLY4	BHY10 *vps33^{D88K}-ttx-GFP$_{A207K}$::NAT*	This work
BLY5	BHY10 *vps33^{R281A}-ttx-GFP$_{A207K}$::NAT*	This work
BLY6	BHY10 *vps33^{G297V}-ttx-GFP$_{A207K}$::NAT*	This work
BLY7	BHY10 *vps33^{D300G}-ttx-GFP$_{A207K}$::NAT*	This work
Yeast Expression Plasmids		
pRS416	*URA3 CEN/ARSH4 Amp^{R}*	(Sikorski & Hieter, 1989)
pBL1	*pRS416 VPS33pr::VPS33-ttx-GFP$_{A207K}$*	This work
pBL2	*pRS416 VPS33pr::vps33^{L75P}-ttx-GFP$_{A207K}$*	This work
pBL3	*pRS416 VPS33pr::vps33^{D88K}-ttx-GFP$_{A207K}$*	This work
pBL4	*pRS416 VPS33pr::vps33^{I278N}-ttx-GFP$_{A207K}$*	This work
pBL5	*pRS416 VPS33pr::vps33^{R281A}-ttx-GFP$_{A207K}$*	This work
pBL6	*pRS416 VPS33pr::vps33^{G297V}-ttx-GFP$_{A207K}$*	This work
pBL7	*pRS416 VPS33pr::vps33^{D300G}-ttx-GFP$_{A207K}$*	This work
pBL8	*pRS416 VPS33pr::vps33^{D300E}-ttx-GFP$_{A207K}$*	This work
pBL9	*pRS416 VPS33pr::vps33^{F305L}-ttx-GFP$_{A207K}$*	This work

pBL10	*pRS416 VPS33pr::vps33^{T553I}-ttx-GFP$_{A207K}$*	This work
pBL11	*pRS416 VPS33pr::vps33^{E653A}-ttx-GFP$_{A207K}$*	This work

Bacterial Expression Plasmids

pHIS parallel1	pET22B- *amp^R GST-(tev)-*	(Sheffield *et al.,* 1999)
pGST parallel1	pGEX4T1- *amp^R GST-(tev)-*	(Sheffield *et al.,* 1999)
pRP1	pRSF- *kan^R His$_7$-MBP-(tev)-*	This work
pBL12	pRSF- *kan^R His6-GFP$_{A207K}$-(tev)-*	This work
pBL12	pRSF- *kan^R -(tev)-GST*	This work
pBL13	pBL12- *kan^R SSO1(1-265)-(tev)-GST*	This work
pBL14	pBL12- *kan^R VAM3 (1-264)-(tev)-GST*	This work
pBL15	pBL12- *kan^R VAM3$_{Habc}$ (1-145)-(tev)-GST*	This work
pBL16	pBL12- *kan^R VAM3$_{Linker}$ (116-186)-(tev)-GST*	This work
pBL17	pBL12- *kan^R VAM3$_{SNARE}$ (182-264)-(tev)-GST*	This work
-	pGST parallel1- *amr^R* GST-Vti1 (1-194)	(Stroupe *et al.,* 2006)
AMB73	pGEX-KET- *amp^R GST-VAM7 (2-316)*	(Merz *et al.,* 2004)
AMB74	pGEX-KET- *amp^R GST-VAM7$_{PX}$ (2-123)*	(Merz *et al.,* 2004)
pBL18	pGST paralle1- *amp^R GST-(tev)-NYV1 (1-231)*	This work
pBL19	pRP1- *kan^R His$_7$-MBP-(tev)-VTI1 (1-194)*	This work
AMB225	pTYB3- *amp^R His6-Vam7 (1-316)*	(Schwartz *et al.,* 2009)
pBL20	pHIS paralle1- *amp^R His$_6$-(tev)-NYV1 (1-231)*	This work
pBL21	pHIS paralle1- *amp^R His$_6$-(tev)-NYV1$_{5\Delta}$ (1-211)*	This work
pBL22	pBL12- *kan^R His6-GFP$_{A207K}$-(tev)-Vam7 (190-316)*	This work
pBL23	pGST paralle1- *amp^R GST-(tev)-Vam7$_{SNARE}$ (190-316)*	This work
pBL24	pGST paralle1- *amp^R GST-(tev)-NYV1$_{SNARE}$ (162-231)*	This work
pBL25	pGST paralle1- *amp^R GST-(tev)-SED5$_{SNARE}$ (170-319)*	This work
pBL26	pHIS paralle1- *amp^R His$_6$-(tev)-BOS1 (1-222)*	This work
pBL27	pHIS paralle1- *amp^R His$_6$-(tev)-SE22 (1-188)*	This work
pSN358	pET14b- *amp^R His$_6$-BET1 (1-123)*	(Stone *et al.,* 1997)
pBL28	pGST paralle1- *amp^R GST-(tev)-YKT6 (1-195)*	This work
pBL29	pGST paralle1- *amp^R GST-(tev)-SE22 (1-188)*	This work
pBL30	pHIS paralle1- *amp^R His$_6$-(tev)-YKT6 (1-195)*	This work

pBL31	pBL17- *kan^R VAM3$_{SNARE(-9\Delta)}$ (192-264)-(tev)-GST*	This work
pBL32	pBL17- *kan^R VAM3$_{SNARE(-7\Delta)}$ (199-264)-(tev)-GST*	This work
pBL33	pBL17- *kan^R VAM3$_{SNARE(-5\Delta)}$ (206-264)-(tev)-GST*	This work
pBL34	pBL17- *kan^R VAM3$_{SNARE(-3\Delta)}$ (213-264)-(tev)-GST*	This work
pBL35	pBL17- *kan^R VAM3$_{SNARE(-1\Delta)}$ (220-264)-(tev)-GST*	This work
pBL36	pBL17- *kan^R VAM3$_{SNARE(+1\Delta)}$ (227-264)-(tev)-GST*	This work
pBL37	pBL17- *kan^R VAM3$_{SNARE(+3\Delta)}$ (234-264)-(tev)-GST*	This work
pBL38	pBL17- *kan^R VAM3$_{SNARE(+5\Delta)}$ (241-264)-(tev)-GST*	This work
pBL39	pBL17- *kan^R SSO1$_{SNARE}$ (184-265)-(tev)-GST*	This work
pBL40	pGST paralle1- *amp^R GST-(tev)- VAM3$_{SNARE}$ (182-264)*	This work
pBL41	pBL40- *amp^R GST-(tev)- VAM3$_{SNARE(+9\Delta)}$ (182-257)*	This work
pBL42	pBL40- *amp^R GST-(tev)- VAM3$_{SNARE(+7\Delta)}$ (182-250)*	This work
pBL43	pBL40- *amp^R GST-(tev)- VAM3$_{SNARE(+5\Delta)}$ (182-243)*	This work
pBL44	pBL40- *amp^R GST-(tev)- VAM3$_{SNARE(+3\Delta)}$ (182-236)*	This work
pBL43	pBL40- *amp^R GST-(tev)- VAM3$_{SNARE(-1\Delta)}$ (182-222)*	This work
pBL43	pBL40- *amp^R GST-(tev)- VAM3$_{SNARE(-5\Delta)}$ (182-208)*	This work
pBL44	pBL18- *amp^R GST-(tev)-NYV1$_{(+9\Delta)}$ (1-225)*	This work
pBL45	pBL18- *amp^R GST-(tev)-NYV1$_{+7\Delta)}$ (1-218)*	This work
pBL46	pBL18- *amp^R GST-(tev)-NYV1$_{(+5\Delta)}$ (1-211)*	This work
pBL47	pBL18- *amp^R GST-(tev)-NYV1$_{(+5\Delta)}$ (1-211)*	This work
pBL47	pBL12- *kan^R PEP12 (1-268)-(tev)-GST*	This work
pBL48	pBL12- *kan^R SED5 (1-319)-(tev)-GST*	This work